DETERMINATION OF MECHANISMS CAUSING AND LIMITING SEPARATIONS IN COLUMN CRYSTALLIZATION

Walter Collins Gates, Jr.

A dissertation submitted in partial fulfillment
of the requirements for the degree of
Doctor of Philosophy in the
University of Michigan
1967

Doctoral Committee:

Professor John E. Powers, Chairman
Professor Edward E. Hucke
Associate Professor Robert H. Kadlec
Professor Edgar E. Westrum, Jr.
Professor J. Louis York

ACKNOWLEDGEMENTS

This dissertation is the result of contributions from many sources. These contributors and contributions are acknowledged with gratitude.

Professor J. E. Powers, chairman of the doctoral committee, for his continuing guidance and criticism.

Professor R. H. Kadlec, committee member, for his generous assistance throughout the course of the study.

Professors E. E. Hucke, E. E. Westrum, Jr., and J. L. York, committee members for their beneficial assistance and helpful suggestions.

Dr. R. Albertins and Mr. J. D. Henry, Jr. for their critical remarks and general assistance.

The personnel of the shops of the Department of Chemical and Metallurgical Engineering who were helpful beyond the call of duty.

Mr. F. Drogosz who assisted in the operation and maintenance of the analytical equipment.

The National Science Foundation, Union Carbide Corporation, The Riggs Foundation, and the Chemistry Department of the University of Michigan for financial support.

The Upjohn Company for the donation of the drive mechanism for the column crystallizer.

Mr. Gary J. Powers for his assistance and stimulation during the early stages of the experimental work.

Mr. Murray Player whose comments significantly improved the manuscript.

Mr. R. Stewart and Professor C. W. Peters for their gentlemanly conduct during trying periods.

Mr. M. Newberger for his assistance with some of the computing.

The staff of the Industry Program of the College of Engineering of the University of Michigan for its complete cooperation and efficient production of the final form of this dissertation.

My wife, Lorna, for her encouragement, support, and assistance. Without these, this research would have been neither started nor completed.

TABLE OF CONTENTS

TABLE OF CONTENTS (CONT'D)

TABLE OF CONTENTS (CONT'D)

LIST OF TABLES

LIST OF FIGURES

LIST OF FIGURES (CONT'D)

LIST OF APPENDICES

NOMENCLATURE

A	Cross-sectional area of column, measured perpendicularly to flow of liquid and solid phases, cm^2.
a	Area available for interphase mass-transfer per unit volume of column, cm^{-1}.
B	Slope of phase Equation (29), C°.
b	Intercept of phase relation (3), weight fraction.
$C_{unsubscripted}$	Flow of liquid adhering to crystals, g/sec.
$C_{subscripted}$	Constant in general solution to differential equation; or specific heat, cal/g-C°.
D	Coefficient of diffusion, cm^2/sec.
E	Diffusion faction (D FACTOR) defined by Equation (16), g-cm/sec.
F	Mass-transfer factor defined by Equation (16), g/cm-sec.
f	Frequency of spiral oscillation, sec^{-1}; or notation for "function of".
G	Collection of terms defined by Equation (34), cal/g.
g	Notation for "function of".
H	Grouping of variables, defining the separating power of a column crystallizer operating at specified conditions, cm; or heat of fusion, cal/g.
h	Position in the column, measured from melting section, cm.
h_o	Length of purification section, cm.
J	Thermal conduction in liquid phase, cal/sec.
K	Coefficient of mass-transfer between solid and liquid phases, cm/sec.
k	Rate at which concentration changes with time (see Equation (40b)), weight fraction/sec.
L	Mass flow of solid, g/sec.

NOMENCLATURE (CONT'D)

m	Slope of phase relation (3), dimensionless.
N	Diffusional flow of material, g/sec.
n	Counting integer.
P	Collection of terms used in Equation (49), weight fraction/cm^2.
Q	Symbol representing differentiation (d/dh), cm^{-1}.
q	Constant in general solution to differential equation, defined by characteristic equation, cm^{-1}.
R	Constant defined by Equation (5); or collection of terms defined by Equation (35), cal/sec-C°-weight fraction.
R_o	Outside radius of spheres, cm.
r	Radius of sphere, cm.
S	Collection of terms defined by Equation (36), cal/g; or slope of composition profile, weight fraction/cm.
s	Stroke of spiral oscillation, cm.
T	Temperature of liquid phase, °C; or reduced weight fraction in solid phase, weight fraction.
t	Temperature of solid phase, °C.
U	Overall heat-transfer coefficient between liquid and solid phases, cal/cm^2-sec-°C.
V	Mass flow of liquid, g/sec.
W	Collection of terms defined by Equation (47c), cm^2/sec.
X	Weight fraction in solid, g/g. The high melting component in solid solutions, and that excluded from the solid in eutectics.
Y	Weight fraction in liquid, g/g (see definition of X).
Z	Weight fraction cyclohexane in liquid adhering to crystals.
z	Position in column measured from freezing section, cm.

NOMENCLATURE (CONT'D)

Greek Symbols

α	Grouping of other constants, or ratio of adhering liquid to crystal.
Δ	Small increment.
ϵ	Eddy-thermal diffusivity of liquid, cal/sec-cm-C°.
η	Volume fraction, dimensionless.
ρ	Density, g/cm^3.
Σ	Summation symbol.
θ	Time, sec.

Superscripts

B	Refers to BNB
C	Refers to CNB
L	Refers to solid phase.
o	Refers to position, h=o.
V	Refers to liquid phase.
*	Equilibrium value.
—	Average value.

ABSTRACT

The process of column crystallization was analyzed mathematically and experimentally in order to determine the mechanisms by which separations are achieved and limited. The results of the study indicate that, at total reflux, separation is produced by the formation of crystals in the freezing section and by interphase mass-transfer in the adjacent purification section. The separation is mainly limited by eddy diffusion in the liquid phase.

Data obtained from three binary chemical systems were used in the study. The first system, m-chloronitrobenzene - m-bromonitrobenzene, forms a solid solution with a small phase separation, less than 6 weight per cent. The second system, azobenzene-stilbene, forms a solid solution with a phase separation which exceeds 20 weight per cent. The third system,benezene-cyclohexane, has essentially no solid solubility in the range of compositions used (1/2 to 3 weight percent cyclohexane).

Four mathematical models of column crystallization were developed and compared with experimental data. These models were based on different sets of assumptions as to the mechanisms which control the overall separation. The models which are consistant with the experimental results describe column crystallization as follows.

Crystals form in a freezing section and undergo changes as they pass through an adiabatic purification section to a melting section. The changes manifest in the crystals depend on the type of crystals present. Crystals with considerable solid solubility undergo melting and recrystallization. Crystals which have little dissolved impurity are

washed by the reflux liquid. In either case, mass-transfer between the countercurrently passing phases is controlled (limited) by the mass-transfer coefficient, not by the heat-transfer coefficient. Eddy diffusion in the liquid phase opposes the separation being effected by interphase mass-transfer.

The concentration of a component in the liquid phase, if a system which has a small phase separation is used, is described by the following equation: $Y = Y_o - (Y-X^*)_o \, h/(E/L + L/F)$. Y and X^* are the liquid and equilibrium solid compositions, h is the distance from the melting section, L is the rate of crystal flow, and E and F are terms relating to diffusion in the liquid and interphase mass-transfer respectively. A system which exhibits little solid solubility is adequately described by $Y = C_1 + C_2 \exp[h/(E/L + L/F)]$. C_1 and C_2 are experimental constants, C_1 probably being related to the extent of the small solid solubility.

Concurrent to the generation of data to evaluate the mathematical models, operational characteristics of a one inch by 24 inch column crystallizer were observed. Maximum crystal rates were influenced by:

(a) the area of the heat-transfer surface in the freezing section (FS),

(b) the local heat-transfer coefficient in the FS, and

(c) probably the size of the crystals.

Separation with respect to agitation had a maximum at about 30 RPM and 30 oscillations/min. Liquid phase diffusivities and mass-transfer coefficients, in satisfactory agreement with published values, were determined. Diffusivities increased linearly with the one-half power of

the agitation frequency, and varied between 1.3 cm^2/sec and 4.6 cm^2/sec. The values of the mass-transfer coefficient varied between 0.07 cm/sec and 0.64 cm/sec.

CHAPTER I

INTRODUCTION

The study reported in this dissertation was undertaken with a two-fold purpose. The primary goal was the quantitative determination of the mechanisms involved in the process of column crystallization. Such a determination would confirm or invalidate the theoretical and qualitative predictions of Powers[32] which had not previously been subjected to a complete test. The secondary aim, the mathematical description of the concentration profiles produced in a column crystallizer, was established to accomplish the primary goal. The results of the study indicate that mass-transfer between phases and dispersion within the liquid phase are the two mechanisms involved.

In order to obtain the data from which the above conclusions are drawn, a column crystallizer was built and operated at total reflux. A system which forms a continuous solid solution was used as the mixture to be separated. This type of system was chosen because it affords a severe test of the general applicability of this relatively new separation process.

With preliminary data from this system in hand, several possible mathematical models of column crystallization were formulated. Additional data were taken which showed that only one of these models is consistent with experimental results. Also, previously published data concerning one solid solution and one eutectic system were reanalyzed with models derived from the one consistent model. These analyses indicated that the mechanisms which effect and limit the separation

achieved by column crystallization are independent of the type of system being separated.

The dissertation is divided into two sections. Descriptions, the existing literature, theoretical models, and experimental results and interpretations which bear on the elucidation of the mechanisms just described are presented in the first section. This section is followed by a group of appendices which present in greater detail the descriptions of equipment, procedures, and analyses which are needed to repeat the experiments. Results which do not relate to the stated purposes of the research are also presented as an appendix. These several appendices support the first part of the dissertation but are not required for the full appreciation of the material presented therein.

A. Definitions

Several terms, used throughout this dissertation, have precise definitions which must be made clear.

"Separation" is the difference in composition which occurs in the liquid phase between two points in a crystallization column.

"Eutectic system", or "system which forms a eutectic" is a chemical mixture which exhibits little or no solid solubility and which has a eutectic point.

"Mass-transfer" or "heat-transfer" is used exclusively to refer to the exchange of material or energy which occurs between the phases which are in countercurrent contact in a column crystallizer.

"Diffusion" is used to describe that movement of material which occurs within a single phase either by molecular diffusion or by Taylor diffusion. "Diffusion" is distinguished from "backmixing," defined below.

"Backmixing" is used to describe the movement of material within a single phase caused by the turbulence of that phase. Backmixing is synonomous with eddy-diffusion.

"Dispersion" is the net effect of diffusion and backmixing as they are defined above.

"Phase Separation" refers to the difference between the compositions of two phases existing at equilibrium.

"Phase Relation" is the curve or equation describing the compositions of two phases in equilibrium.

"Agitation" is the net effect of the motion of the spiral within the column.

"Performance" is the separation per unit length of column.

"Crystal Rate" is the rate of crystal flow across a given cross-section; if the column crystallizer is adiabatic, then the crystal rate is equal to the crystallization rate.

CHAPTER II

REVIEW OF LITERATURE PERTAINING TO COLUMN CRYSTALLIZATION AND ITS ANALYSIS

A. Description of Process

Column crystallization was invented by Arnold[5] in 1951. This process incorporates the inherent theoretical attractiveness of crystallization in a separation process which eliminates some of the disadvantages previously associated with crystallization.

Column crystallization occurs in three distinct sections which are illustrated in Figure 1. In the freezing section, two phases of differing composition are formed. One is a disperse solid phase and the other a continuous mother liquor. The solid phase passes through a purification section countercurrently to a liquid moving toward the freezing section. A melting section, adjacent to the purification section and opposite the freezing section, supplies energy to the system. This energy transforms the solid crystals to a liquid to produce reflux.

Based on this brief description, simple analogies can be drawn for clarification. The melting and freezing sections are similar to parts of distillation equipment. The melting section is like a total condenser in which energy transfer causes a phase change with no change in composition. Contrarily, the energy transfer in the freezing section, like that in a reboiler, produces a phase change and a composition change. In addition, both distillation and column crystallization can be operated at total reflux or with continuous feed and removal of products. Figure 1 illustrates operation in the latter mode.

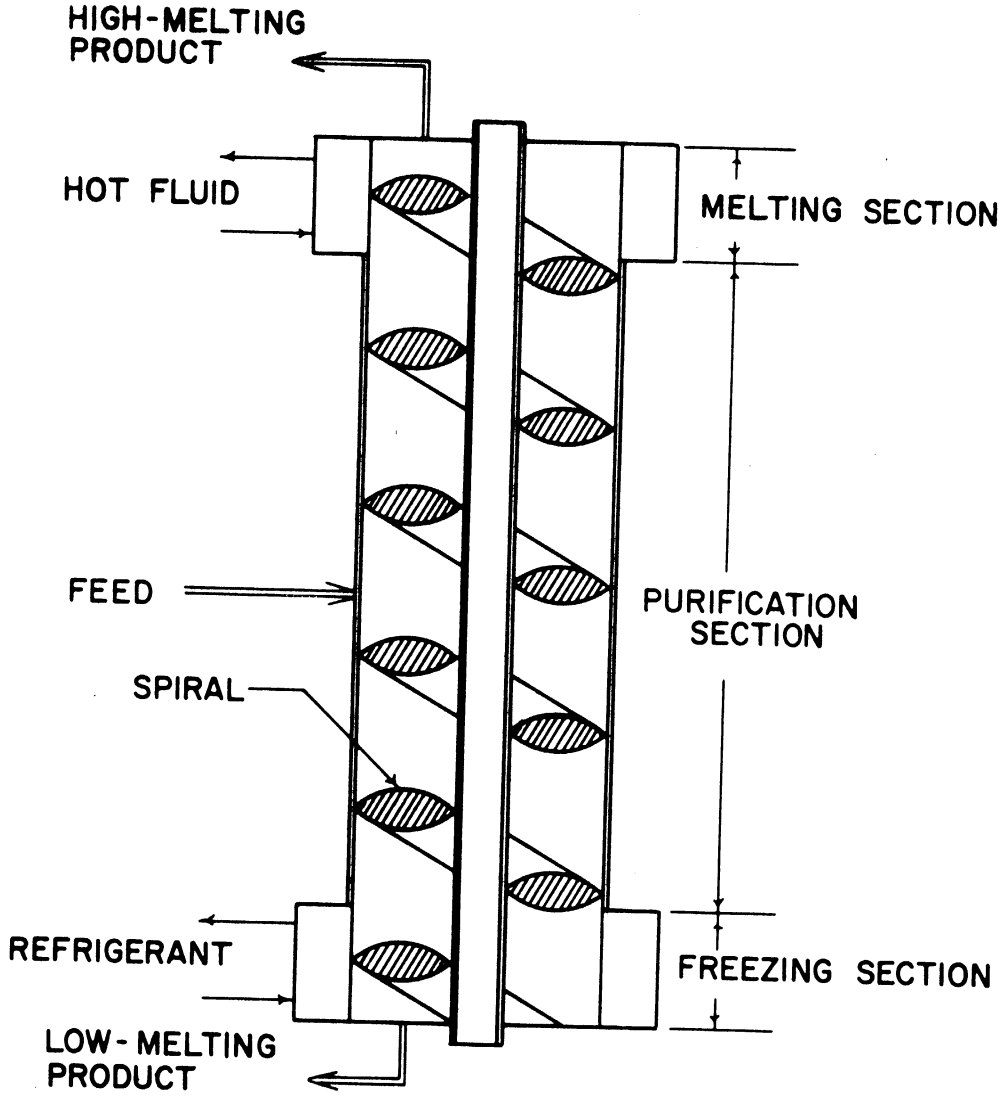

Figure 1. Sections Used in Column Crystallization.

The separation section of a column crystallizer is analagous to an extraction tower. Both contain a continuous phase and a disperse phase which has some degree of integrity. These two phases move countercurrently, with mass-transfer between phases and with dispersion in the continuous phase.

1. Configurations

Subsequent to Arnold's invention, two significantly different modifications of column crystallization have evolved. The first, deriving from the invention of Arnold, is called the Phillips column crystallizer. This device is primarily used in the industrial scale production of materials, especially p-xylene from its isomers. References to the Phillips column by Weedman[44], Thomas[39], Findlay[9], and McKay[30] have dealt with improvements in its construction, operation, and control.[10,29,38,17]

The other type of crystallizer is that developed by Schildknecht (Reference 36). It is used in the laboratory to produce materials of high purity. Modifications of the Schildknecht-type column have been described by Schildknecht[35] and Albertins.[1]

The literature concerning both Phillips- and Schildknecht-type crystallizers has been recently reviewed by Albertins, Gates, and Powers (Reference 2) and by Albertins.[1]

B. Applications

The separation and purification by column crystallization of a great variety of materials has been described and reviewed.[1,2] Aqueous systems[11,14,27] and organic mixtures have been processed.

These mixtures include light hydrocarbons, both aliphatic[12,27] and aromatic,[14,43,44] and such heavy materials as fatty acids.[33] Binary[14,44] and multicomponent[12,14,16] separations have been described.

C. Analysis

Analyses applicable to column crystallization are found in two areas of the literature. The first deals specifically with column crystallization, and the second deals generally with processes involving countercurrent contacting of two phases.

1. Column Crystallization

Early attempts to describe column crystallization mathematically were reported by Powers[32], Yagi et al.[45], and Anikin[3,4] and have been reviewed.[1,2] The analyses of Powers[32] and Yagi et al.[45] were tested experimentally and were in qualitative agreement with their data. Powers analyzed the separation of eutectic systems and systems which form solid solutions. He postulated that the mechanisms which are involved in column crystallization are dispersion and mass-transfer, but he did not determine the quantitative contributions of these mechanisms.

Albertins[1] recently analyzed the column crystallization of a eutectic system, benzenze - cyclohexane. He predicted modified exponential profiles of the liquid composition based on a model including only dispersion within the liquid phase. The agreement between this model and the considerable amount of experimental data was satisfactory.

All of the analyses mentioned above consider dispersion within the liquid phase as one mechanism limiting the effectiveness of column crystallization.

2. Other Processes

Many previous articles have dealt with the analyses of processes in which liquid-phase dispersion is considered. Li and Ziegler[26] recently reviewed much of this literature as it pertains to extraction in simple and in pulsed columns. Hartland and Mecklenburgh[18] presented an analysis of processes involving countercurrent contact of two phases for which there is a linear equilibrium relation. Their analysis included dispersion in each phase and mass-transfer between phases.

D. Results of Previous Investigations

1. Column Crystallization

Albertins,[1] in his study of benzene-cyclohexane, indicated that a mathematical description of column crystallization which includes mass-transfer between phases may be incompatible with his data. He also showed that effective diffusivities in the liquid phase were in good agreement with values reported by Jones[21] and by Moon[31] who studied pulsed-column, liquid extraction. No attempt was made, however, to correlate diffusivity with agitation.

Several operational limitations of column crystallization have been reported but not discussed. For example, a column capacity as high as 0.5 gm/cm^2-sec has been described,[1,28] but capacities much lower than this are common.[8] No mention has been made of the factors which might limit these fluxes.

Previous reports of column crystallization have not correlated the size of the crystals with the maximum possible flux of the reflux liquid.

2. Other Processes

Work by Hayford[20] and others,[31] who studied the effect of agitation on diffusivity (D) in fluid flow through packed beds, suggests that D is linearly related to the 1/2 power of the pulse frequency. These studies also suggest that D is proportional to the stroke (twice the amplitude) of the pulsation. The study of Smoot and Babb[37] indicated that effective diffusivities between 0.8 and 2.6 cm^2/sec result in pulsed extraction columns when the pulse frequency varies between 30 and 100 oscillations per minute.

The literature on packed beds indicates that the size of particles influences the maximum flow of liquid through a bed. Leva[24] shows that the maximum flux of a liquid increases as the square of the particle size.

CHAPTER III

INTRODUCTION TO EXPERIMENTAL INVESTIGATION

A. Equipment

A small Schildknecht-type column crystallizer was designed and built to carry out the experiments described in this report. A sketch of the column appears in Figure 2. An insulated glass column, 2.60 cm ID and 38 cm long, was used. The freezing section was at the bottom and the melting section at the top. The column was equipped with 7 taps through which samples of the reflux liquid could be taken. A stainless-steel tube which could be rotated and oscillated passed through the three sections of the column. This spiral was maintained concentric with the glass by a 1/2 inch diameter stainless-steel rod. A detailed description of the apparatus is included in Appendix A1-a.

B. Materials

Meta-bromonitrobenzene and meta-chloronitrobenzene (BNB and CNB) were used in this investigation. This system forms a continuous solid solution as is illustrated in Figures 3 and 4.

This system was chosen for several reasons. First, equilibrium data from two sources[19,22] which were in agreement were available. Second, the liquidus and solidus lines, as seen in Figure 3, are very close to one another. A system with such a phase diagram offers a severe test of the general applicability of column crystallization to solid solutions. Third, the mixture is solid at room temperature and melts at slightly above room temperature. Such a mixture eliminates the need for an extensive refrigeration system or for excessive insulation or guard heaters.

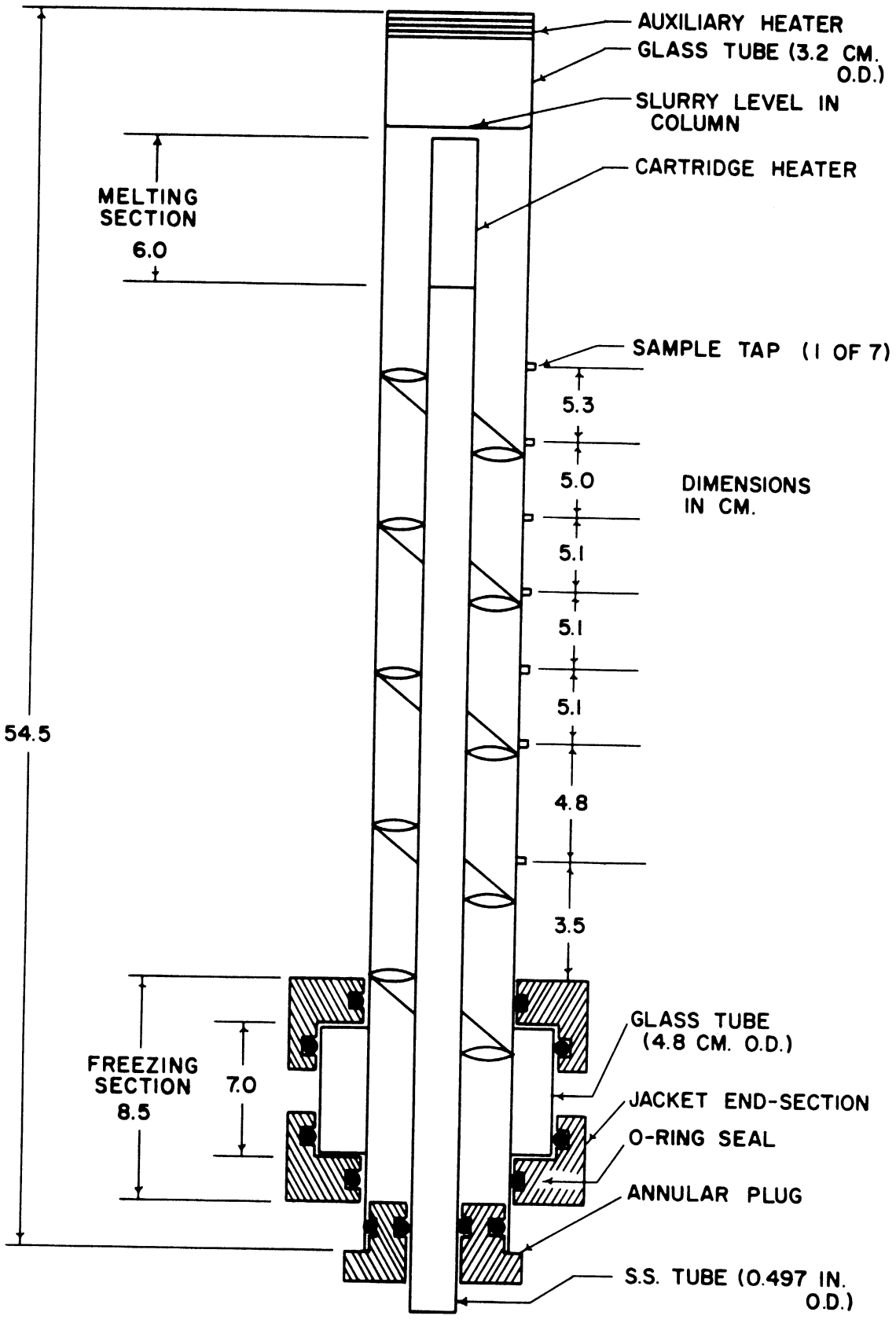

Figure 2. Diagram of Column Crystallizer.

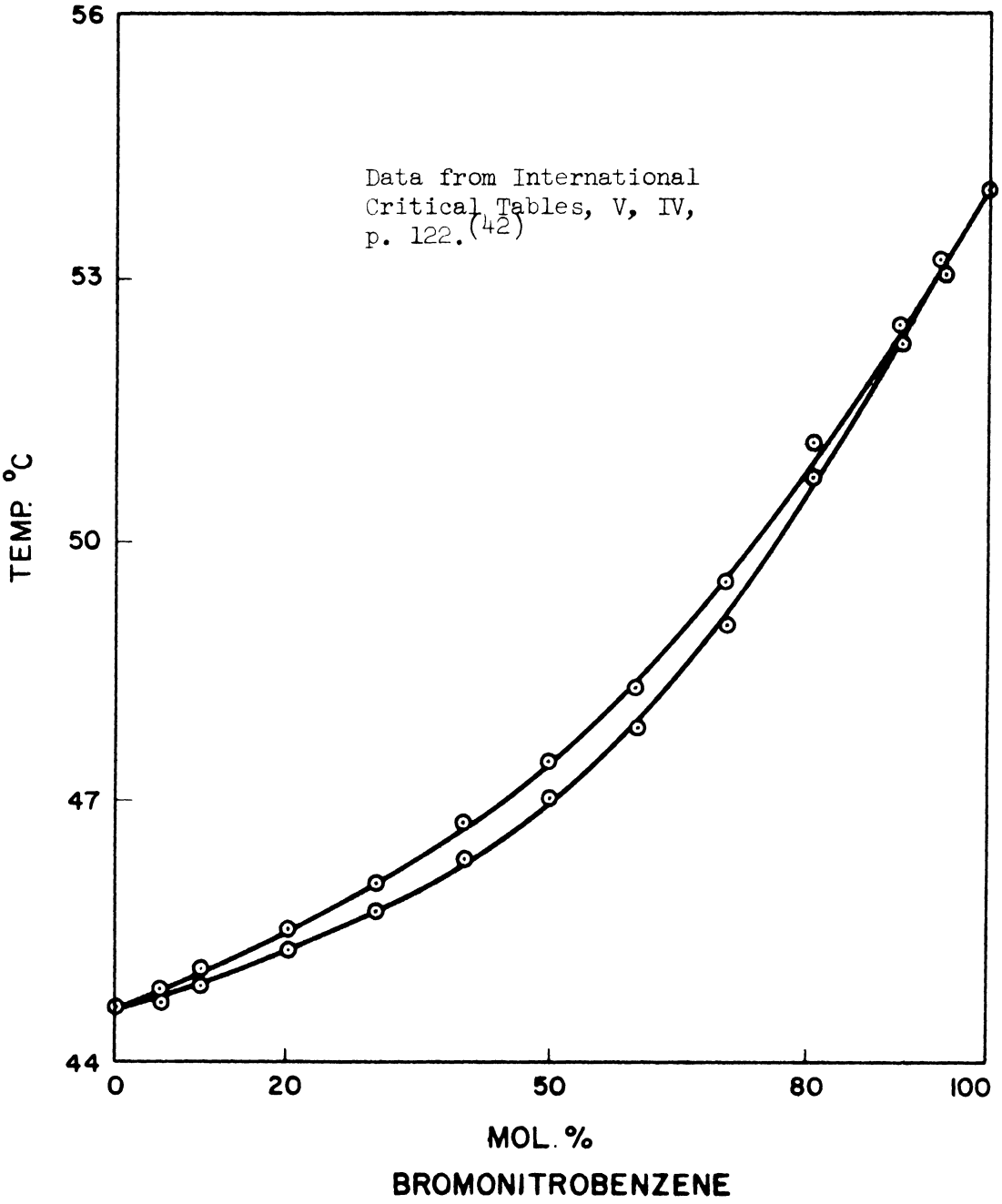

Figure 3. Phase Diagram of m-chloronitrobenzene - m-bromonitrobenzene.

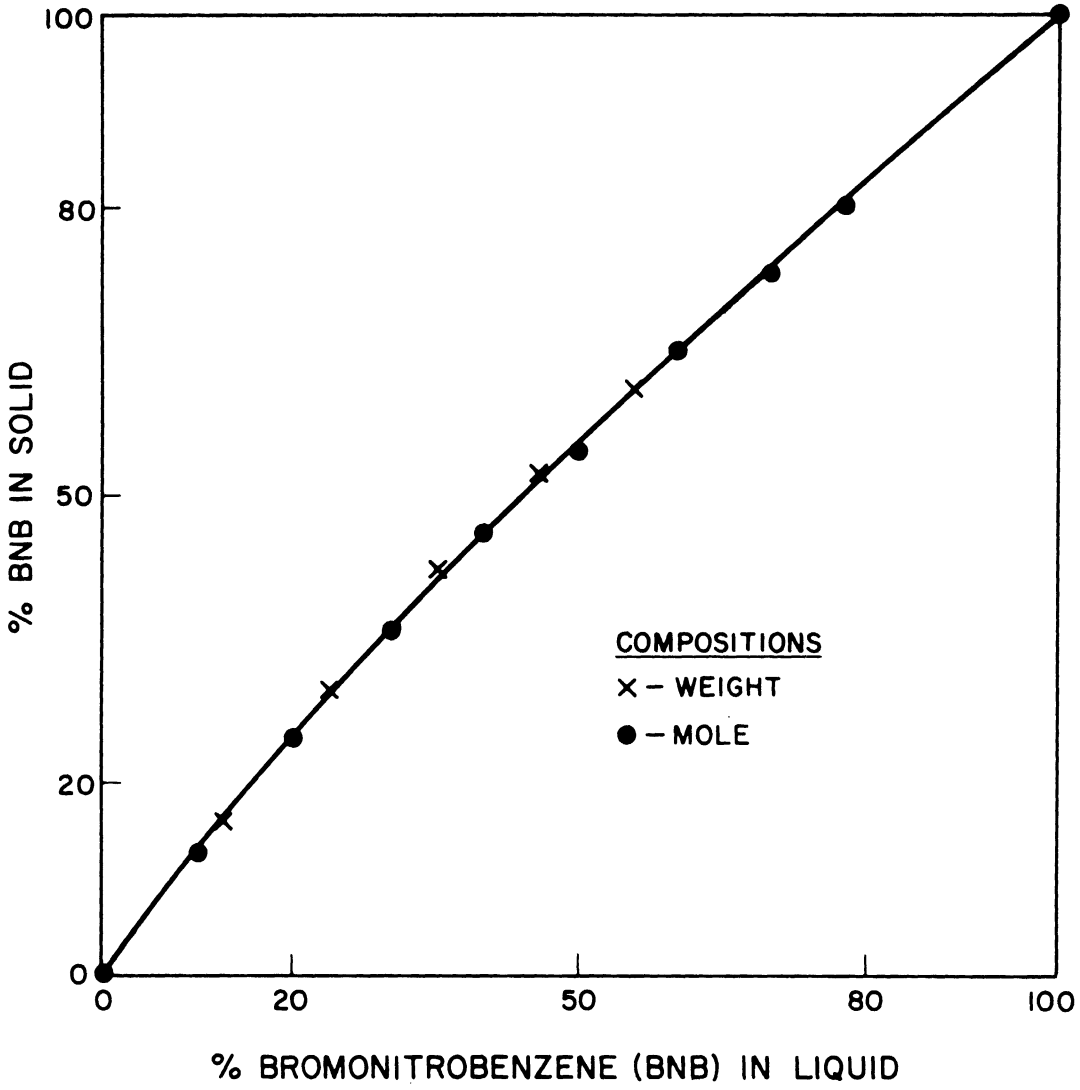

Figure 4. Phase Relation of m-chloronitrobenzene - m-bromonitrobenzene.

C. Procedures

Summarized below are the procedures used in the operation and sampling of the equipment and in the analyses of samples and data. These procedures are spelled out in greater detail in Appendices A1-b and A1-c.

Liquid of the desired composition was charged to the heated column. Warm water at a known temperature was fed to the freezing section to produce crystals in the charge. These crystals were agitated by the action of the rotating and oscillating spiral. About 90 minutes after the first crystals formed, the entire column contained a slurry of crystals and liquid. This slurry appeared to be uniform throughout. No material was fed to the column after the initial charge.

The power input to the melter was adjusted to maintain a constant proportion of crystals. About 8 hours after the first crystals formed, and at least 2 hours subsequent to any significant adjustment in operating conditions, samples of the liquid in the column were withdrawn and analyzed chromatographically.

Plots were constructed of the liquid composition vs. position in the column, and the slopes of these plots were determined. To accomplish the purpose of this study, the elucidation of the mechanisms involved in column crystallization, the influence of 6 operating variables on these slopes was determined. These variables were:

1. the charge composition,
2. the crystal rate through the column,
3. the length of the column,
4. the rate of rotation of the spiral,
5. the frequency of spiral oscillation, and
6. the stroke of the spiral oscillation.

D. Results

The experimental results which bear on the elucidation of the mechanisms involved in column crystallization are summarized in Figures 5 to 14 and in Table I. These results are discussed in detail later in the dissertation. However, this summary collects in one place the important results.

Figures 5 to 14 are plots of liquid composition vs. column position which is indicated by tap number. Tap number 7 was immediately above the freezing section, and the lowest numbered tap for a given run was immediately below the melting section.

The variables listed on each figure, as well as charge composition, were varied among the runs included on each graph. Because the charge composition was changed only slightly between runs presented on each graph, each figure shows the effect of the variables listed on that graph.

Table I summarizes the conditions used for each run.

The line drawn on each figure is the linear regression line through the data points. The slope of this line is a measure of the effectiveness which a set of operating conditions has in causing a separation between two compounds. A large slope corresponds to a highly effective set of operating conditions. The variation of this slope with changes in several operating conditions was the object of investigation in this dissertation. Thus, the separation per unit length within the column is the important dependent variable resulting from each run. Runs made at the same conditions gave the same slope to within two per cent. (See Appendix A2-a).

As it was to be expected, data points scattered somewhat about the regression lines. However, only in 5 runs, Runs 7, 13, 31, 34, and 35, did the difference between the regression line and a data point exceed one weight per cent BNB for more than 1 data point. Eleven runs were made for which no points exceeded the difference just mentioned.

Figures 5 and 6 indicate that the length of the purification section was not an important variable in determining the separation per unit length, the column performance. Rather, the performance was constant for a given set of operating conditions.

Figures 7, 8 and 9 show that the performance decreased as the degree of agitation was increased, either by increasing the stroke of oscillation or by increasing the rate of spiral rotation.

Figures 10 and 11 illustrate that the performance increased as the crystal rate increased. Each of the three figures represents a single charge composition and set of agitation conditions.

Figures 12, 10, 9, 13, 11 and 14 show the effect of charge composition. Charges which were nearby pure (Figures 12 and 14) gave a low separation per unit length. Charges of about 50% BNB (Figures 9, 10, 11 and 13) resulted in much higher performances.

Other experimental results are presented in Appendix A3. These relate to the design and operation of the column crystallizer rather than to the mechanisms involved in column crystallization.

The data on which the experimental results are based are presented in Appendix A7.

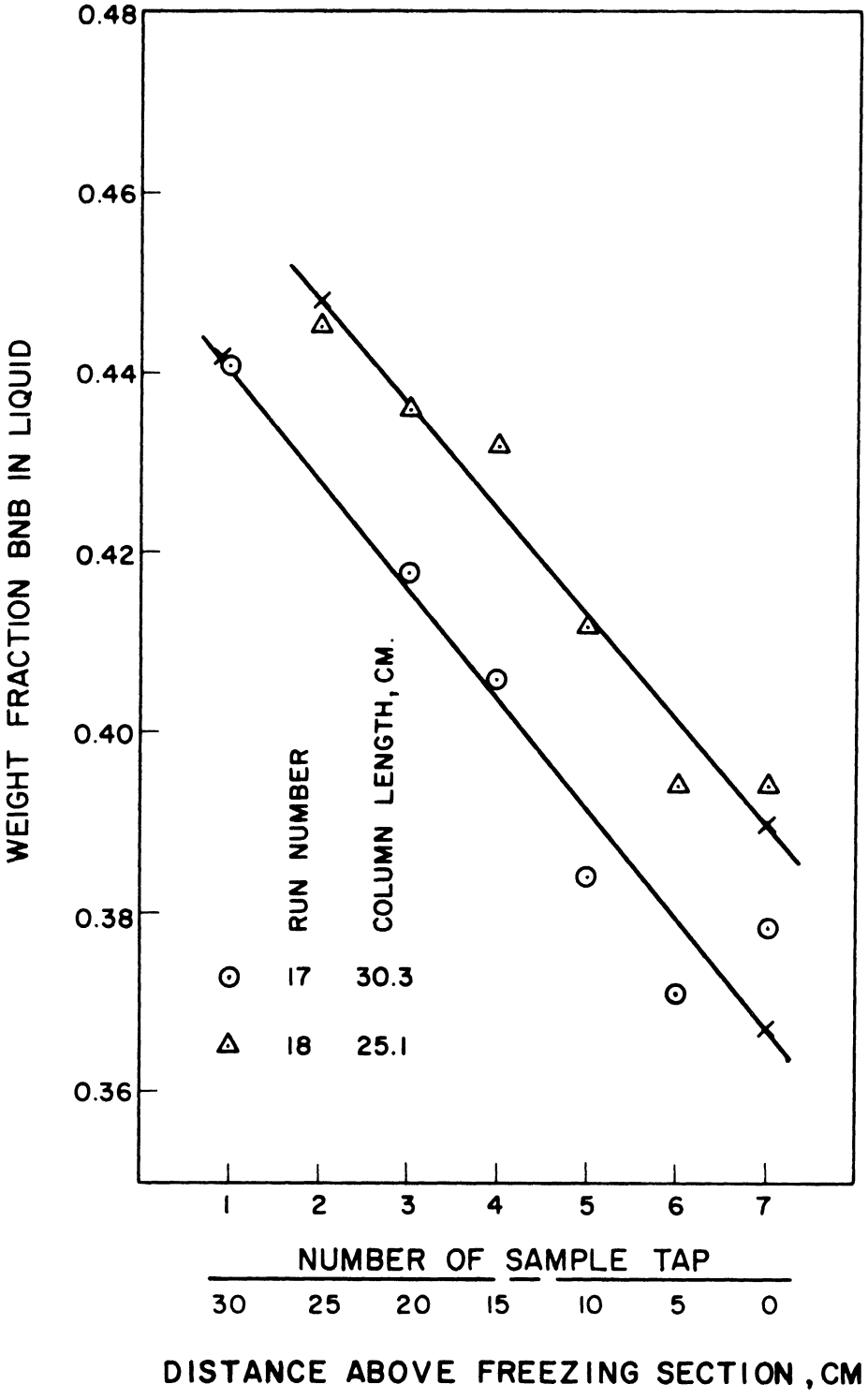

Figure 5. Effect of Column Length on Column Performance.

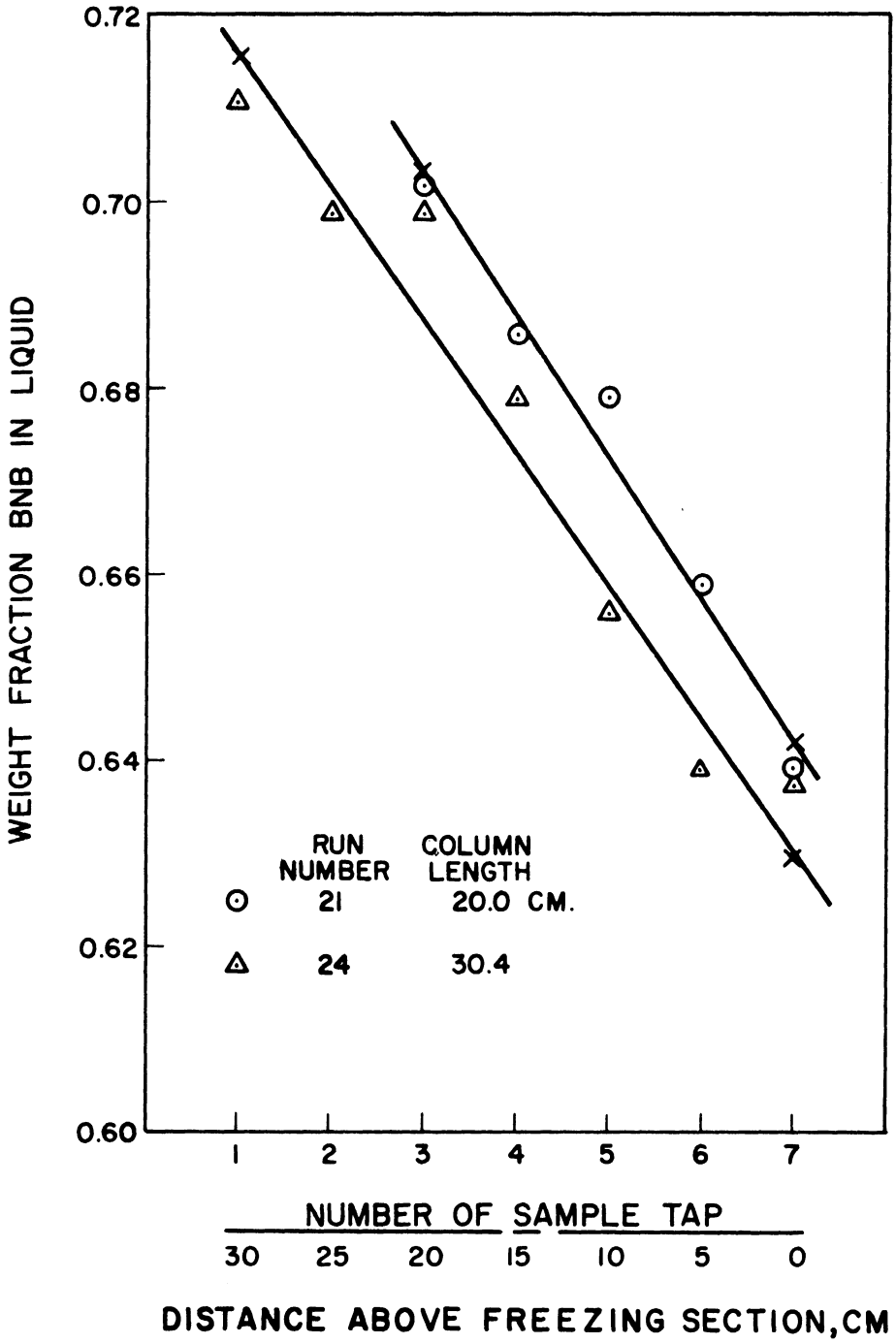

Figure 6. Effect of Column Length on Column Performance.

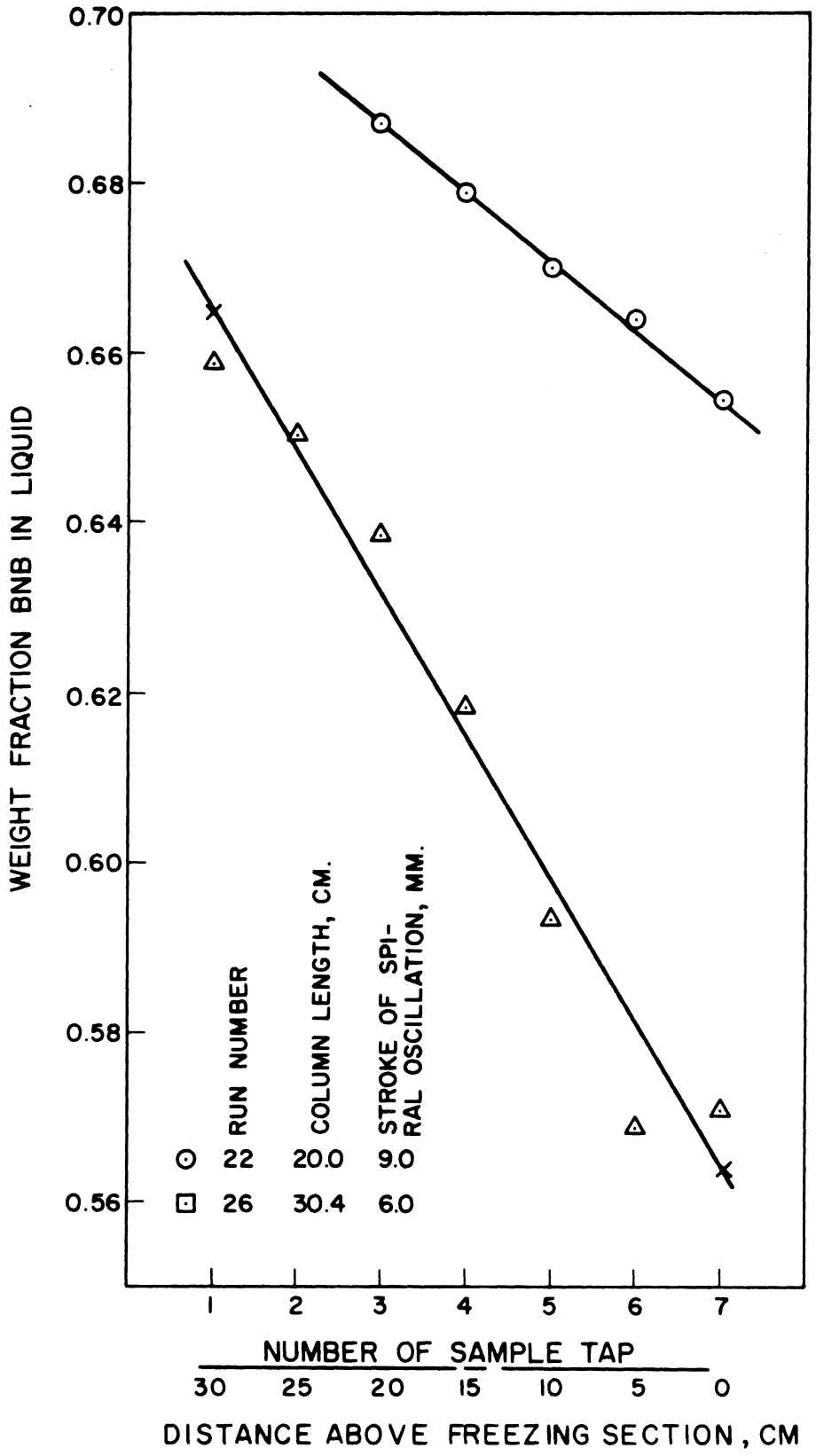

Figure 7. Effect of Stroke of Spiral Oscillation on Column Performance.

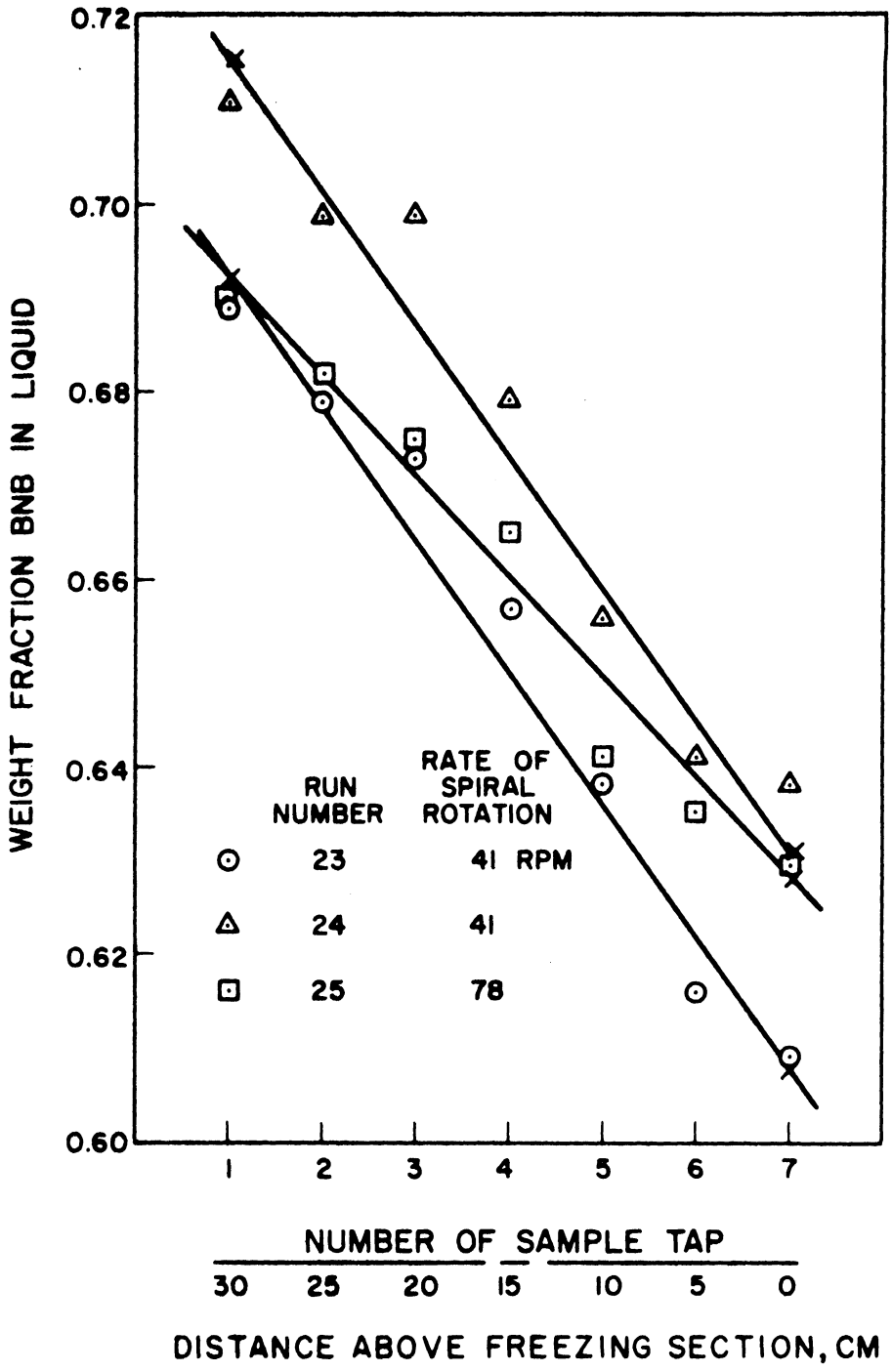

Figure 8. Effect of Rate of Spiral Rotation on Column Performance.

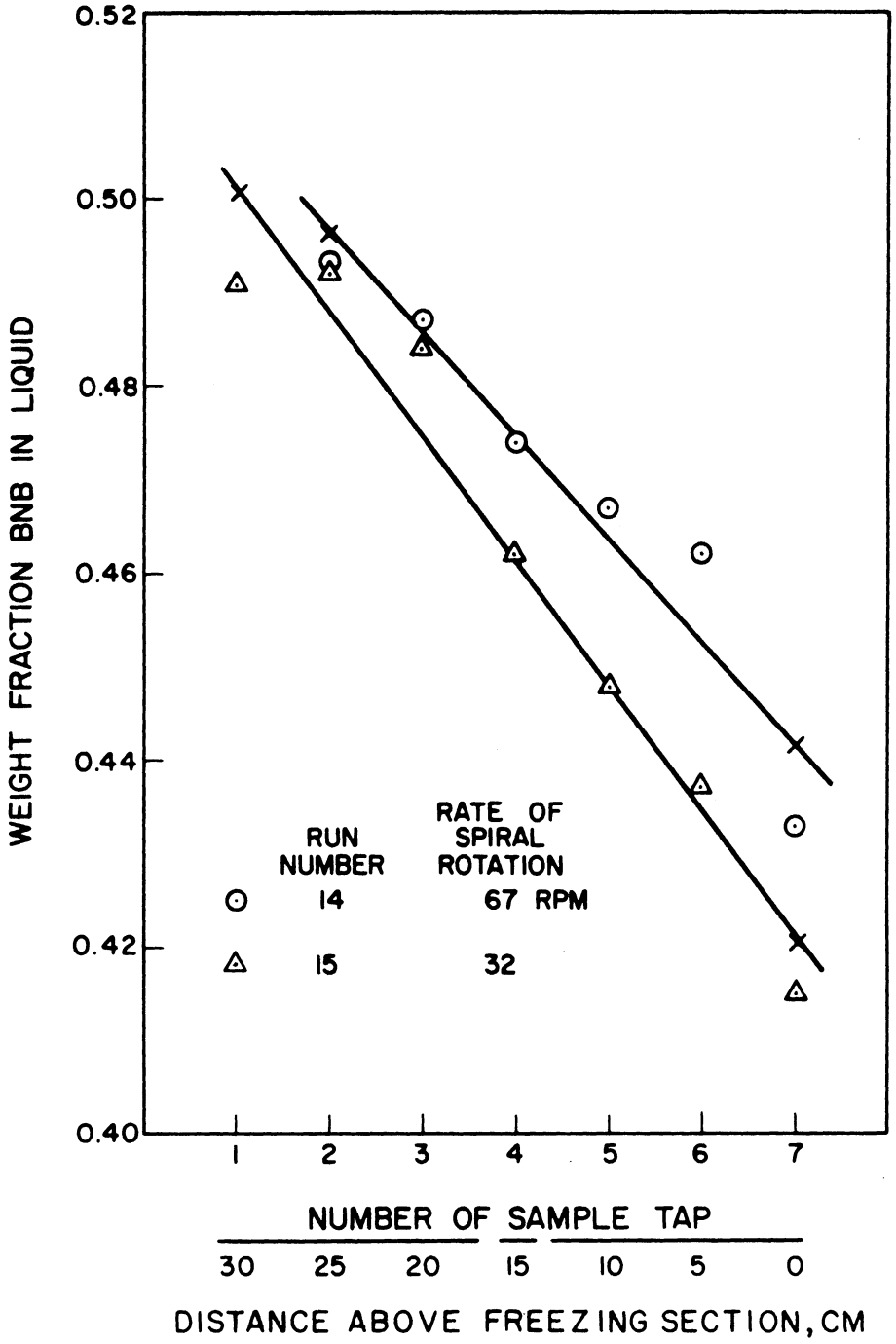

Figure 9. Effect of Rate of Spiral Rotation on Column Performance.

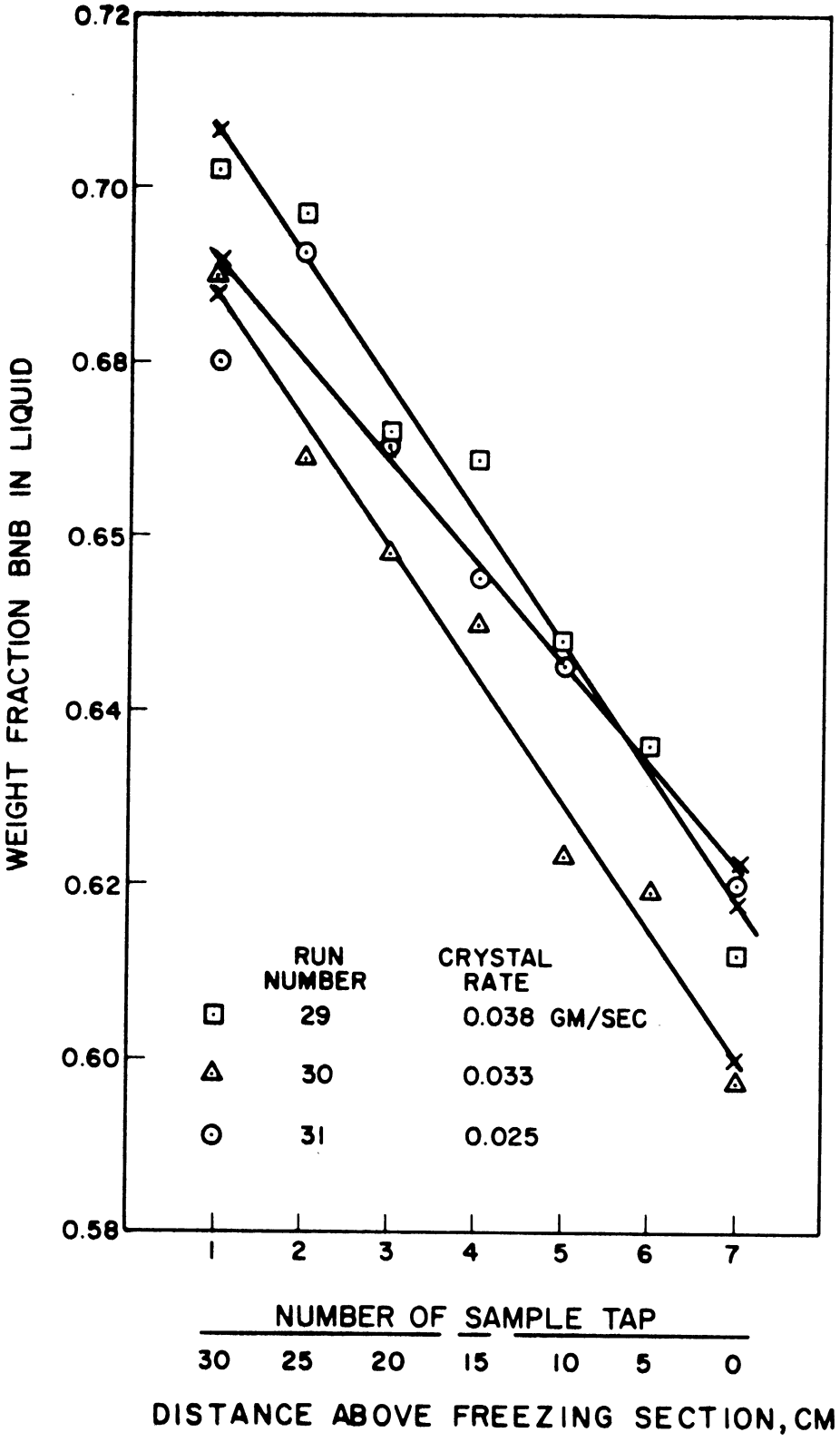

Figure 10. Effect of Crystal Rate on Column Performance.

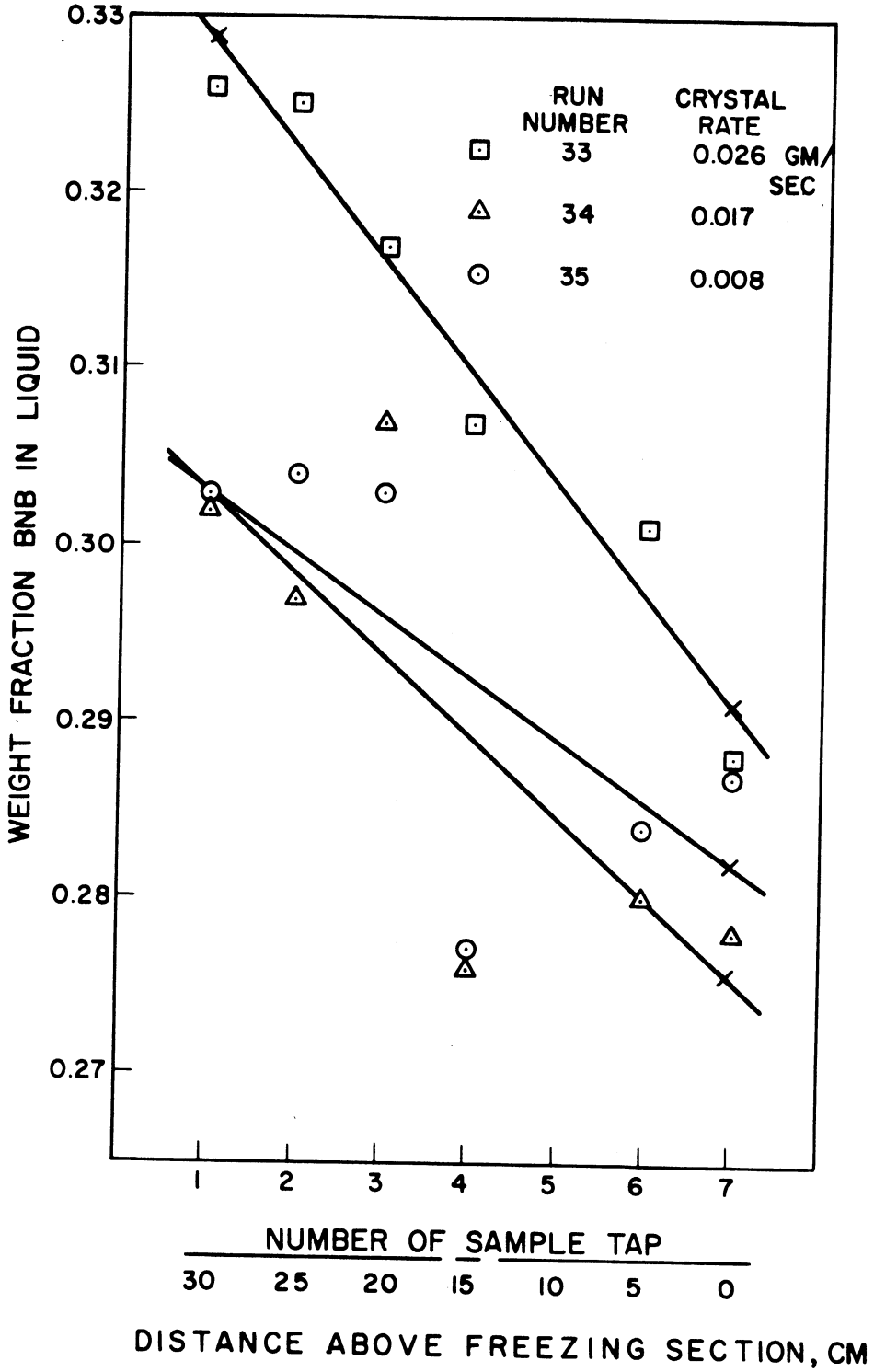

Figure 11. Effect of Crystal Rate on Column Performance.

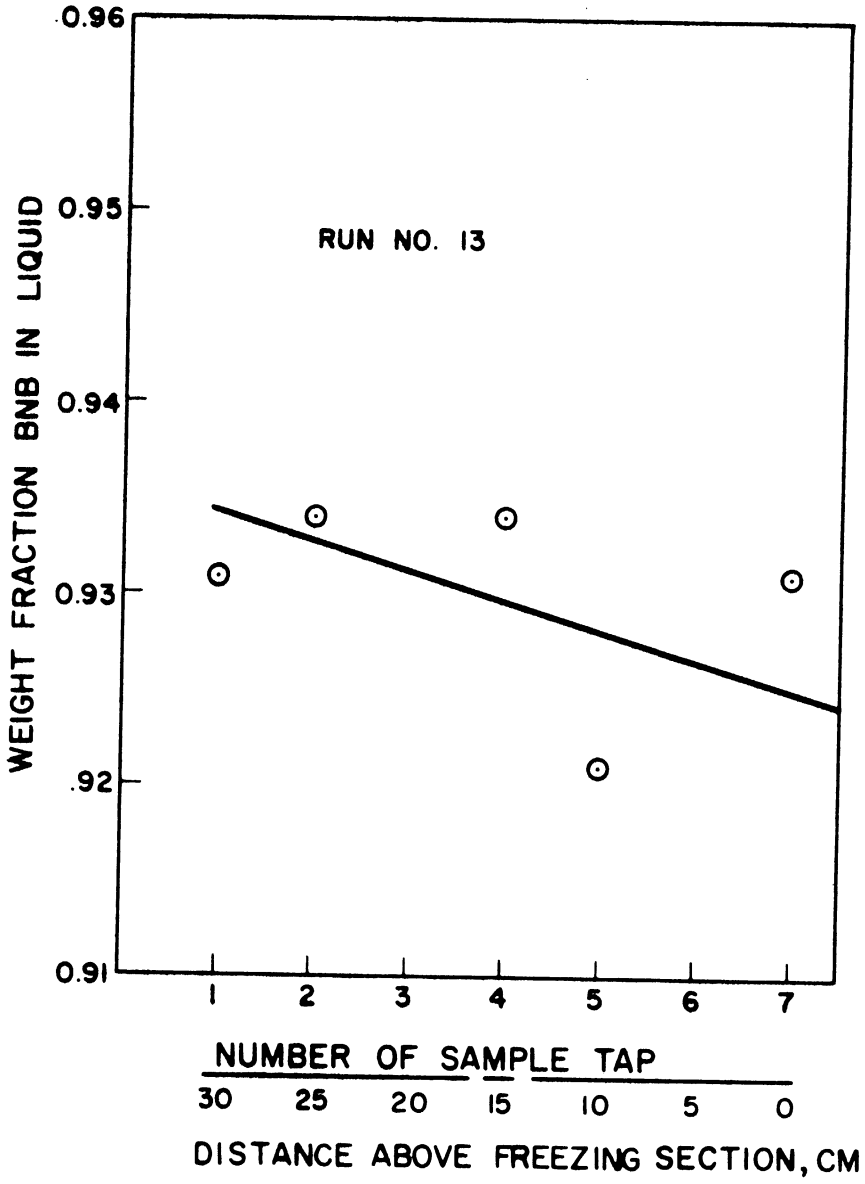

Figure 12. Composition Profile in Column.

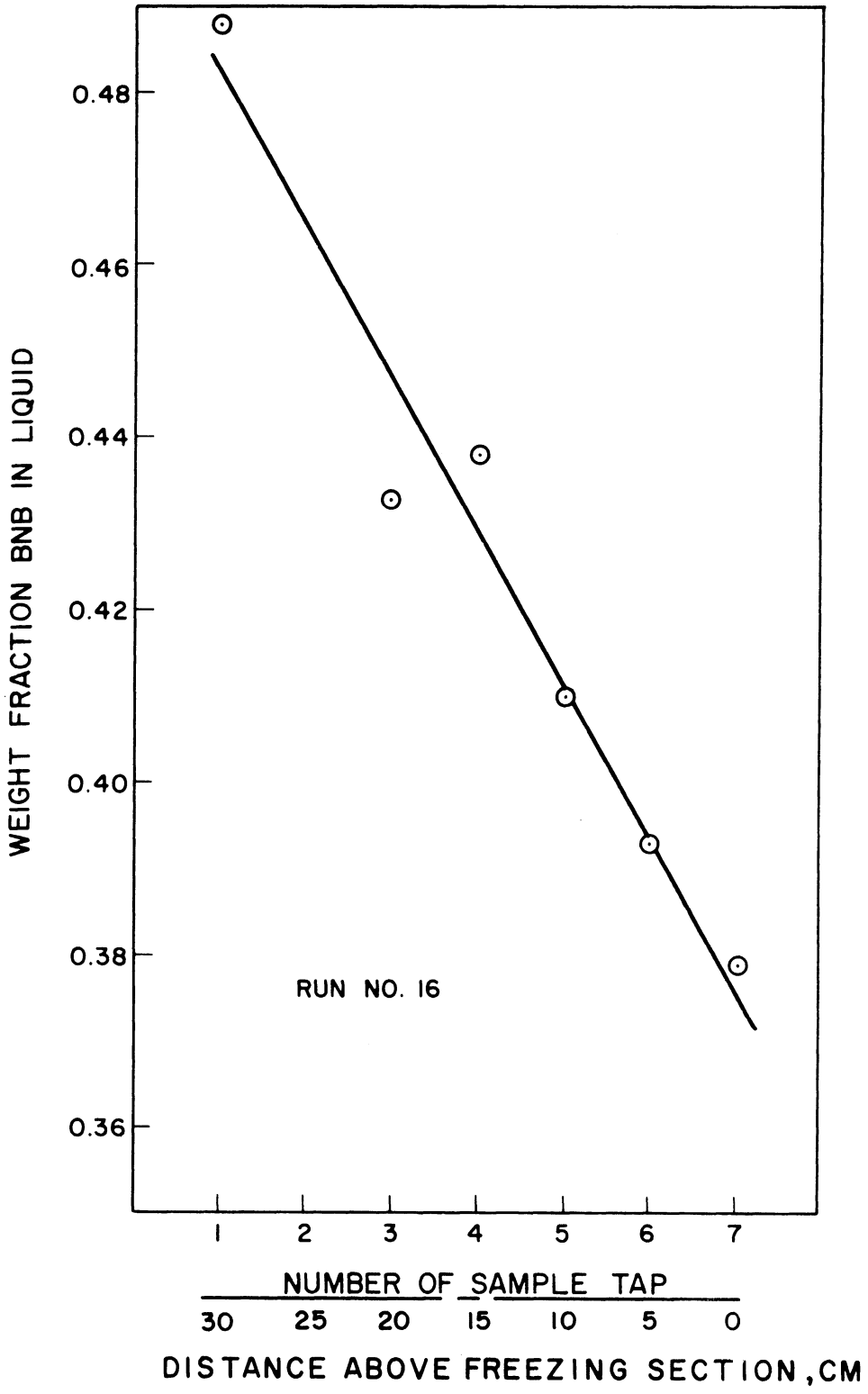

Figure 13. Composition Profile in Column.

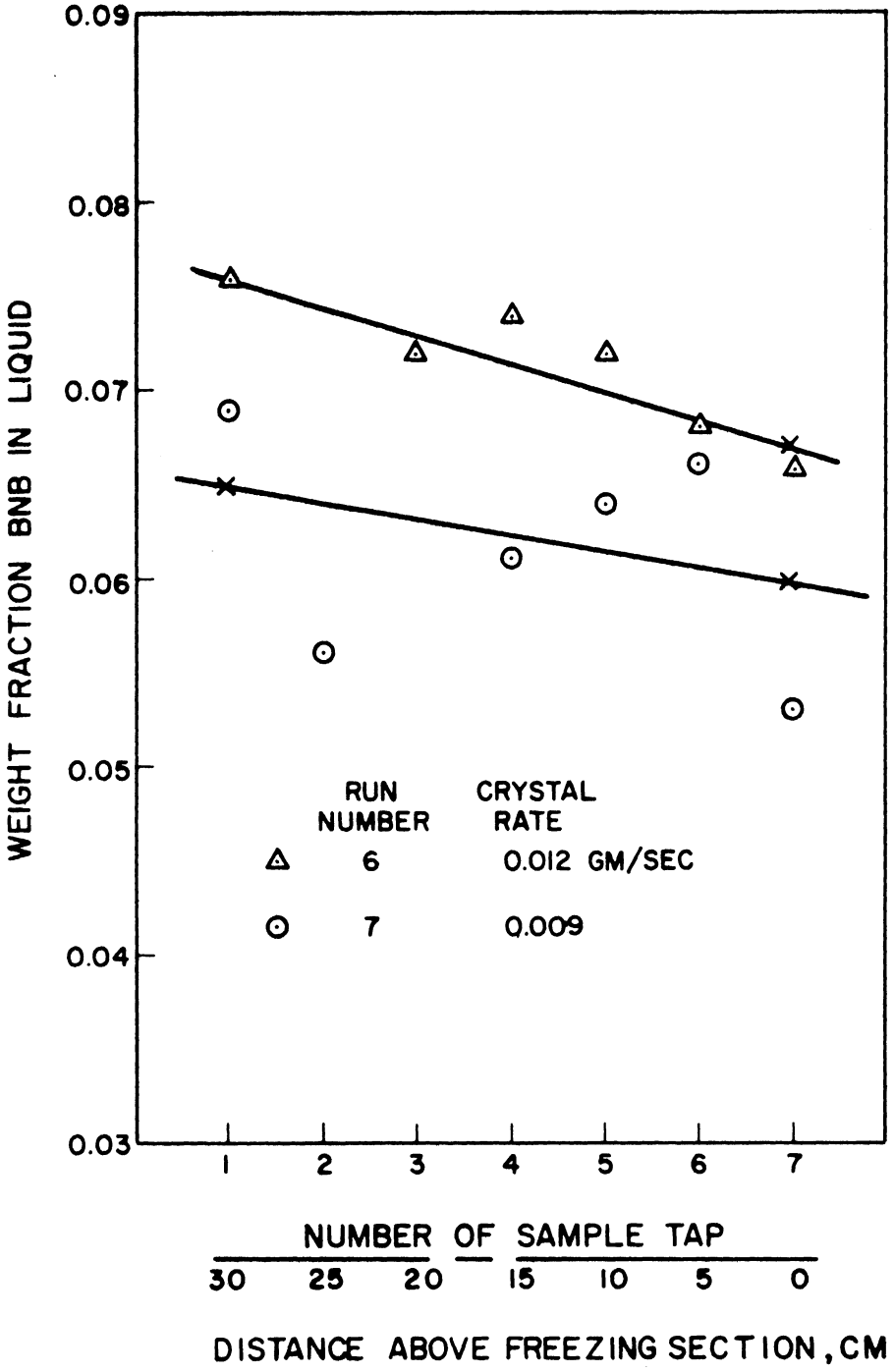

Figure 14. Effect of Crystal Rate on Column Performance.

TABLE I

SUMMARY OF CONDITIONS USED IN REPORTED RUNS

Run	Nominal Charge Composition	Crystal Rate	Agitation			Column Length
			Rate of Oscillation	Stroke of Oscillation	Rate of Rotation	
	Weight Fraction BNB	g/sec	OPM	mm	RPM	cm
17	0.50	0.018	31	6.0	29	30.3
18	0.50	0.018	31	6.0	29	25.1
21	0.65	0.034	43	6.0	45	20.0
24	0.65	0.035	45	6.0	41	30.3
22	0.65	0.031	43	9.0	45	20.0
26	0.65	0.032	43	6.0	48	30.3
23	0.65	0.033	45	6.0	41	30.3
24	0.65	0.035	45	6.0	41	30.3
25	0.65	0.033	43	6.0	78	30.3
14	0.50	0.036	25	4.5	67	30.3
15	0.50	0.036	25	4.5	32	30.3
29	0.65	0.038	67	4.2	60	30.3
30	0.65	0.033	67	4.2	60	30.3
31	0.65	0.025	67	4.2	60	30.3
33	0.35	0.026	130	2.0	60	30.3
34	0.35	0.017	130	2.0	60	30.3
35	0.35	0.008	130	2.0	60	30.3
13	0.95	0.040	22	4.5	67	30.3
16	0.50	0.027	40	6.0	46	30.3
6	0.05	0.012	72	4.5	67	30.3
7	0.05	0.009	72	4.5	67	30.3

CHAPTER IV

MATHEMATICAL DESCRIPTION OF COLUMN CRYSTALLIZATION

Four mathematical models of column crystallization, each based on different assumptions as to what occurs physically, are developed in this section. These models are similar in that dispersion in the liquid phase is assumed. They are different in that several modes of mass-transfer between phases are considered.

Examination of the bromonitrobenzene - chloronitrobenzene phase diagram in Figure 3 indicates that BNB will concentrate in the melting section. Thus as a crystal moves toward this section, it moves into a region of increasingly high temperature. The crystal thereby becomes unstable. This instability must be relieved by a change in the composition of the crystal. The change can occur in one of several ways, each leading to a different mathematical model. Three such models are described.

One possible mechanism for change is melting and recrystallization. The unstable crystal melts by absorbing energy. This energy is supplied by the formation of new crystals. These new crystals, relative to the ones formed in the freezing section, are enriched in BNB because they are formed from a liquid itself enriched in BNB.

Melting and recrystallization involve the simultaneous interchange of both mass and energy. One would expect that these mechanisms would be governed by a mass-transfer coefficient and by a heat-transfer coefficient. In the general mathematical description both coefficients would be considered. Such a model would probably be very complex. Consequently, two simplified cases are described here. If neither of the

simple models is sufficient to describe the experimental data, then the general case should be developed and investigated.

In the first simplified model, it is assumed that the heat transfer coefficient is large and that the rate of mass-transfer is limited by a mass-transfer coefficient. The model describing this case is Model I or the mass-transfer-limiting model. This model is consistent with experimental results.

The second case of melting and recrystallization which is considered assumes that the mass-transfer coefficient is large and that the interphase transfer is restricted by a heat-transfer coefficient. This model is referred to as Model II, or as the heat-transfer-limiting model. This model is not consistent with experimental results.

Another possible mechanism for the relief of composition instability is diffusion within the solid itself. Rather than becoming enriched by recrystallization, the solid is enriched by diffusion of BNB from the liquid into the solid. This possibility and its mathematical description are discussed in Model III. This model is not consistent with experimental results.

Another case which was evaluated, Model IV, assumes a constant crystal composition. This model can not be justified on physical grounds. However, since this model is said to describe eutectic systems,[1] it might also describe data for a solid solution. As was expected, this model disagreed with experimental results.

Each of the four models just described is developed in this section. Following each development is a description of the predictions of the model. The four models are then evaluated in Chapter V by comparing experimental results with these several predictions.

A. Mass-Transfer-Limiting - Model I

The mathematical description of column crystallization based on this model follows the developments of Hartland and Mecklenburgh[18] and Powers.[32]

1. Description

The physical description is as follows. Solid of weight fraction X moves through the column at rate L without backmixing. This solid, which is radially homogeneous, contacts liquid of weight fraction Y moving at rate V . There is dispersion in the liquid axially but not radially. Mass-transfer occurs between the two phases which pass countercurrently. The elemental description of the process is illustrated in Figure 15.

The flows of liquid and solid respectively contribute VY and LX to the movement of BNB. The rate of dispersion of BNB within the liquid is assumed to follow Fick's Law, Equation (1).

$$N_B = -DA\eta\rho\, dY/dh \qquad (1)$$

Here N_B is the rate of dispersion of BNB in gm/sec, ρ is the density of the liquid in gm/cm^3, η is the volume fraction liquid, A is the area in cm^2 through which the liquid and solid flow, and D is the effective diffusivity in cm^2/sec containing contributions from molecular and Taylor diffusion and from backmixing. The last four factors, ρ , η , A and D , are assumed to be independent of position , h .

According to the model, the rate, J , of BNB mass-transfer from the solid to the liquid phase follows Equation (2).

$$J = K_a A \rho \Delta h (Y - Y^*) \qquad (2)$$

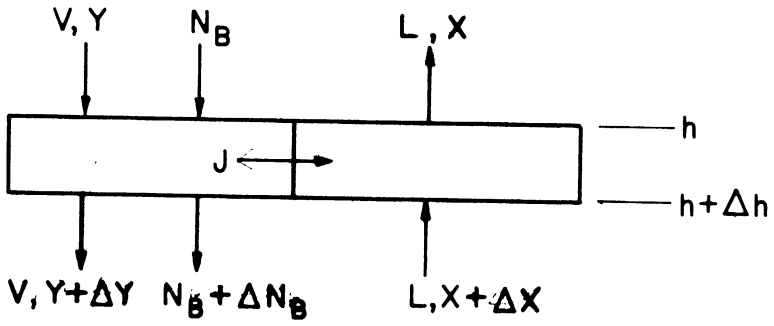

$$N_B = -D\eta A\rho \quad dY/dh$$

$$J = KaA\rho \quad \Delta h(Y-Y^*)$$

Figure 15. Elemental Description of Column Crystallization--Mass-Transfer-Limiting Model.

J is considered to be proportional to the difference between the existing liquid phase composition, Y , and the equilibrium composition, Y* . This latter composition is that ficticious value which is in equilibrium with the solid contacting the liquid Y . In Equation (2), h is the column position measured from the melting section in cm , a is the interfacial area between the two phases per unit volume, cm^2/cm^3 , and K is the mass-transfer coefficient, cm/sec . K and a are assumed to be constant.

Based on the rate equations listed above and considering BNB, a mass balance on an element of the liquid phase yields Equation (3).

$$DA\eta\rho\frac{d^2Y}{dh^2} - V\frac{dY}{dh} - KaAp(Y-Y^*) = 0 \qquad (3)$$

The first term in this equation describes the dispersion within the liquid phase. The next two terms relate to the bulk flow of BNB, and to the mass-transfer between phases. V is assumed to be independent of h.

A BNB balance on the upper part of the column, considering operation at total reflux, yields Equation (4).

$$DA\eta\rho\, dY/dh - VY + LX = 0 \qquad (4)$$

The first term relates to dispersion, and the last two terms to bulk flow of the liquid and of the solid, respectively.

A total balance on the upper part of the column yields Equation (5).

$$-V + L = 0 \qquad (5)$$

The solution to Equations (3) to (5) requires another relationship between the dependent variables. The liquid-solid phase equilibrium furnishes the necessary relation. In general, the phase equilibrium will be such that an analog or numerical solution to the system of equations (Equations (3) to (5) and the equilibrium relation) will be required. However, BNB-CNB has a phase relation, as shown in Figure 4, which is linear over a wide range of compositions. Thus Equation (6) may be used as the required phase relation.

$$X = mY^* + b \tag{6}$$

Values of m and b can be determined from Figure 4 for the range of composition which applies in a given separation.

The elimination of Y^*, X, and V from Equations (3) to (6) produces Equation (7).

$$d^2Y/dh^2 - (L/DA\eta\rho + Ka\,Ap/Lm)\,dY/dh + (1/m - 1)\,Ka\,Y/D\eta = bKa/mD\eta \tag{7}$$

This equation has as variables Y, L, and h which are all relatively easy to determine experimentally. Thus, the model can be tested for agreement with data. The definitions 8a to 8c are introduced into Equation (7) in order to simplify further manipulations. Equation (9), which is the differential equation describing the mass-transfer-limiting model of column crystallization, is the result.

$$R_1 = L/DA\eta\rho + Ka\,Ap/Lm \tag{8a}$$

$$R_2 = Ka/D\eta \tag{8b}$$

$$R_3 = 1/m - 1 \tag{8c}$$

$$R_4 = 1 - m \tag{8d}$$

$$\frac{d^2 Y}{dh^2} - R_1 \frac{dY}{dh} + R_2 R_3 Y = \frac{R_2 b}{m} \qquad (9)$$

2. Limitations

It is useful to restate the limitations inherent to Equation (9) before considering its solution. Equation (9) is strictly a material balance. Energy effects are involved, but only implicitly. That is, it is assumed that V and L are constant, independent of position. This assumes that heat capacities, heats of fusion and mixing, and heat leaks to ambient have a certain inter-relation. This relation is not set forth, but the constancy of V and L is considered in Appendix A2-b.

Other factors are considered to be constant. These factors include all those which make up R_1 , R_2 , and R_3 . This assumption was not tested experimentally. However, the variations in R_1 , R_2 , and R_3 probably are second order effects and can be neglected for the purposes of this study. The success of the model incorporating these assumptions is the only justification of the assumptions.

The given form of the differential equation explicitly assumes a phase relation which can be approximated by a linear equation. In a chemical system in which the liquidus and solidus lines are very far apart, such an assumption could only be applied to a very small range of compositions. Thus one would expect that Equation(9) would have to be applied piecewise along a column separating such a system. The constants m and b would vary markedly along the length of a column. If a piece-wise application were undesirable, then a numerical or analog solution to Equations (3) to (5), using an equation more closely describing the equilibrium relation than does a linear one, would be required.

3. Solution to Differential Equation

The solution to Equation (9) has the form given in Equation (10).

$$y = C_1 + C_2 \exp(q_2 h) + C_3 \exp(q_3 h) \tag{10}$$

The last two terms of this equation are the general solution to the homogenous part of Equation (9). The constant C_1 is the particular solution to the non-homogeneous part and is given by Equation (11).

$$C_1 = b/(1-m) \tag{11}$$

The constants q_2 and q_3 must satisfy the characteristic Equation (12).

$$q^2 - R_1 q + R_2 R_3 = 0 \tag{12}$$

This is a quadratic equation whose roots are given by Equation (13).

$$q = R_1 \left[1 \pm (1 - 4 R_2 R_3 / R_1^2)^{1/2} \right] / 2 \tag{13}$$

In many cases, the collection of terms $R_2 R_3 / R_1^2$ will be less than 0.1 in which case the square root term in Equation (13) can be closely approximated as in Equation (14).

$$(1 - 4 R_2 R_3 / R_1^2)^{1/2} = 1 - 2 R_2 R_3 / R_1^2 \tag{14}$$

The roots of Equation (12) thereby become Equations (15).

$$q_2 = R_1 \left[1 - R_2 R_3 / R_1^2 \right] \tag{15a}$$

$$q_3 = R_2 R_3 / R_1 \tag{15b}$$

The root q_2 can be further simplified, subject to the above limitation on R_2R_3/R_1^2, to yield Equation (16).

$$q_2 = R_1 \tag{16}$$

Thus the solution to the differential Equation (9) becomes Equation (17).

$$Y = b/(1-m) + C_2 \exp(hR_1) + C_3 \exp(hR_4/H) \tag{17}$$

In this equation, R_1 and R_4 are given by Equations (8a) and (8d), and H by Equation (18). Equation (18) defines E and F which will

$$R_1 = L/DA\eta\rho + K_a A\rho/Lm \tag{8a}$$

$$R_4 = 1-m \tag{8d}$$

$$H = R_1/R_2 = DA\eta\rho/L + Lm/K_a A\rho = E/L + L/F \tag{18}$$

be discussed later. The term H/R_4 is a measure of the effectiveness that a given set of operating conditions has in achieving a separation between components in a column crystallizer. This term has the units of cm and therefore indicates the length of column required to produce a certain separation. Throughout chemical engineering literature a term of this type is called the height of a transfer unit, HTU.

4. Boundary Conditions

The constants C_2 and C_3 in Equation (17) can be evaluated using appropriate boundary conditions. The first boundary condition is that the solution must be applicable at all conditions of operation. Specifically, the value of Y must be between zero and one for all values of L. The second boundary condition is that the composition of

the liquid at $h = 0$ is known or can be determined experimentally. That is, $Y = Y_o$ at $h = 0$.

Examination of Equation (8a) indicates that R_1 becomes very large as L increases or approaches zero. Because R_1 appears in the argument of the exponential, the term $C_2 \exp R_1 h$ would become exceedingly large under either of these conditions unless C_2 were small. In fact C_2 must be zero if this term is to remain finite as L approaches zero. A specific case may clarify this argument.

As it will be demonstrated later, the terms in Equation (8a) have values near those given below.

$$R_1 \approx L/0.2 + 0.04/L \qquad (8a)$$

The crystallizer can be operated, with some difficulty, with a crystal rate as low as 0.005 gm/sec . At this condition R_1 is about 8 cm^{-1} The second term in Equation (17) thereby becomes $C_2 \exp 8h$. For large $h(h = 30)$ the exponential part of this term becomes very large. As neither of the other two terms in Equation (17) can counteract the influence of this large term, C_2 must be very small, on the order of $\exp(-250)$. C_2 can reasonably be assumed to be zero. Thus Equation (17) reduces to Equation (19).

$$Y = b/R_4 + C_3 \exp(h R_4/H) \qquad (19)$$

The reduction of Equation (17) from two exponential terms to one can be based on an argument other than that just discussed. The factors R_1 and R_4/H from Equation (17) can be estimated by using typical or extreme values for D and K taken from the literature, and by using values for a , A , η and ρ approximated or determined from experimental

data. The result of such estimation is that R_1 is always much larger that R_4/H, and for most cases, R_1 is about equal to the reciprocal of R_4/H.

Further, because of the particular dependence of R_1 and R_4/H on the crystal rate, R_4/H is bounded regardless of the values estimated for D and K or the value of L. R_1 on the other hand becomes very large for some ranges of L regardless of the values of D and K.

These two characteristics of R_1, its large value in relation to R_4/H, and its unboundedness with regard to L, make it reasonable to require that C_2 be zero. Application of the second boundary condition to Equation (19) indicates that C_3 is given by $Y_o - b/R_4$.

The exponential in Equation (19) can be approximated by the linear form given in Equation (20) because, as it will be shown later, H/R_4 is large.

$$\exp(h R_4/H) = 1 + h R_4/H \tag{20}$$

Thus the solution to the differential equation becomes Equation (21).

$$\begin{aligned} Y &= Y_o + (Y_o - b/R_4)\, h R_4/H \\ &= Y_o + (R_4 Y_o - b)\, h/H \end{aligned} \tag{21}$$

By the earlier assumption regarding phase equilibrium, $mY_o + b$ is equal to X_o^*. Applying this to Equation (21) yields Equation (22), the final form for the solution.

$$\begin{aligned} Y &= Y_o + (Y_o - X_o^*)\, h/H \\ &= Y_o - (X^* - Y)_o\, h/H \end{aligned} \tag{22}$$

5. Limitations

The limitations discussed earlier were on the differential equation describing the mass-transfer-limiting model. Additional assumptions are applied to the general solution to the differential equation in order to produce Equation (22). These assumptions and their justification are reiterated below. If Equation (22) is to be applied to another chemical system then the validity of these approximations should be checked in view of the new experiments.

The first two terms of the binomial expansion for the exponential in Equation (19) were used as an approximation of the whole expansion. Experimental evaluation of the variables making up this exponential indicates that the approximation is excellent. Similarly, the approximation of q_2 by R_1 (Equation (16)) is very good.

Results of experiments used to evaluate terms in the general solution justify two other approximations. The determination that R_1 is greater than 5 for some conditions of operation and greater than 1 for almost all conditions of operation, shows that C_2 must be zero. The approximations used in obtaining Equation (21) from Equation (19) is justified by the large experimental values determined for H/R_4 . H was always greater than 10 cm , and R_4 did not exceed 0.1. H/R_4 was therefore always greater than 100 cm , and hR_1/H was less than 0.3.

6. Predictions

Equation (22) predicts that the composition of the liquid in the column will vary linearly with position. The magnitude of this variation, the concentration gradient, should increase as the phase separation, $(X^* - Y)_o$, increases. Thus, as the concentration of material charged to

the column approaches 0 or 100 per cent, the concentration gradient should approach zero.

The model also predicts that the composition profile will be dependent on the crystal rate, and that this dependence will be determined by the magnitude of the operating parameters, especially D and K (see Equation (18)).

Another prediction of this model is that, if D and K are constant, the product HL will be a linear function of L^2. This can be seen by multiplying the terms in Equation (18) by L.

The final prediction of the mass-transfer-limiting model is that H, which is evaluated from the concentration gradient, is a function of composition. The inclusion of m, the slope of the phase relation, Equation 4, in the second term in H is the basis of this prediction.

The first three of these predictions were substantiated by the experimental results. The fourth prediction could not be tested directly, but an indirect test seems to substantiate it, also.

B. Heat-Transfer-Limiting - Model II

The heat-transfer-limiting model is similar to the mass-transfer-limiting model in its development although it is mathematically more complex. Unless specifically noted to the contrary, the symbols used in Model II have the same significance as in Model I.

1. Description

The physical description for Model II is illustrated in Figure 16. Solid of weight fraction X at t°C moves through the column crystallizer at L gm/sec. Countercurrently, a liquid of weight fraction Y at T°C flows at V gm/sec. Material moves axially within

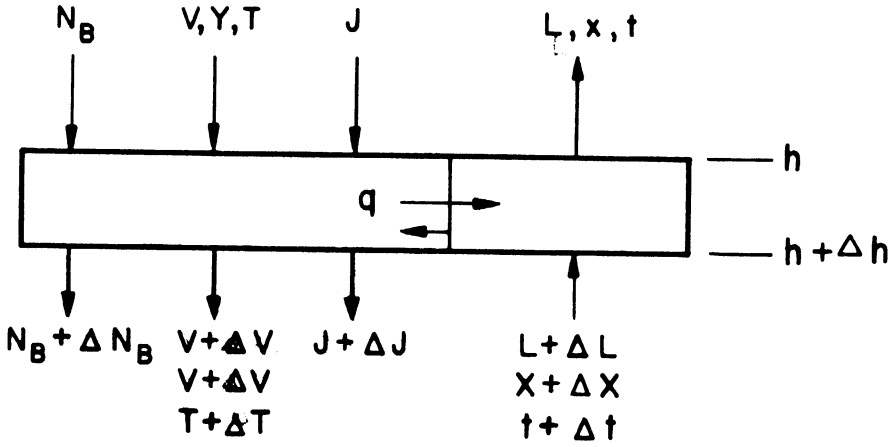

$$N_B = -DA\eta\rho \; dY/dh$$

$$J = -\epsilon A\eta \; dT/dh$$

$$q = u_a A \; (T-t)$$

Figure 16. Elemental Description of Column Crystallation--Heat-Transfer-Limiting Model.

the liquid phase by dispersion at N_B g/sec. There is no dispersion of material within the solid or radially in the liquid.

The energy associated with the dispersion of materials in the liquid phase is assumed to be negligible. This assumption is probably justified because the dispersion of CNB will be about equal to that of BNB. Thus the associated energies will be about equal. There is heat conduction, J cal/sec , in the liquid but there is none in the solid because it is a disperse phase held in no fixed orientation. This conduction, given by Equation (23), is proportional to the cross-sectional area of the liquid phase $A\eta$ cm^2 , to the temperature gradient in the liquid, dT/dh C°/cm , and to the eddy-thermal diffusivity, ϵ cal/cm-C° -sec, which contains effects of simple conduction and eddy convection.

$$J = -\epsilon A \eta \, dT/dh \tag{23}$$

Heat-transfer, q cal/sec , between phases is proportional to the heat-transfer coefficient, U cal/cm^2-sec-C° , to the interfacial area, $a A \Delta h$ cm^2 , and to the temperature difference, T-t . q is given by Equation (24).

$$q = U a A \Delta h (T - t) \tag{24}$$

The energy associated with mass-transfer is equal to the product of the change in V times the specific enthalpy of the solid which is produced.

The third rate equation used in the heat-transfer-limiting model, Equation (25), is the same as Equation (1) used in Model I.

$$N_B = -D A \eta \rho \, dY/dh \tag{25}$$

This equation gives the rate of axial dispersion in the liquid phase.

The three rate equations presented above permit energy balances to be written on an element of the liquid phase, Equation (26), and on the top end of the column, Equation (27).

$$\frac{d}{dh}\left[VY(H_B + TC_{v,B})\right] + \frac{d}{dh}\left[V(1-Y)(H_C + TC_{v,C})\right] - \epsilon A\eta \frac{d^2T}{dh^2} = Ua\Delta(T-t) - \frac{dV}{dh}\left[xC_{L,B} + (1-x)C_{L,C}\right]t \qquad (26)$$

$$VY(H_B + TC_{v,B}) + V(1-Y)(H_C + TC_{v,C}) - \epsilon A\eta \frac{dT}{dh} = L\left[xC_{L,B} + (1-x)C_{L,C}\right]t \qquad (27)$$

The first two terms in these equations represent the energy associated with the bulk flow of liquid, V . The third terms relate to heat conduction in the liquid. The last term in Equation (26) is the energy lost by the liquid resulting from a change in V. The last term of Equation (27) represents the energy associated with the bulk flow of solid, L .

In these equations, the subscripted C's are specific heats in cal/gm-C° . The first subscript, L or V , identifies the phase as solid or liquid, and the second subscript, B or C , identifies the material as BNB or CNB. It is assumed that specific heats are constant with respect to temperature and composition.

The derivation of Equation (26) and (27) is based on the assumption that the enthalpies of solid BNB and CNB are zero at an arbitrary temperature T_o°C and that at this same temperature the liquid enthalpies are H_B and H_C , respectively. It is further assumed that there is no

heat of mixing within either phase. These assumptions are justified by the small separations achieved using BNB-CNB.

Material balances on one end of the column yield Equations (28) and (29), just as in Model I.

$$D A \eta \rho \, dY/dh - VY + LX = 0 \qquad (28)$$

$$-V + L = 0 \qquad (29)$$

Equation (28) is a BNB balance, and (29) is a total balance.

The heat-transfer-limiting model is completed by using two further equations which relate the dependent variables. These equations are the phase equilibrium Equations (30) and (31).

$$T = 44.6 - 4.056 \ln(1-Y) - T_o \qquad (30)$$

$$t = 44.6 - 3.207 \ln(1-x) + 0.3829 \left[\ln(1-x)\right]^2 - T_o \qquad (31)$$

These equations are incorporated into the model based on the assumptions that the liquid is at its freezing point and that the solid is at its melting point. The first assumption is justified by the conditions of agitation maintained in the crystallizer. Such conditions, as well as the presence of small crystals, make the possibility of supercooling very small.

The numerical constants used in Equations (30) and (31) apply for X and Y between 0 and 0.7 and were determined by fitting phase equilibrium data by regression lines (see Appendix A5-b).

V is eliminated from the equations above to reduce the equations and dependent variables by 1. This produces a solution in terms of the crystal rate, L , which is easily measured at one point in the column.

T_o , which is arbitrary, is set equal to 44.6°. This eliminates two terms from each of Equations (30) and (31). This elimination simplifies the solution considerably.

The solution of the heat-transfer-limiting model can be further simplified by converting the derivatives of T to derivatives of Y. This is accomplished by noting that $dT/dh = (dT/dY)(dY/dh)$ and that dT/dY is equal to $4.056/(1-Y)$ as determined from Equation (30).

Another simplification is possible based on experimental results. It was shown in Figures 5 to 14 that plots of Y vs. h were linear. Thus d^2Y/dh^2 is zero. If this is incorporated into the second derivatives of T , then d^2T/dh^2 is given by $4.056\ dY/dh)/(1-Y)^2$.

Based on the simplifications listed above, Equations(26) to (31) reduce to Equations (32) to (36).

$$(H_B - H_c)\frac{d}{dh}(LY) + (C_{v,B} - C_{v,c})\frac{d}{dh}(LYT) - C_{v,c}\frac{d}{dh}(LT) - \frac{4.056\,\epsilon A\eta}{(1-Y)^2}\frac{dY}{dh} = Ua\,A(T-t) - \frac{dL}{dh}\left\{\left[C_{L,c} + X(C_{L,B} - C_{L,c})\right]t - H_c\right\} \quad (32)$$

$$LH_c + (H_B - H_c)LY + LTC_{v,c} + LYT(C_{v,B} - C_{v,c}) - \frac{4.056\,\epsilon A\eta}{1-Y}\frac{dY}{dh} = Lt\left[C_{L,c} + X(C_{L,B} - C_{L,c})\right] \quad (33)$$

$$DA\eta\rho\frac{dY}{dh} - LY + LX = 0 \quad (34)$$

$$T = -4.056\ \ln(1-Y) \quad (35)$$

$$t = -3.207 \ln(1-x) + 0.3829[\ln(1-x)]^2 \qquad (36)$$

The increase in the number of terms appearing between Equations (26) and (27), and Equations (32) and (33) is the result of collecting like terms subject to the previous assumption that heats of fusion and specific heats are constant.

2. Solution

Equations (32) to (36) cannot be solved analytically. However, they can be solved numerically when put in proper form, Equations (37) to (42).

Equations (37) to (42) derive from Equations (32) to (36) if all the derivatives of products are expanded, all like terms are collected, and simple rearrangements of terms made. There are no approximations made in these transformations other than those already made. Consequently, the simple algebra is omitted and only the result shown.

$$T = -4.056 \ln(1-Y) \qquad (37)$$

$$X = \left\{ Y + \frac{D\rho(1-Y)}{\epsilon B} \left[C_{L,c} t + (H_c - H_B) Y + (C_{v,c} - C_{v,B}) YT - C_{v,c} T \right] \right\} / \left\{ 1 - \frac{D\rho(1-Y)}{\epsilon B} (C_{L,B} - C_{L,c}) t \right\} \qquad (38)$$

$$t = -3.207 \ln(1-x) + 0.3829[\ln(1-x)]^2 \qquad (39)$$

$$\frac{dY}{dh} = V(Y-X)/DA\eta\rho \qquad (40)$$

$$\frac{dV}{dh} = \left[\mu_a A (T-t) - (QV+R) \frac{dY}{dh} \right] S \qquad (41)$$

$$Q = (C_{v,c} - C_{v,B})T - BC_{v,c} - BC_{v,B}\frac{Y}{1-Y} + H_c - H_B \qquad (42a)$$

$$R = \frac{\epsilon A \eta}{(1-Y)^2}\frac{dY}{dh} \qquad (42b)$$

$$S = (C_{v,c} - C_{v,B})YT - C_{v,c}T + (H_c - H_B)Y - H_c - C_{L,c}t - (C_{L,B} - C_{L,c})Xt \qquad (42c)$$

The method of solution is as follows. A set of values for U, ϵ, and D is chosen. These parameters are respectively the heat-transfer coefficient, the effective eddy thermal-diffusivity of the liquid, and the effective mass-diffusivity of the liquid. As mentioned earlier, these two diffusivities contain contributions from the mixing action of the spiral within the column as well as from processes on a molecular scale.

A set of conditions for Y and V at $h = 0$ is selected. These values correspond to conditions encountered during the experiments. T is calculated from Equation (37). X and t are determined by an iteration on Equations (38) and (39). The two derivatives, dY/dh and dV/dh, are evaluated from Equations (40) and (41). A fourth order Runga - Kutta integration is performed to determine new values for Y and V. The procedure is repeated until a length equal to the length of the column has been traversed. A table of Y vs. h is prepared and compared with experimental results.

3. Predictions

By proper selection of values for U, ϵ, and D, profiles of Y vs. h which are linear with small separations are predicted. The effect of increasing the crystal rate, L, at $h = 0$ is to increase the separation.

C. Diffusion Within the Solid Phase - Model III

The two previously developed models each considered the liquid and solid phases to be radially homogeneous at all positions within the column. Only axial variations were assumed. The model developed in this section, which assumes diffusion within the solid phase, necessarily removes the limitation of radial homogeneity in the solid. This introduces considerable complexity to the model and to its mathematical description. Such complexity is reduced by considering the crystals in the purification section to have a simple geometry.

The general solution to a model which includes diffusion in the solid, dispersion in the liquid, and simultaneous heat- and mass-transfer between phases would indeed be complex. Such a solution was not attempted. Rather, one limiting case of such a solution, one which considers a single mechanism to be controlling, is developed. That mechanism is diffusion within the crystal. It is therefore assumed that heat-transfer and mass-transfer occur sufficiently rapidly to permit the diffusion but not so rapidly so as to destroy the crystals.

1. Description

The description of the model which embodies the conditions stated above is as follows. Spheres of radius R_o are formed in the freezing section and move toward the melting section. Initially these spheres are of uniform weight fraction X_o, and they are in equilibrium with the liquid in the freezing section. The surface of the spheres remains in equilibrium with the liquid throughout the column.

In order to describe the concentration profile in the crystals, it is assumed that the surface concentration varies linearly with the

position in the column. This assumption is predicated on two previous assumptions and on one piece of experimental evidence. The previous assumptions are that:

(1) the concentration at the surface of the solid is in equilibrium with that in the liquid, and

(2) the phase relation is linear.

The pertinent experimental observation is that the concentration in the liquid phase varied linearly with position (see Figures 5 to 14).

Based on the assumption concerning the surface concentration, the spheres can be considered independently of the liquid. The concentration profile is then a function of the rate of variation at the surface, the radius R_o, the position in the column, and the diffusivity of the solid.

2. Solution to Concentration Profile in Solid

The diffusion of BNB in the crystal is assumed to follow Fick's Law. With the spherical geometry assumed in this model, the rate of diffusion N_B is therefore given by Equation (43).

$$N_B = 4\pi \rho_s D_s r^2 \partial X / \partial r \qquad (43)$$

In this equation, X is the weight fraction BNB in the crystal, r is the distance from the center of the crystal in cm, ρ_s is the density of solid BNB in g/cm^3, and D_s is the molecular diffusivity of solid BNB in cm^2/sec.

In the standard way, a BNB balance on a shell element of the crystal yields Equation (44).

$$\partial(rX)/\partial\theta = D_s \partial^2(rX)/\partial r^2 \qquad (44)$$

The first term in this equation relates to the variation of X at a given position in the crystal with time, and the second term describes the movement of BNB within the crystal.

The time, Θ, is related to the position in the column, h, by the crystal rate, L, the area through which the liquid and solid pass, A, the length of the column, h_o, and the crystal holdup, $Ah_o\rho_s(1-\eta)$. Thus the time is given by Equation (45).

$$\Theta = A h_o \rho_s (1-\eta)/L h_o \tag{45}$$

The boundary conditions which apply to Equation (45) are Equations(46).

$$X = X_o \text{ at } \Theta = 0 \tag{46a}$$

$$X = X_o + k\Theta \text{ at } r = R_o \tag{46b}$$

Here k is the rate of variation of the surface concentration of the crystal, weight fraction/sec.

By defining a new variable T equal to $X-X_o$, the problem reduces to Equations (47).

$$D_s \partial^2(rT)/\partial r^2 = \partial(rT)/\partial\Theta \tag{47a}$$

$$T = 0 \text{ at } \Theta = 0 \tag{47b}$$

$$T = k\Theta \text{ at } r = R_o \tag{47c}$$

The solution to Equation (47) is given by Carslaw and Jaeger[6] as Equations(48).

$$T = k\left[\Theta - \frac{R_o^2 - r^2}{6D}\right] - \frac{2kR_o^3}{D\pi^3 r}\sum_{n=1}^{\infty} f(n) \tag{48a}$$

$$f(n) = \frac{(-1)^n}{n^3}\exp\left(-\frac{D_s n^2 \pi^2 \Theta}{R_o^2}\right)\sin\left(\frac{n\pi r}{R_o}\right) \tag{48b}$$

Integration of these equations from $r = 0$ to $r = R_o$ leads to Equations (49). These give the average concentration, $\overline{T}$, of a sphere at any time (position).

$$\overline{T} = k\left[\theta - \frac{k}{15 D_s}\right] + \frac{\quad}{D\pi^4} \sum_{n=1} g(n) \qquad (49a)$$

$$g(n) = \frac{1}{n^4} \exp\left(-\frac{D_s n^2 \pi^2 \theta}{R_o^2}\right) \qquad (49b)$$

If it is assumed that D_s is less than $10^{-8} cm^2/sec$, which is a high diffusivity for the solid phase, and that R_o is greater than 0.05 mm, which is a very small radius, then the $g(n)$ for n greater than 1 can be collected into a constant term. The single exponential given in Equation (50) is produced.

$$\overline{T} = k\theta + \frac{k R_o^2}{15\pi^2 D_s}\left[90 \exp\left(-\frac{\pi^2 D_s \theta}{R_o^2}\right) - \pi^4\right] \qquad (50)$$

This equation gives the average composition of the solid to which is imposed a linearly varying liquid composition.

From Equation (49), it can be shown that the derivative of the solid concentration at the surface of the sphere is given by Equation (51).

$$\left(\frac{\partial T}{\partial r}\right)_{R_o} = \frac{2 k R_o}{D_s}\left[\frac{1}{6} - \frac{1}{\pi^2} \exp\left(\frac{-D_s \pi^2 \theta}{R_o^2}\right)\right] \qquad (51)$$

This derivative governs the rate at which BNB enters the solid.

The preceding equations complete the first part of the overall problem of the solid-phase - diffusion model. The second part, the description of the liquid, is presented below.

3. Solution to Profile in Liquid

A BNB balance on an element of the liquid yields Equation (52).

$$DA\eta\rho \frac{d^2Y}{dh^2} + L\frac{dY}{dh} = D_s \rho_s a A \left(\frac{\partial T}{\partial r}\right)_{R_o} \qquad (52)$$

The first term relates to the diffusion within the liquid, and the second to bulk flow in the liquid. The term on the right-hand side of the equation is the rate of diffusion of BNB into the solid and is given by Equation (51). Introducing Equations (45) and (51) into Equation (52) produces Equation (53).

$$\frac{d^2Y}{dh^2} + R_1 \frac{dY}{dh} = R_2\left[\frac{1}{6} - \frac{1}{\pi^2}\exp(-wh)\right] \qquad (53)$$

In this equation W_1, R_1 and R_2 are given by Equations (54).

$$R_1 = L/DA\eta\rho \qquad (54a)$$

$$R_2 = 2hR_o a \rho_s / D\eta\rho \qquad (54b)$$

$$W = D_s \pi^2 A(1-\eta)\rho_s / L R_o^2 \qquad (54c)$$

The solution to Equation (53) is given by Equation (55).

$$Y = C_1 + C_2 \exp(-R_1 h) + R_2 h/6R_1 + R_2 \exp(-wh)/[\pi^2 w(R_1 - w)] \qquad (55)$$

Two boundary conditions are used to evaluate C_1 and C_2. Let the concentration in the liquid, and the derivative of this concentration, be determined experimentally at $h = 0$. Thus at $h = 0$, $Y = Y_o$, and $dY/dh = S_o$. Application of these conditions defines C_1 and C_2 as

shown in Equations (56).

$$C_2 = R_2/6R_1^2 - R_2/[\pi^2 R_1(R_1 - W)] - S_o/R_1 \qquad (56a)$$

$$C_1 = Y_o - C_2 - R_2/[\pi^2 W(R_1 - W)] \qquad (56b)$$

The form of the composition profile can be rearranged if the restrictions on R_o and D_s, which were imposed in the first part of the problem, are applied. Namely that $R_o > 0.05$ mm and $D_s < 10^{-8}$ cm^2/sec. This application permits the expansion of $\exp(-Wh)$ to its linear form $1-Wh$ giving Equation (57).

$$Y = Y_o + \left[h + \left(\frac{\exp(-R_1 h) - 1}{R_1}\right)\right] - S_o\left(\frac{\exp(-R_1 h) - 1}{R_1}\right)$$

$$- \frac{R_2}{\pi^2(R_1 - W)}\left[h + \left(\frac{\exp(-R_1 h) - 1}{R_1}\right)\right] \qquad (57)$$

If D_s is larger than 10^{-8}, or R_o less than 0.05 mm, then this linearization is not valid and a more complicated form for Equation (57) would result.

Equation (57) can be further reduced if $R_1 h$ is such that $\exp(-R_1 h)$ can be expanded to its linear form $1-R_1 h$. If this expansion is valid, then the terms in Equation (57) which are enclosed in parentheses reduce to $-h$, and those enclosed in square brackets reduce to zero. Under this condition, Equation (57) becomes Equation (58).

$$Y = Y_o + S_o h \qquad (58)$$

If the two term expansion of exp $(-R_1 h)$ is invalid, but the three term expansion is valid, then Equation (57) reduces to Equation (59).

$$Y = Y_o + S_o h + \left[1 - S_o - \frac{R_2}{\pi^2 (R_1 - W)} \right] \frac{R_1 h^2}{2} \qquad (59)$$

4. Predictions

The model incorporating diffusion in the solid phase, in its simpliest form, predicts that the concentration gradient within the liquid will be linear. This prediction is based on the restrictions placed on the values of $R_1 h$. If these restrictions are loosened slightly, then the model predicts a parabolic concentration profile.

The boundary conditions which were applied to Equation (55) permit no further predictions to be made. The constants Y_o and S_o are entirely empirical. The dependence of these constants on operational variables can not be predicted. Only correlations with experimental data will give information as to the possible functional forms of Y_o and S_o.

Such a solution is not altogether satisfying especially because the variation of S_o with operating conditions was studied in this investigation. If the model in the form presented here cannot be evaluated satisfactorily, then boundary conditions which are not empirical should be used and the new form of the diffusion model tested.

D. Constant-Crystal-Composition - Model IV

The model which assumes that the crystals pass unchanged through the purification section of the column is presented because this model was used successfully by Albertins[1] to interpret data for a eutectic system. The development which is presented below will facilitate a later discussion of the differences between the conclusions drawn by Albertins and those extracted from the current results.

1. Description

In this model, crystals of weight fraction X_o are considered to form in the freezing section and pass unchanged to the melting section at L gm/sec. An adhering liquid of weight fraction Z accompanies the crystals at C gm/sec . Mass-transfer occurs at J gm/sec between this adhering liquid and the free liquid which moves countercurrently at V gm/sec and weight fraction Y . Dispersion occurs in the liquid phase at N gm/sec . The model for this case is illustrated in Figures 17 and 18.

The development of the constant-crystal-composition model closely parallels the development of the mass-transfer-limiting model. As in the earlier case, the rate of dispersion of BNB is proportional to the effective diffusivity, D , the area available for dispersion, $A\eta$, the density of BNB, ρ , and the concentration gradient, dY/dh . That is, N_B is given by Equation (60).

$$N_B = -D\eta A\rho\, dY/dh \tag{60}$$

The rate of mass-transfer, J , is given by Equation (61).

$$J = Ka\,A\rho\,\Delta h\,(Y-Z) \tag{61}$$

The factors K , a , A , and Δh are the same as in Model I. The driving force for mass-transfer is assumed to be the difference in concentration between the two liquid phases.

A BNB balance on an element of the free liquid phase gives Equation (62).

$$DA\eta\rho\frac{d^2Y}{dh^2} - V\frac{dY}{dh} - Ka\,A\rho\,(Y-Z) = 0 \tag{62}$$

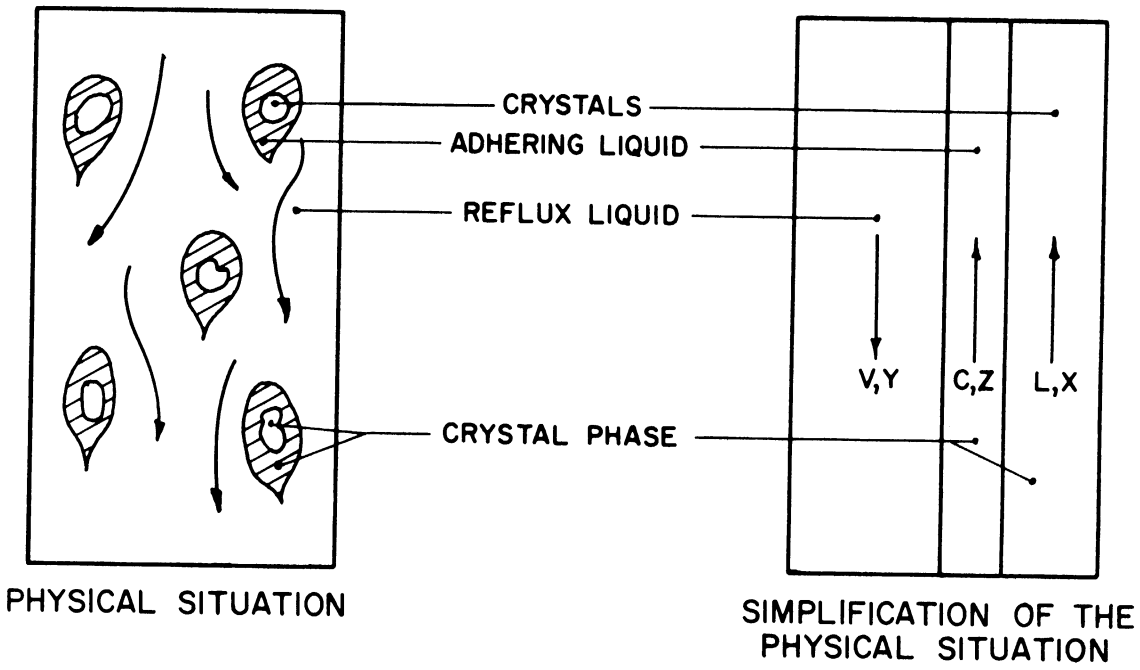

Figure 17. Illustration of Flows in Constant-Crystal-Composition Model.

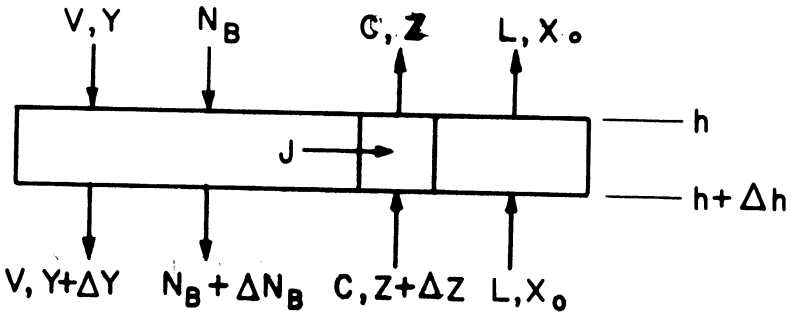

$$N_B = -D\eta A\rho \; dY/dh$$

$$J = KaA\rho \; \Delta h(Y-Z)$$

Figure 18. Elemental Description of Column Crystallization--Constant-Crystal-Composition Model.

As in Equation (3), the terms in this equation refer to dispersion, bulk flow, and mass-transfer, respectively. It is assumed that the flows V and L and the coefficients D , A , η , ρ , and K are independent of position, h .

A BNB balance on one end of the column gives Equation (63).

$$DA\eta\rho \frac{dY}{dh} + LX_o + CZ - VY = 0 \qquad (63)$$

Only the flow term, CZ is different from the terms in Equation (4). A total balance on one end of the column gives Equation (64).

$$L + C - V = 0 \qquad (64)$$

In order to solve Equations (62) to (64), it is assumed that $C = \alpha L$. In general, α will be small because C and V are both liquid phases. A numerical value for alpha must be estimated, but data on "drained crystals" probably should not be used. The surface which forms on draining does not occur in the present situation. An approximation for alpha can be made on the basis of boundary-layer theory, or outright guesses can be made.

When Z , which is very difficult to measure experimentally, is eliminated from Equations (62) and (63), Equation (65) is produced.

$$\frac{d^2Y}{dh^2} = -R_1 \frac{dY}{dh} + R_2 Y = R_2 X_o \qquad (65)$$

The constants R_i are defined by Equations (66).

$$R_1 = K\alpha A\rho / L\alpha + L(1+\alpha) / DA\eta\rho \qquad (66a)$$

$$R_2 = K\alpha / D\eta\alpha \qquad (66b)$$

2. Solution

According to the model, X_o is constant. Thus the solution to Equation (65) is given by Equation (67).

$$Y = C_1 + C_2 \exp(q_2 h) + C_3 \exp(q_3 h) \qquad (67)$$

In this equation, q_2 and q_3 are given by the characteristic Equation (68).

$$q^2 - R_1 q + R_2 = 0 \qquad (68)$$

C_1 must be equal to X_0 and by applying the same valid approximations which were used in Model I, the roots of Equation (68) are given by Equations (69).

$$q_2 = R_1 \qquad (69a)$$

$$q_3 = R_2 / R_1 \qquad (69b)$$

C_2 and C_3 are defined by appropriate boundary conditions.

As in the mass-transfer-limiting model, R_1 becomes large as L becomes large or small. Therefore C_2 must be zero if Equation (67) is to apply to all conditions of crystal flow. Equation (67) thus reduces to Equation (70).

$$Y = X_0 + C_3 \exp(h R_2 / R_1) \qquad (70)$$

The reduction of Equation (67) from three terms to two can be accomplished on a base similar to that suggested in Model I. Because the constant-crystal-composition model was said to describe a eutectic system[1], data from such a system are used as the basis for the reduction.

Values of D and K can be extracted from Equation (67) by relating it to experimental data. In one method for doing this, it is assumed that the three terms in Equation (67) are non-zero. Then for a given set of data, the values determined for D and K depend on the value chosen for X_0. In any case, the resulting values of D agree

with the values appearing in the literature. On the contrary, regardless of the value chosen for X_o, the resulting value of K is 3 or 4 orders of magnitude smaller than values presented in the literature.

In the second method of applying Equation (67), C_2 is assumed to be zero. The resulting equation is then used to evaluate D and K. The values which result are in essential agreement with published values.

The second of these two methods seems preferable, although it is by no means mathematically exact. Thus, C_2 is assumed to be zero, thereby yielding Equation (70).

3. Prediction

This model predicts that a plot of $\ln (Y-X)$ vs. h will be linear with slope R_2/R_1. This is the result found by Albertins[1] in his study of cyclohexane-benzene, a eutectic system.

Another prediction can be made on a purely physical basis although this prediction is in apparent contradiction to the one just presented.

According to the model, the crystals formed in the freezing section pass unchanged through the purification section to the melting section where they melt to form the reflux which is analyzed. Because the crystals melt completely, the composition of the liquid at $h = 0$ should differ from that of the crystals only as the result of dilution by the small amount of impure clinging liquid. Thus the composition of the liquid at $h = 0$ must be less than that of the crystals.

The crystals which reach the melting section are of the same composition as those in the freezing section, and are approximately in equilibrium with the liquid in the freezing section. Thus the prediction

obtains. The difference in the composition of the liquid at the two ends of the column should be no more than the difference achieved by a single equilibrium phase separation. That is, if the liquidus and solidus compositions differ by 6 weight per cent at the temperature maintained in the freezing section, then the difference $Y_{30}-Y_0$ should not exceed 6 per cent.

CHAPTER V

EVALUATION OF MODELS

The four models developed in the previous section are evaluated in this section. The evaluations are made by comparing the predictions of each model with experimental results. As was already mentioned, only the mass-transfer-limiting model, Model I, is consist nt with the data.

The models are evaluated in the same order as that in which they were presented. Thus five tests of the mass-transfer-limiting model are discussed in view of experimental data. Then pertinent results are compared with the predictions of the other models to indicate the inconsistencies of these models.

A. Mass-Transfer-Limiting

Five tests were made of the mass-transfer-limiting model. In four of the tests, the results presented below demonstrate that this model of column crystallization is consistent with experimental data. These data were presented earlier, on Figures 5 to 14. The result of the fifth test was inconclusive.

1. Test 1

The mass-transfer-limiting model includes the term $(Y-X^*)_o$ which relates to the difference in composition between phases in equilibrium at the top of the column. The inclusion of this term, the phase separation, predicts that separations will decrease as the charge to the column is made more nearly pure. This prediction was fulfilled in the experiments as summarized in Table II.

TABLE II

INFLUENCE OF DIFFERENCE IN PHASE COMPOSITIONS ON SEPARATION

Run	Charge	Phase Separation X^*-Y	Separation Y_0-Y_{30}	Crystal Rate	Rotation	Oscillation Rate	Oscillation Stroke
		Weight Fractions BNB		g/sec	RPM	OPM	mm
13	0.95	~0.01	0.015	0.040	67	22	4.5
29	0.65	0.037	0.089	0.038	60	67	4.2
30	0.65	0.039	0.089	0.033	60	67	4.2
31	0.65	0.039	0.070	0.025	60	67	4.2
14	0.50	0.057	0.055	0.036	67	25	4.5
15	0.50	0.057	0.080	0.036	32	25	4.5
16	0.35	0.058	0.106	0.027	46	40	6.0
17	0.35	0.059	0.072	0.018	29	30	6.0
6	0.05	~0.01	0.005	0.012	67	72	4.5
7	0.05	~0.01	0.005	0.009	67	70	4.5

Table II presents the separations achieved in several runs for which the charge composition varied widely. It is clearly seen that as the nominal weight fraction m-bromonitrobenzene (BNB) in the charge was increased from 0.05 to 0.95, the separation attained passed through a maximum. For nearly pure charges (Runs 6, 7, and 13) the ultimate separation was only 0.015 weight fraction. For charges of intermediate concentration (Runs 14-17 and 29-31) the separation reached 0.106 weight fraction.

Figures 19 and 20 summarize the data in Table II. It must be emphasized that variables other than charge composition varied among the several runs.

2. Test 2

The mass-transfer-limiting model also contains the expression $E/L + L/F$, which is referred to as H. In this expression, E and F are factors which are defined in Equations (71), as presented in Equation (18).

$$\epsilon = D A \eta \rho \tag{71a}$$

$$F = m / K \alpha A \rho \tag{71b}$$

They relate to dispersion and mass-transfer, respectively.

The model thus predicts that the concentration gradient within the column is a function of the crystal rate, L. Data on Figures (21) and (22) show this variation. For the range of crystal rate which could be achieved, H decreased as L increased. Examination of the derivative dH/dL, as demonstrated in Appendix A5-d, indicates that H reaches

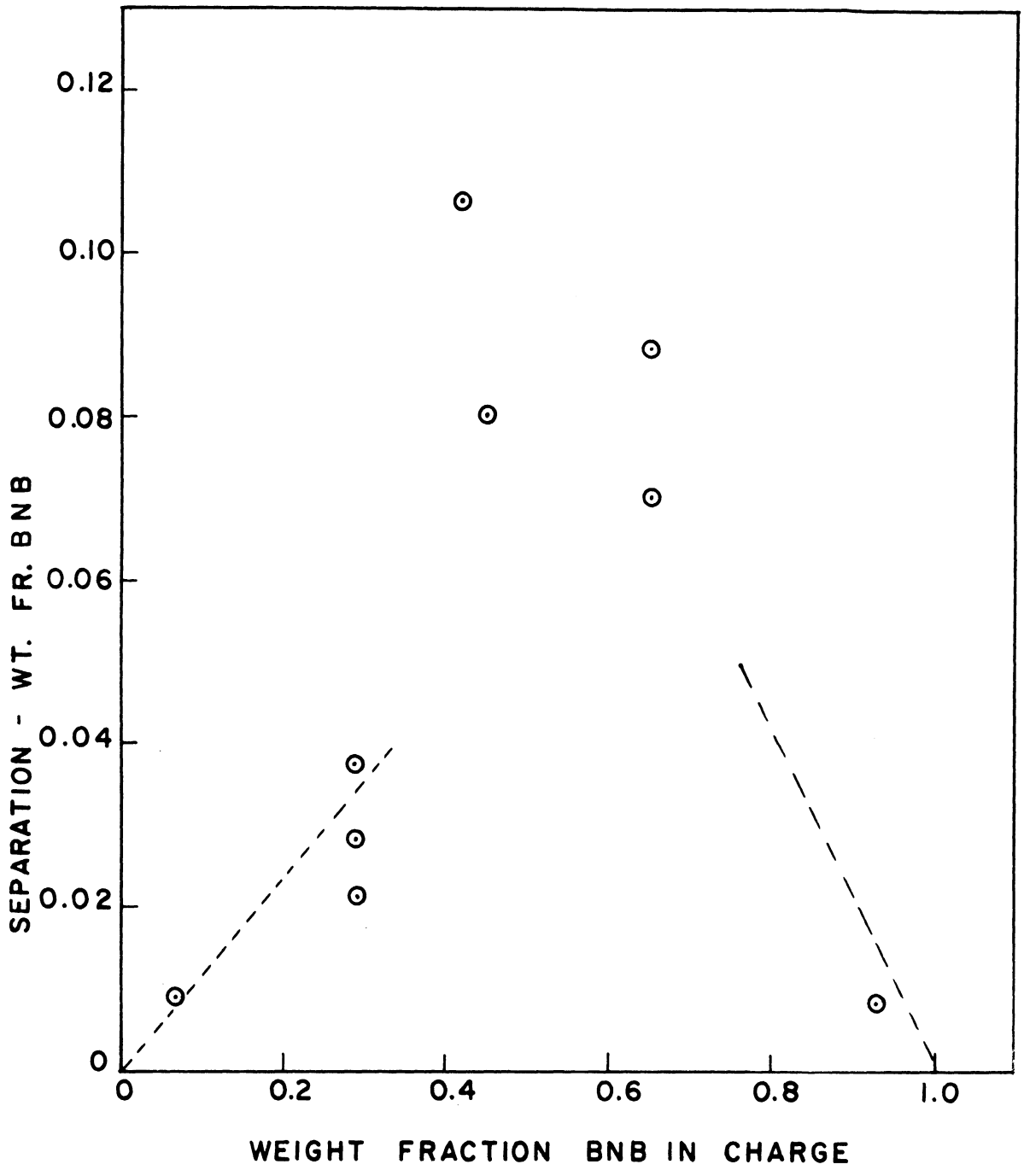

Figure 19. Effect of Charge Composition on Separation.

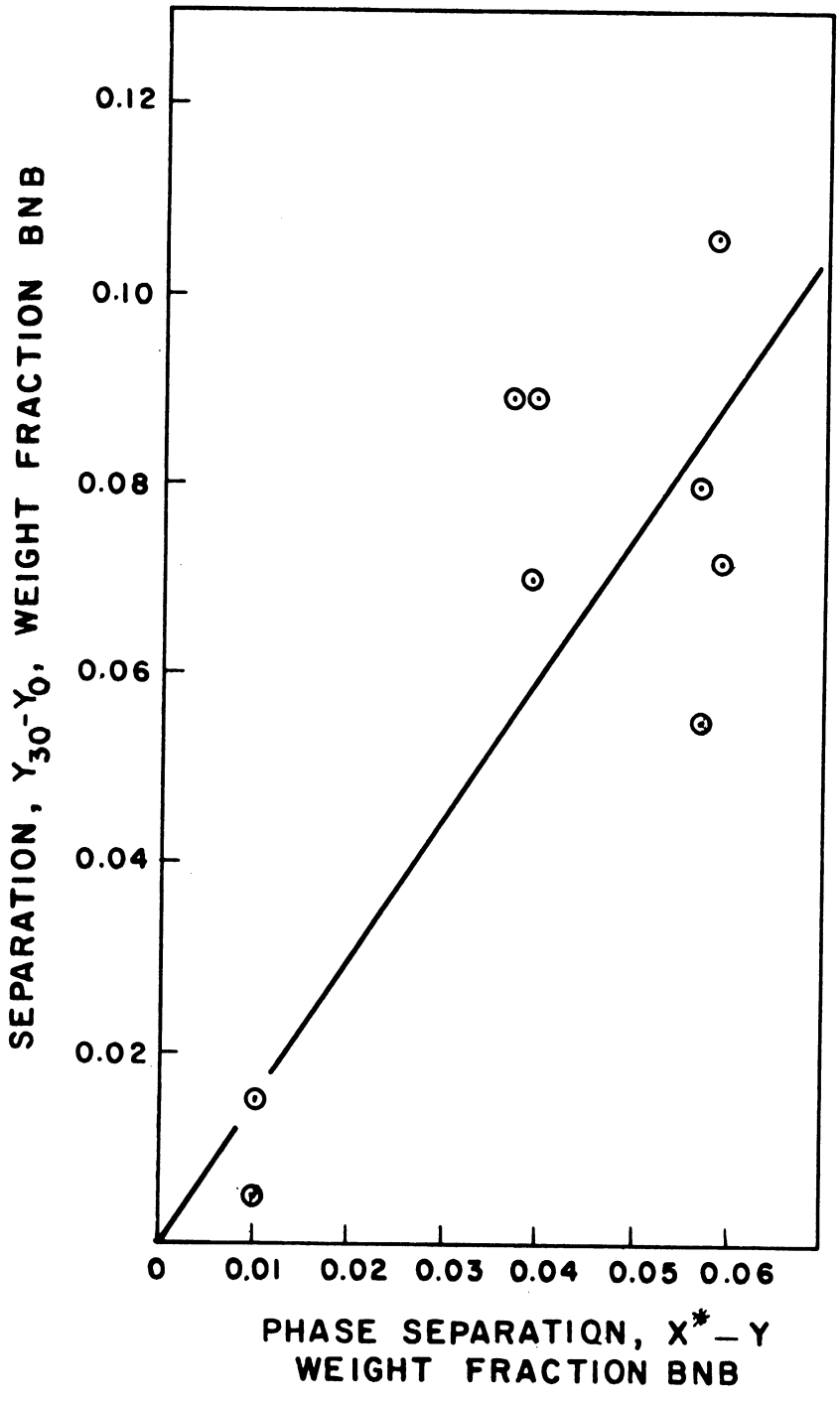

Figure 20. Effect of PPhase Separation on Separation.

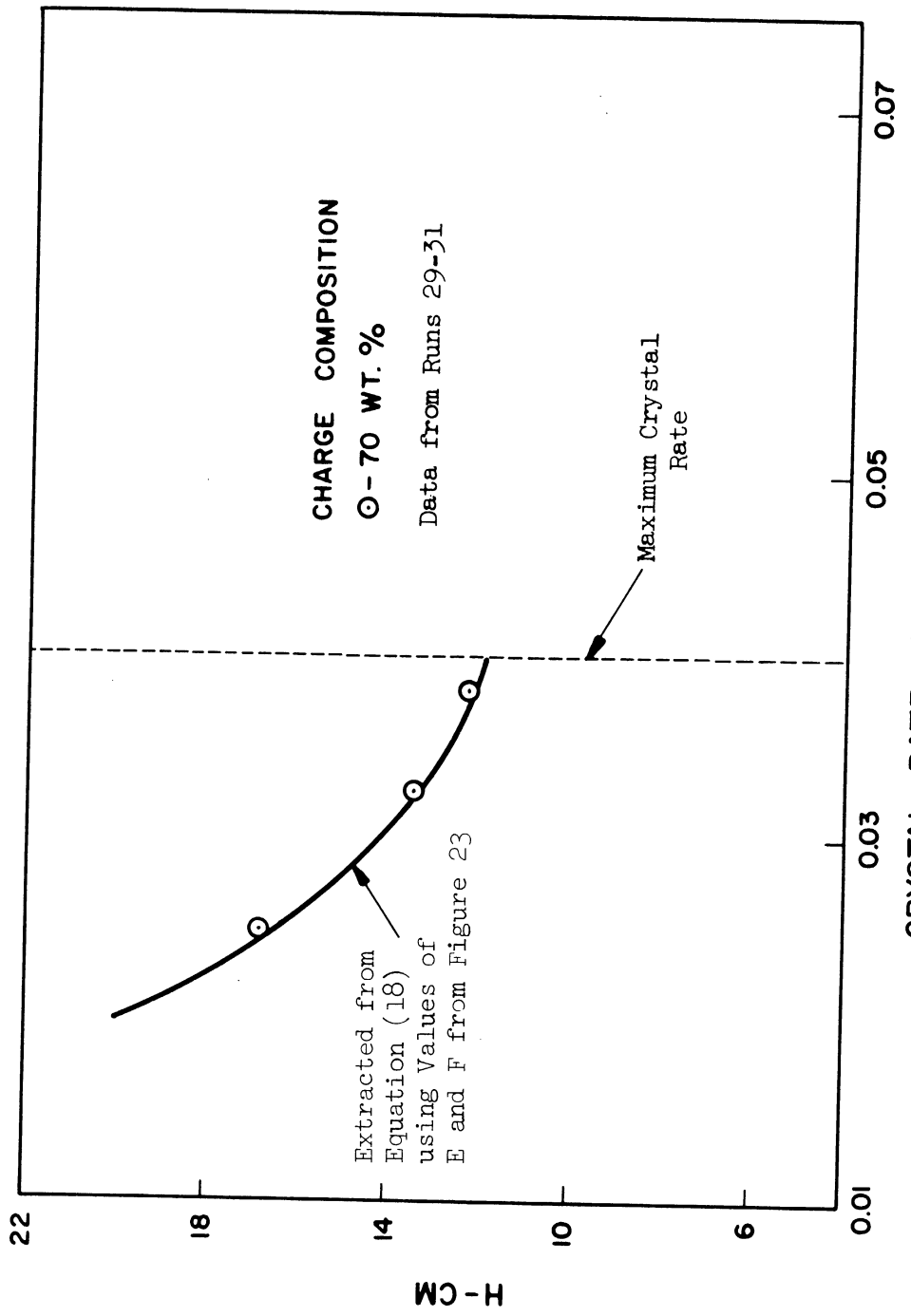

Figure 21. Effect of Crystal Rate on Column Performance.

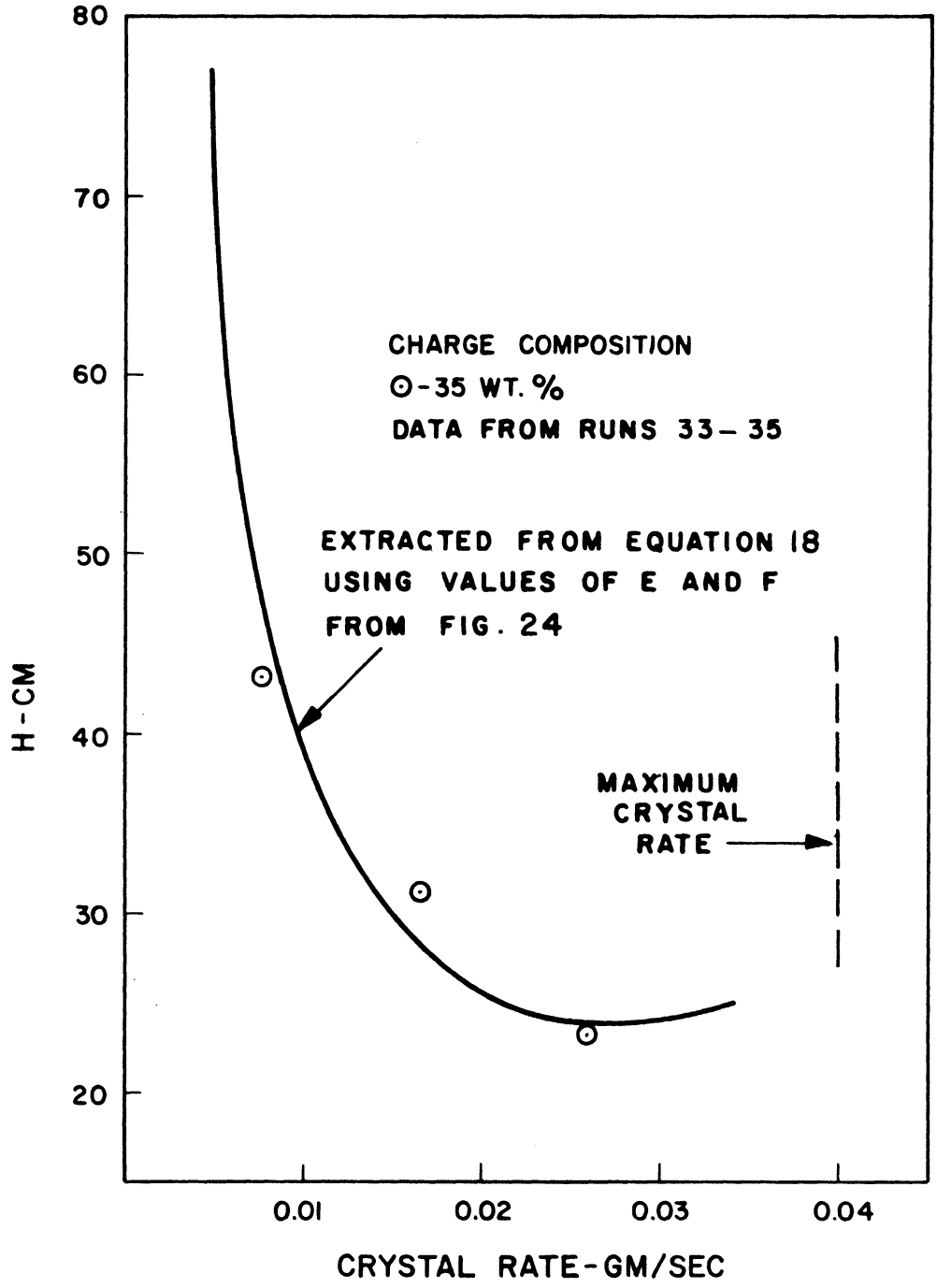

Figure 22. Effect of Crystal Rate on Column Performance.

a minimum when the term E/L is equal to L/F. Relating this to the data shows that axial dispersion within the liquid, not mass-transfer between phases, is the dominant effect in column crystallization. This result is in agreement with that of Albertins.[1]

3. Test 3

As it was mentioned earlier, Equation (18), when multiplied by L to produce Equation (72), predicts that the HL is a linear function of L^2.

$$H = E/L + L/F \tag{18}$$

$$HL = E + L^2/F \tag{72}$$

Thus plots of HL vs. L^2, as shown on Figures 23 and 24, have intercepts E and slopes $1./F$.

The data on Figures 23 and 24 were fit by linear regression lines in order to give an objective method of analysis. Although there is considerable scatter in the data, especially in those in Figure 24, there is no trend. A parabolic fit of the data would have positive curvature in one case and negative curvature in the other.

It can be inferred from Figures 23 and 24 that E and F are independent of L, as was assumed in the development of the model, and that both dispersion and mass-transfer occur in the column crystallization of a solid solution. Such a conclusion may be opposed to that of Albertins, who studied a eutectic system.

From the slope and intercept of Figures 23 and 24, values of E and F were obtained. Substitution of these values together with estimated or calculated values for A, η, ρ, and a yielded D and K

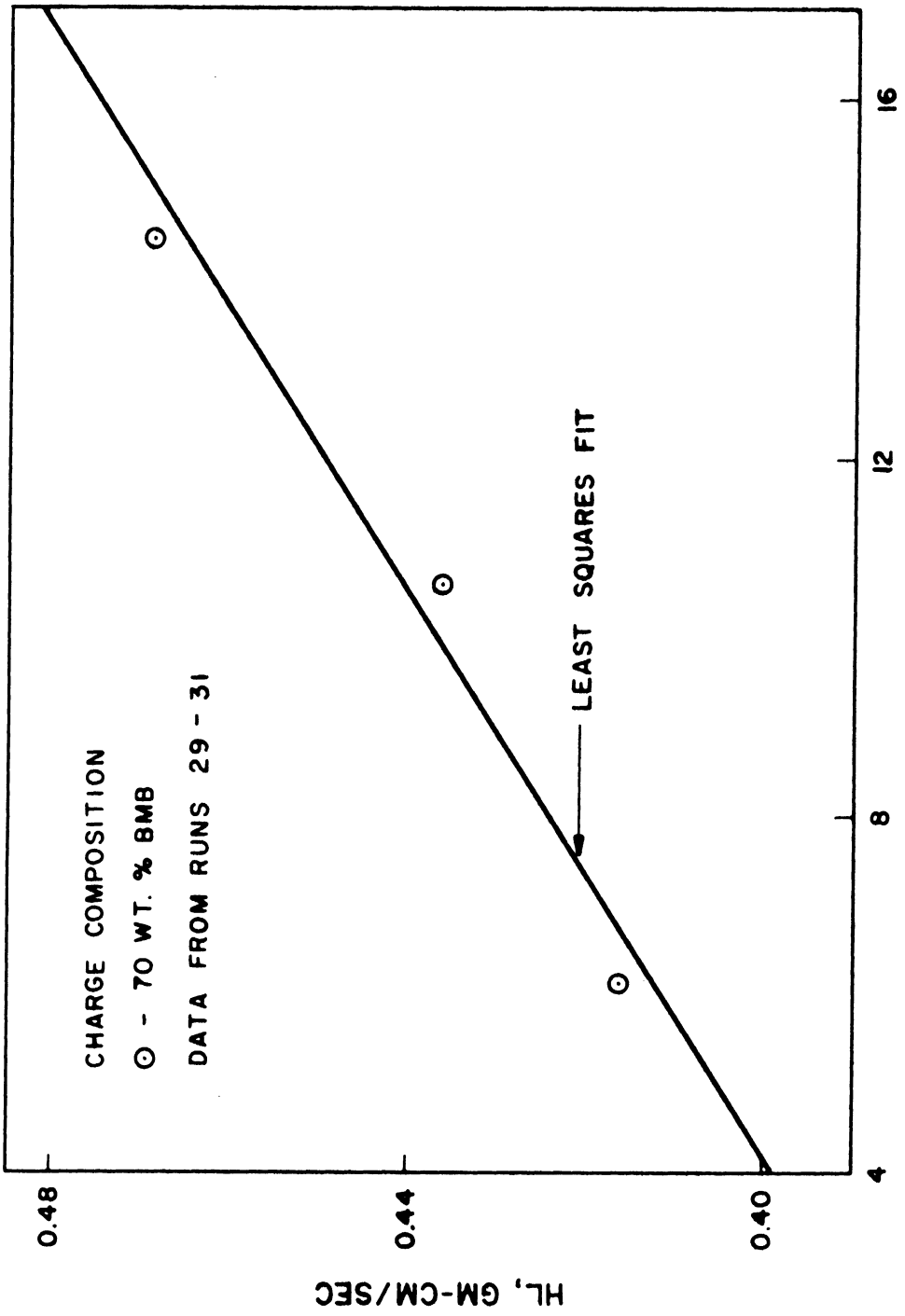

Figure 23. Determination of Diffusivity.

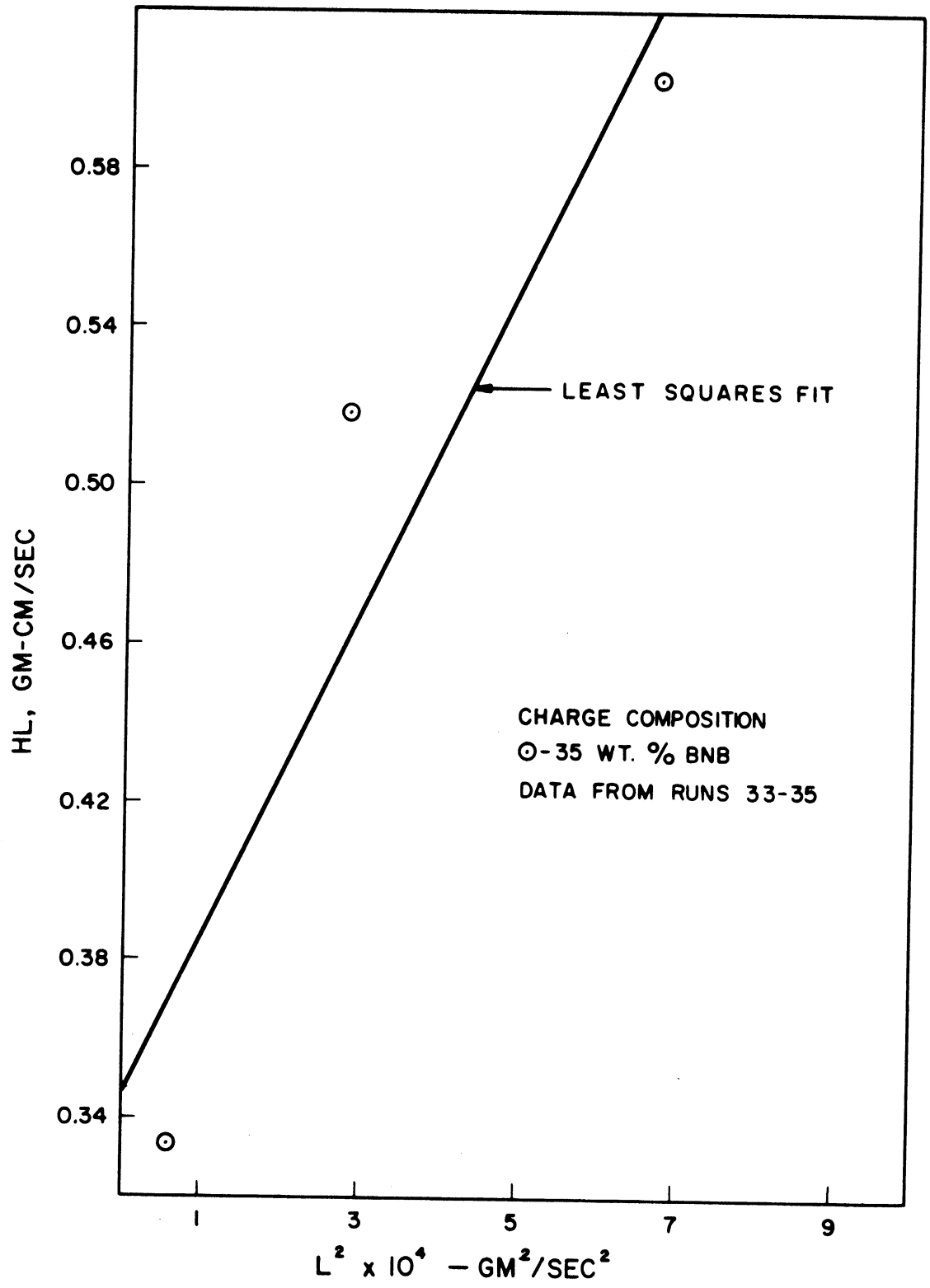

Figure 24. Determination of Diffusivity and Mass-Transfer-Coefficient.

(see Appendix A6). As shown in Table III, the experimental values determined by this procedure, especially those for D, are in agreement with values taken from the literature.

TABLE III

COMPARISON OF EXPERIMENTAL AND LITERATURE VALUES OF DIFFUSIVITY AND MASS-TRANSFER COEFFICIENT

Value		Source
Diffusivity	Mass-Transfer Coefficient	
cm^2/sec	10^3 cm/sec	
4.6	0.44	Figure 23
4.2	0.071	Figure 24
3.5	1.9×10^{-4}*	Albertins[1]
1.7	0.075	Figure 30
1.5, 1.3	0.26, 0.64	Figure 31
0.5-3.0		Jones[21]
	2-5	Lewis[25]
	2-3	Thorsen[40]
0.8-2.6		Smoot and Babb[37]

*Considered to be incorrectly measured.

The preceding paragraphs indicate three predictions of the mass-transfer-limiting model which were demonstrated by the experimental data. These are:

(1) The concentration gradient within the column varies with composition, as indicated by the term $(Y-X^*)_o$.

(2) The concentration varies with the crystal rate. The form of this variation identifies the dominant mechanism in the column crystallization of a solid solution.

(3) Diffusivities and mass-transfer coefficients can be evaluated from appropriate cross plots of experimental data.

4. Test 4

There is one prediction of the model which could not be directly verified with the system BNB-CNB. This relates to the second way in which the concentration gradient should vary with composition.

As was mentioned previously, H, which is inversely proportional to the concentration gradient, contains the term m, which comes from the phase relation $X^* = mY + b$. Table IV shows that m varies from 0.9 to 1.3 as the composition varies from 0 to 100 per cent BNB. H should vary also. However, the influence of m on H is very small because the term L/F, which contains m, is a small part of H. At least this is true in the range of L which was studied. A twenty per cent change in m, the change which occurs between liquid compositions of 25 and 65 per cent BNB, produces a change in H at most equal to 10 per cent and generally less than 5 per cent. Such a small effect can not be determined by the current experiment.

TABLE IV

DEPENDENCE OF SLOPE OF EQUILIBRIUM RELATION ON COMPOSITION FOR SYSTEMS BNB-CNB AND AZOBENZENE-STILBENE - AVERAGE VALUES OF m OVER A COMPOSITION RANGE OF 0.1 WEIGHT FRACTION

Liquid Composition Weight Fraction	$m_{BNB-CNB}$	$m_{Azo.-Stil.}$
0.05	1.3	2.7
0.15	1.2	1.7
0.25	1.1	1.3
0.35	1.0	1.1
0.45	0.9	0.9
0.55	0.9	0.7
0.65	0.9	0.6
0.75	0.9	0.4
0.85	0.9	0.3
0.95	0.9	0.2

5. Test 5

One final test of Model I was made. Equation (22), which was derived for a linear phase relation, predicts that the concentration gradient within the liquid phase is related linearly to $(Y-X^*)_o$. If a system with a non-linear phase relation were separated by column crystallization, one would expect that Equation (22) would be applicable only over small sections of the column. And for each section, $(Y-X^*)_o$ would have a different value.

Equation (22) was hypothetically applied in this manner to the system azobenzene-stilbene, the phase diagram of which is shown in Figure 25. This system has a very non-linear phase relation as shown in Figure 26. Table IV presents the variation of m with composition for the system. These phase data were reported by Powers.[32]

The profile predicted from the hypothetical application is shown in Figure 27. Also shown on this figure are experimental results of Roessler reported by Powers.[32] The agreement is excellent.

The data reported by Powers are for the average composition at each cross-section. Because Equation (22) applies to the composition, Y , of the liquid phase, an estimate of Y was made from Roessler's data. It was assumed that the volume fraction liquid was 2/3 and that the liquid and solid were in equilibrium in order to make this estimate. The volume fraction which was used is the same as that which occurred in the present study. Values for E and F/m were estimated in order to make the calculations of the profile. The details of the calculation are presented in Appendix A5-a.

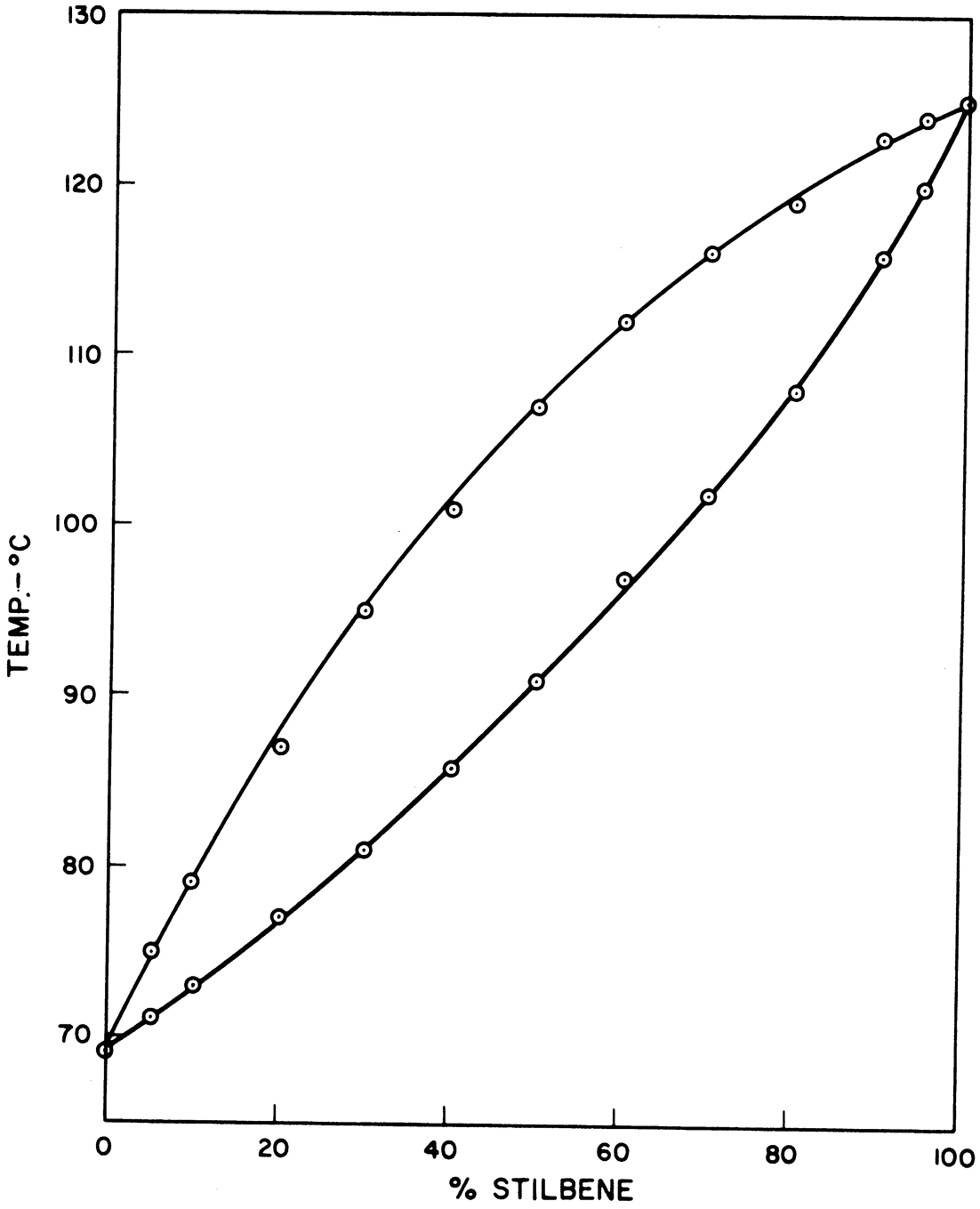

Figure 25. Phase Diagram of Azobenzene-Stilbene.

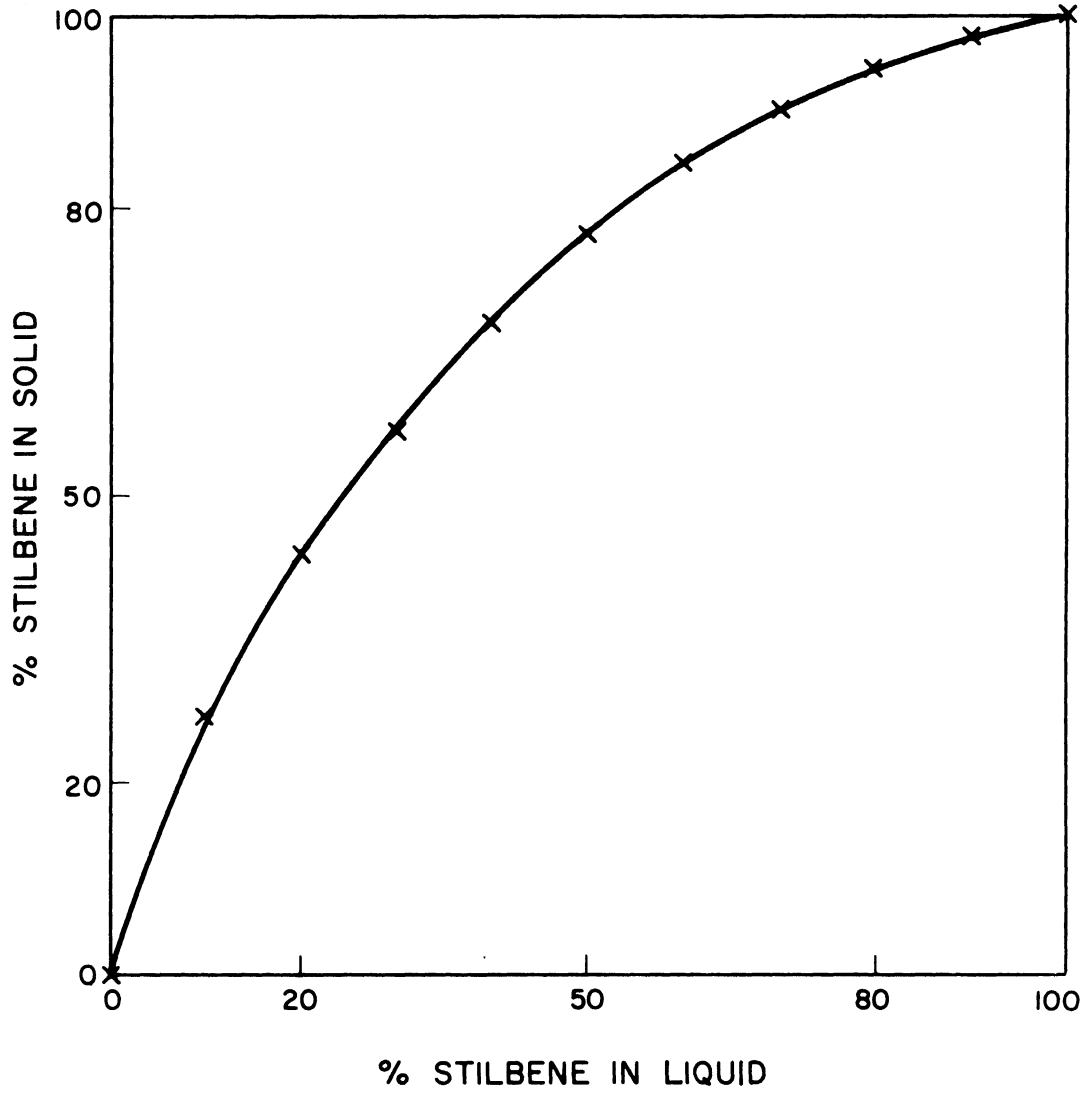

Figure 26. Phase Relation of Azobenzene-Stilbene.

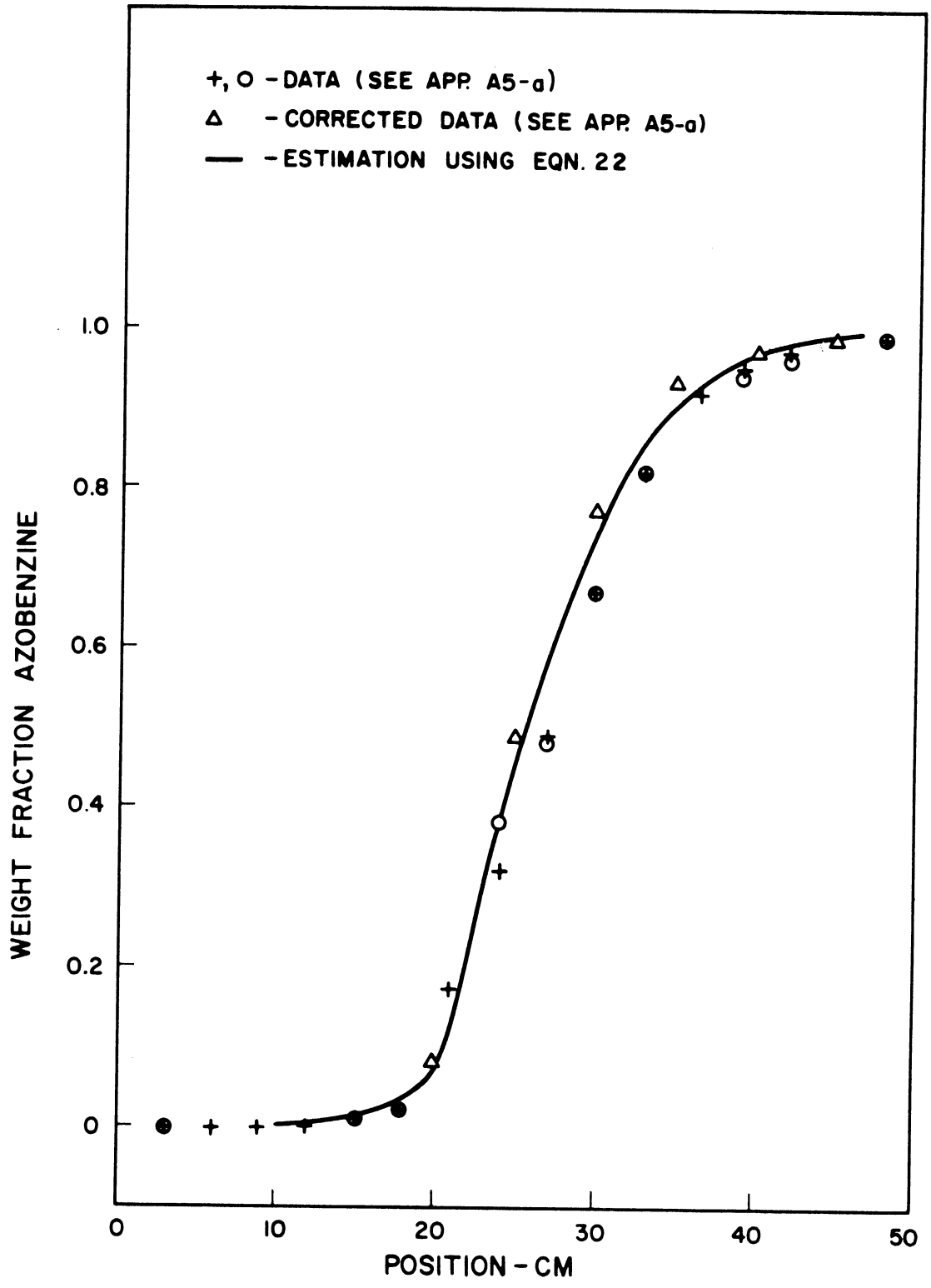

Figure 27. Piecewise Application of Mass-Transfer-Limiting Model to Data Reported by Powers[32].

In applying Equation (22), m was allowed to vary with Y. Better agreement than with m constant was obtained. It seems therefore that, although not tested directly, the inclusion of m in H is correct.

6. Summary of Tests

The five tests presented above indicate that the mass-transfer-limiting model is fully compatible with experimental results. This compatibility is demonstrated for two systems which form solid solutions with widely different characteristics.

B. Heat-transfer-limiting

In order to evaluate the heat-transfer-limiting model, Equations (37) to (42), which describe this case, were solved numerically. The results of several solutions are reported in this section. These results show that the model is contrary to experimental data.

The heat capacities of liquid and solid BNB and CNB were estimated by the method of Sakiadis and Coates given by Reid and Sherwood.[34] The estimates are as follows:

(1) $C_{L,C} = 0.271$ cal/g-C°

(2) $C_{L,B} = 0.209$

(3) $C_{V,C} = 0.348$

(4) $C_{V,B} = 0.268$

Heats of fusion equal to 33.1 and 24.3 cal/g for CNB and BNB, respectively, were used.[42]

1. Effect of Composition

Table V shows that separations predicted by the heat-transfer-limiting model were independent of composition for two widely different sets of operating conditions. The separations were essentially the same although the phase separations (the difference between liquid and solid compositions at equilibrium) varied by more than 20 per cent. Such results are in direct contradiction with the experimental results demonstrated in Table II.

2. Influence of Crystal Rate

A series of solutions was made for which the crystal rate was varied over an order of magnitude, from 0.005 g/sec to 0.05 g/sec. The results of this series are presented in Table VI and in Figure 28.

It is clearly seen that the crystal rate divided by the separation, $L_o/\Delta Y$, which is directly analogous to HL in the mass-transfer-limiting model, increased linearly with L_o . Consequently, a plot of $L_o/\Delta Y$ vs. L_o^2 would be highly curved, especially near $L_o = 0$. These results are in contradiction to the experimental results shown on Figures 21 to 24.

3. Effect of Liquid Diffusivity

In the heat-transfer-limiting model, as well as in the other models which were evaluated, dispersion in the liquid was an important variable. However, in order to produce a profile at all similar to those which were actually observed, values of E about four or five times those measured experimentally were required. In other words, if a value for E about equal to the observed value was used in the heat-transfer-limiting model, then a separation three or four times that which occurred physically was predicted.

TABLE V

EFFECT OF COMPOSITION ON COLUMN PERFORMANCE
HEAT-TRANSFER-LIMITING MODEL

Run	Charge Composition	Phase Separation	Predicted Separation
	Weight Fraction BNB	Weight Fraction BNB	Weight Fraction BNB
A	0.65	0.0441	0.0986
B	0.40	0.0593	0.0928
C	0.65	0.0441	0.0454
D	0.40	0.0593	0.0457
E	0.65	0.0441	0.0637
F	0.50	0.0569	0.0668
G	0.35	0.0585	0.0584

Variable	Runs		
	A-B	C-D	E-G
E	1.2	0.3	1.5
L_o	0.025	0.025	0.025
U	5×10^{-6}	5×10^{-6}	5×10^{-6}
MAη	2.5	20.	3.

TABLE VI

EFFECT OF CRYSTAL RATE ON SEPARATION
HEAT-TRANSFER-LIMITING MODEL

Crystal Rate	Separation	Crystal Rate / Separation	Crystal Rate Squared
g/sec	Weight Fraction	g/sec per Weight Fraction	10^4 g^2/sec^2
0.005	0.012	0.410	0.25
0.01	0.024	0.415	1.0
0.02	0.047	0.424	4.0
0.03	0.069	0.433	9.0
0.04	0.091	0.442	16.0
0.05	0.111	0.452	25.0

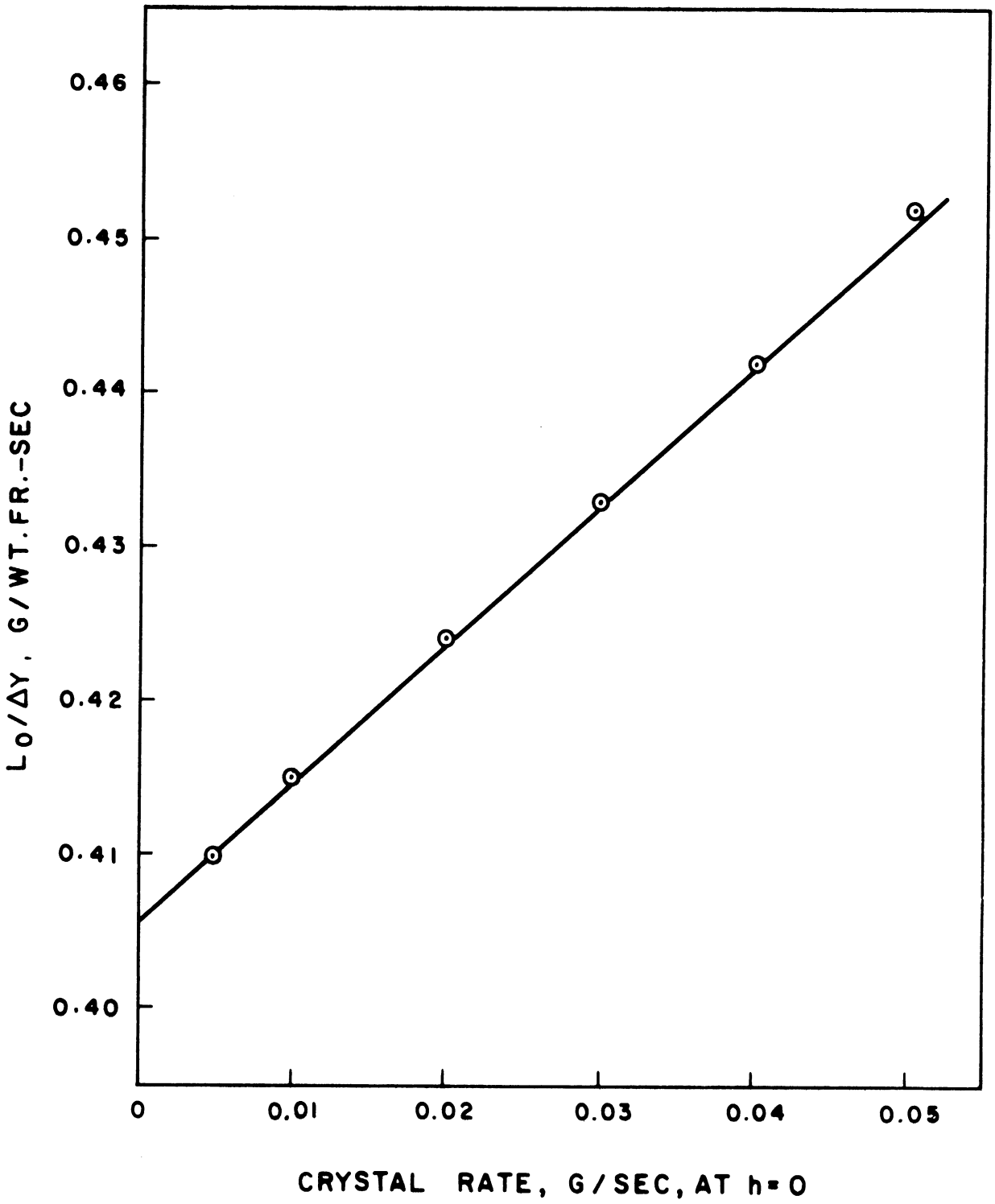

Figure 28. Effect of Crystal Rate on Separation--Heat-Transfer-Limiting Model.

4. Influence of Heat-Transfer Coefficient

One would expect the heat-transfer coefficient between the two phases to have a major influence of the predicted profile inasmuch as the model is a heat-transfer model. Table VII indicates that this expectation is not borne out. A variation of U of three orders of magnitude, from 1 to 1000 Btu/ft^2-hr-F° ($5x10^{-7}$ to $5x10^{-4}$ cal/cm^2-sec-C°), produced a variation in the predicted separation of only 15 per cent. A change in U of one further order of magnitude produced a change in separation equal to a factor of two.

TABLE VII

EFFECT OF HEAT-TRANSFER COEFFICIENT ON SEPARATION

Run	Heat-transfer Coefficient cal/cm^2-sec-C°	Predicted Separation weight fraction BNB
E	$5x10^{-7}$	.0666
F	$5x10^{-6}$	.0667
G	$5x10^{-5}$	.0676
H	$5x10^{-4}$	.0764
I	$5x10^{-3}$	.1530

5. Conclusion

From the discussions presented above, in which contradictions between experimental results and predictions of the heat-transfer-limiting model are demonstrated, it is concluded that this model is incompatible with experiments.

C. Diffusion in Solid Phase

The solution to this model indicates that the liquid composition is, in general, a complex function of position. Under special conditions, the solution can be simplified to a linear or a parabolic form.

If $R_1 h$ is less than 0.4, then the model predicts profiles which are linear to within 10 per cent. This latter quantity is the maximum error introduced into the evaluation of $\exp(-R_1 h)$ by using the linear approximation for $R_1 h$ less than 0.4.

In order that $R_1 h$ be less than 0.4 for eighty per cent of the column, R must be less than 0.016. As it was shown in the evaluation of the mass-transfer-limiting model, D and the product $\eta A \rho$ are less than 1 and 1/2, respectively. Together these terms make up the denominator of R_1 (Equation 54a). Consequently, L must be less than 0.006 in order for the approximation to hold. In other words, if the crystal rate exceeds 0.006 g/sec., then the linearization of $\exp(-R_1 h)$ is invalid, and the model will predict a profile with curvature of at least the second power of h .

The experimental run with the lowest crystal rate had $L = 0.008$ g/sec . Other runs had crystal rates between 0.015 and 0.040 g/sec. Under these conditions the model would not predict the linear composition profiles which were obtained (Figures 5 to 14). The diffusion model is therefore incompatible with experimental results.

D. Constant-Crystal-Composition

The prediction of this model that the separation achieved should be equal to or less than one phase separation did not occur. The data in Table VIII indicate this. For each run in the two pairs, the phase separations in the freezing section were nearly the same. It is clearly

TABLE VIII

COMPARISON OF EXPERIMENTAL RESULTS WITH PREDICTION OF CONSTANT-CRYSTAL-COMPOSITION MODEL

Run	Phase Separation $= Y_{30}-X^*_{30}$	Separation $= Y_0-Y_{30}$	Column Length	Separation Per Unit length $= \frac{Y_0-Y_{30}}{}$
	Weight Fraction	Weight Fraction	cm	Weight Fraction per cm
17	0.0586	0.073	30.4	.0025
18	0.0591	0.058	25.1	.0023
21	0.0465	0.061	20.0	.0031
24	0.0480	0.086	30.4	.0029

seen that the separations achieved had no relation to these equilibrium values. In fact, for each pair of runs, the separation per unit length was nearly constant.

The data in Table IX refute the prediction of the mathematical development that a plot of $\ln(Y-X)$ vs. h will be linear. Examination of the composition data indicates that X cannot be greater than 0.625 if the function $\ln(Y-X)$ is to have meaning. But such a limitation is contrary to the phase equilibrium. The liquid in the freezing section was estimated to have the composition 0.609 weight fraction BNB by extrapolating the composition profile from the purification section. A liquid of this composition would produce crystals with a weight fraction 0.625. Or if the crystals were 0.625 weight fraction, then the liquid in the freezing section at equilibrium with those crystals would have the composition 0.576 weight fraction.

Thus the two predictions of the constant-crystal-composition model are in disagreement with experimental data. This model can not be used to describe the column crystallization of mixtures which form solid solutions although it was used to describe data from a eutectic system.

TABLE IX

PROFILE OF LIQUID COMPOSITION FOR ONE RUN

Tap No.	Position cm	Composition weight fraction
FS	1.0	0.609 '($X^* = 0.658$)
7	6.7	0.625
6	11.9	0.641
5	17.0	0.657
4	22.0	0.672
3	26.8	0.687
2	32.1	0.703
1	37.0	0.708

CHAPTER VI

ANALYSIS OF DATA FROM A SYSTEM FORMING A EUTECTIC

The applicability of the mass-transfer-limiting model, Model I, to two systems which form solid solutions was demonstrated in the previous section. This demonstration indicated that both dispersion within the liquid phase and mass-transfer between phases take place in column crystallization with solid solutions. In this section it is shown that the same mechanisms apply in the column crystallization of a eutectic system.

A. Determination of Diffusion and Mass-Transfer Factors

Equation (19), which is reproduced here, was generated in the description of Model I.

$$Y = b/R_4 + C_3 \exp(hR_4/H) \qquad (19)$$

Development of this equation indicated that the slope of plots of Y vs. h could be used to evaluate H which is defined by Equation (18).

$$H = E/L + L/F \qquad (18)$$

Further, plots of HL vs. L^2 could then be used to evaluate D and K.

A parallel procedure exists for eutectic systems. Equation (70), taken from the model of constant-crystal-composition, is similar to Equation (19).

$$Y = X_o + C_3 \exp(hR_2/R_1) \qquad (70)$$

This equation indicates that the slope, S, of a plot of $\ln(Y-X)$ vs. h

can be used to evaluate R_1/R_2. R_1/R_2 differs from H only in that m is replaced by α. Thus plots of LR_1/R_2 vs. L^2 can be used to evaluate D and K.

In order to prepare plots of LR_1/R_2 vs. L^2, data presented by Albertins[1] were used. His data, which were values of S, were converted to values of R_1/R_2. These values are presented on Figure 29, plotted against L. The crossplots of LR_1/R_2 vs. L^2 which result from Albertins data are shown on Figures 30 and 31. Although there is scatter, the linearity of the curves is clear. The least-squares lines from Figures 30 and 31 were used to calculate the curves presented on Figure 29.

Table III, presented earlier, summarizes the results taken from Figures 30 and 31. This table also shows typical diffusivities and mass-transfer coefficients taken from the literature. The agreement among the various values is satisfactory.

1. Effects of Agitation

Values of D and K are not only in good agreement with literature values, the variations of these parameter with agitation can be adequately explained. Data extracted from Figures 30 and 31 are plotted on Figure 32 as E vs. $f^{1/2}$. Such a plot is suggested by Hayford[20] who studied the effects of pulse frequency and stroke on diffusivity. The agreement between the data and the predicted variation is extraordinary.

The above analyses indicate that a mathematical description of column crystallization which explicitly contains terms relating to

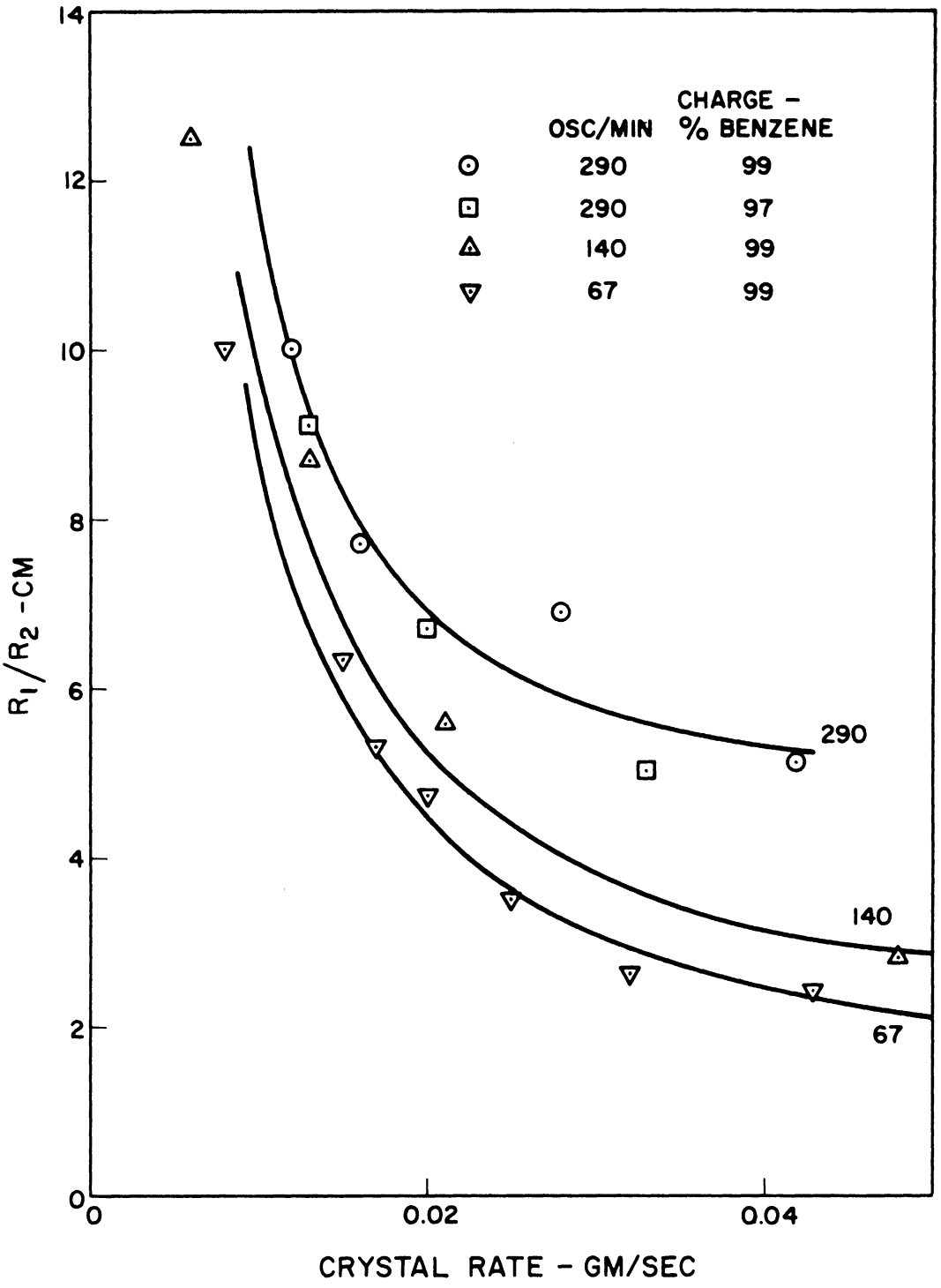

Figure 29. Effect of Crystal Rate on Column Performance.

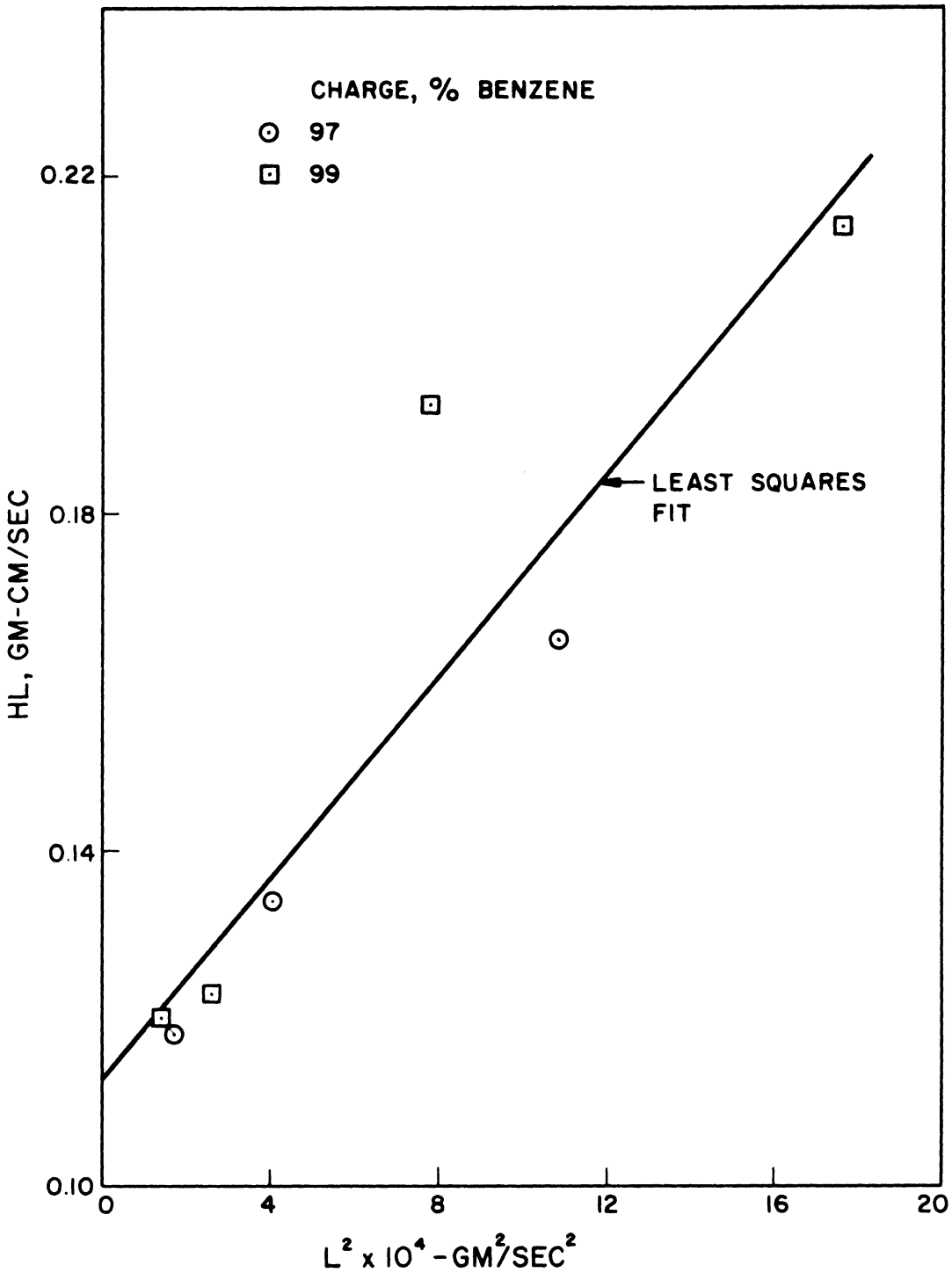

Figure 30. Determination of Diffusivity and Mass-Transfer Coefficient.

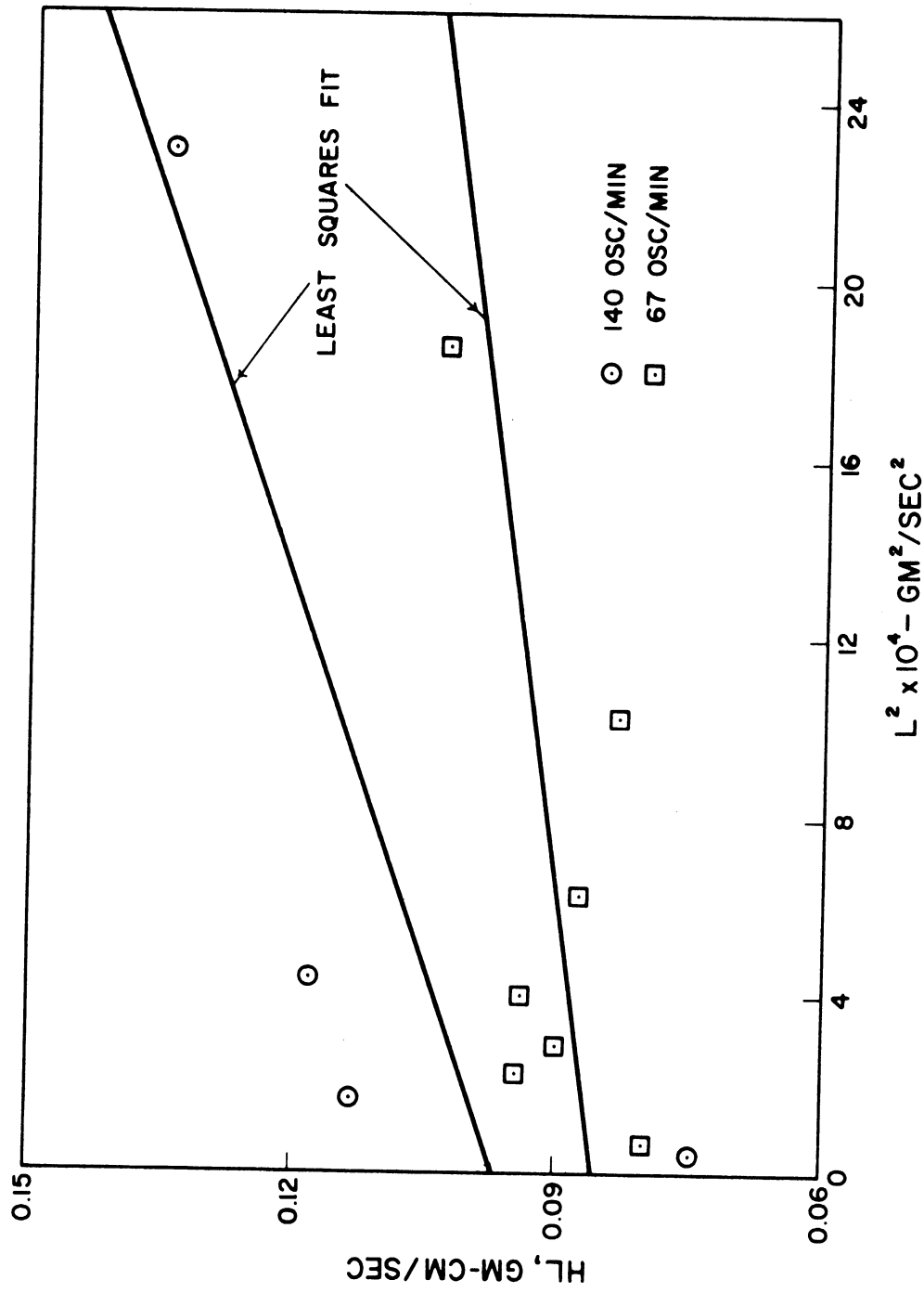

Figure 31. Determination of Diffusivities and Mass-Transfer Coefficients.

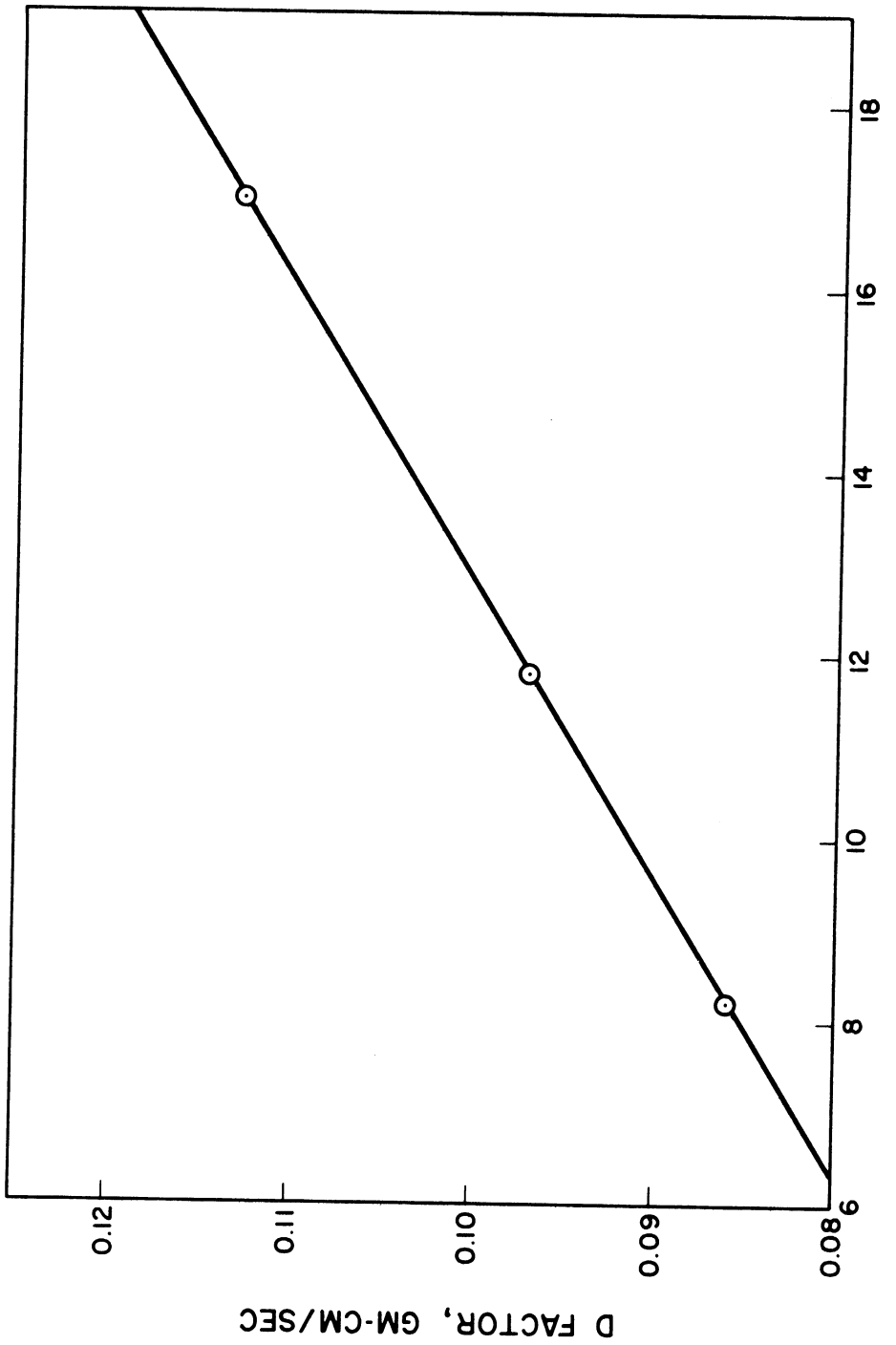

Figure 32. Effect of Agitation on Diffusivity.

mass-transfer and dispersion is entirely compatible with experimental data. This conclusion is true for a eutectic system as well as for two systems which form solid solutions and confirms the prediction of Powers[32].

Such a conclusion, and the agreement indicated in Table III, are contrary to previously published statements.[1] It was contended that the data in Figure 29 should be correlated with a model including only a diffusivity which is a function of crystal rate. It was also indicated that these data, if used to determine a mass-transfer coefficient, give a value which differs from literature values, and thus from the results of the present analysis, by four orders of magnitude. The fallacy in the analysis which permitted such conclusions is indicated below.

2. Fallacy

The previously published analysis indicated that the composition of the liquid could be represented mathematically by Equation (73).

$$Y = X_o + C_1 \exp(q_1 h) + C_2 \exp(q_2 h) \qquad (73)$$

Here q_1 and q_2 both contain factors relating to diffusion and mass-transfer. This equation indicates that a plot of data ln Y vs. h will be linear if X_o and one of the constants C are zero. Such a plot, reproduced from Albertins' paper, is shown in Figure 33. Clearly, the line is not linear.

The curvature indicated on this plot was attributed to the second exponential, and X_o was assumed to be zero. The data were fit statistically to evaluate C_1, C_2, q_1, and q_2. The line drawn on Figure 33

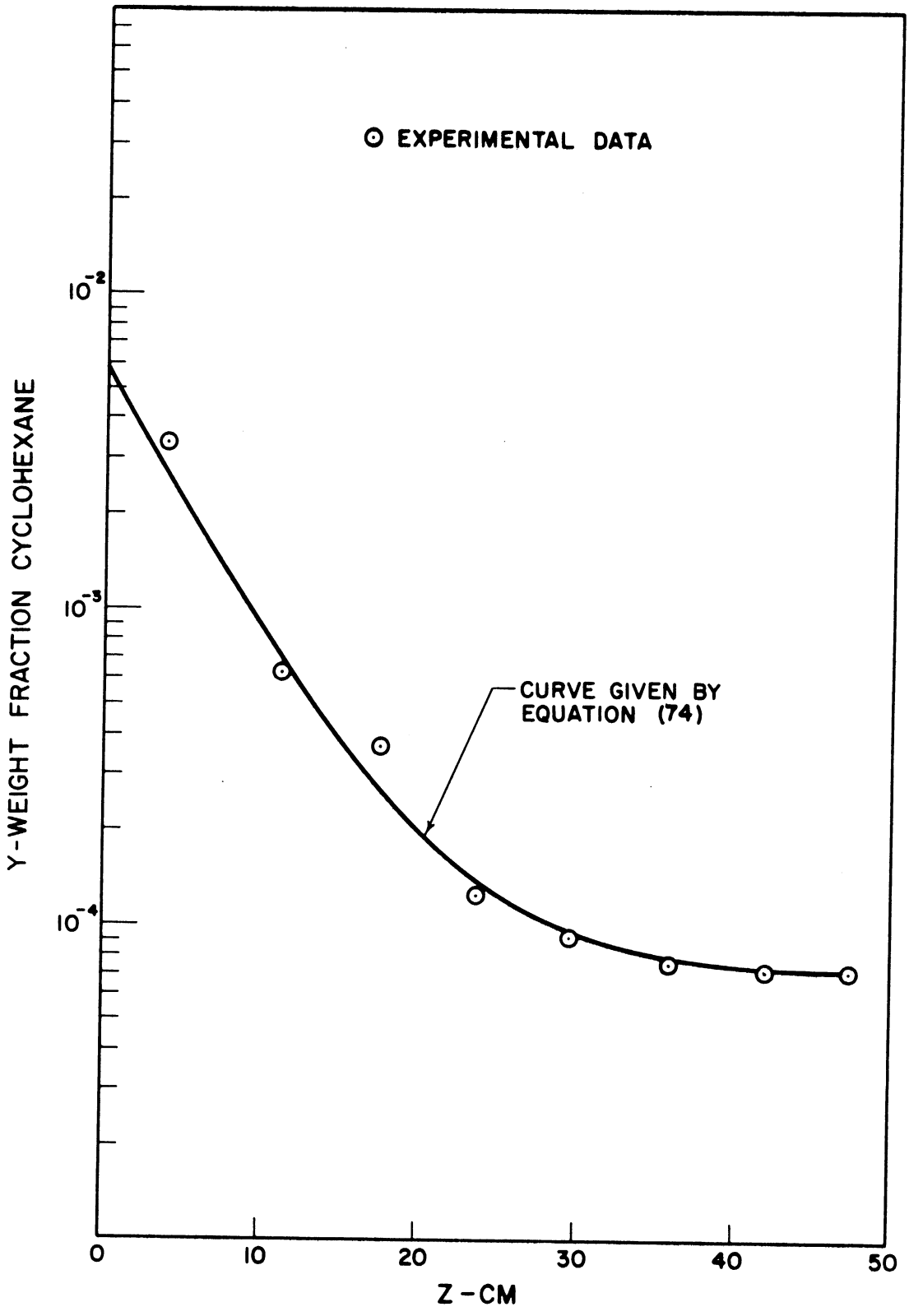

Figure 33. Profile of Liquid Composition for One Run.

is given by Equation (74).

$$Y = 0.0057 \exp(-0.193 Z) + 0.000087 \exp(-0.00442 Z) \quad (74)$$

Here Z is the column position measured from the freezing section ($Z = 50-h$).

Values for K and D were determined from q_1 and q_2. The value of K was about four orders of magnitude different from the values determined by previous investigators in other types of studies. It was therefore concluded that a model including mass-transfer and assuming X_o to be zero was incompatible with the data. Such a conclusion is not dictated by this result. The result does indicate that either:

1. The drawn conclusion is correct, or
2. The assumptions, that $X_o = 0$, and that the curvature of ln Y vs. h is attributable to the second exponential, are incorrect.

It appears that the second of these alternatives was not considered previously.

Detailed examination of the form of q_1 and q_2 in Equation (62) (or in Equation (55)), indicates that the second of these alternatives must be correct. In fact, the constant in front of one of the exponentials must be zero. The same reasoning as applied in the case of the mass-transfer-limiting model can be applied here. For either very high or very low crystal rates, one of the q_i becomes very large. The corresponding C must be zero to keep Y between zero and one for all crystal rates.

Also, the second argument used to reduce Equation (67) from three terms to two, as presented in the development of the constant-crystal-composition model, indicates that C_2 must be zero.

Albertins' data are reanalyzed below applying the second alternative mentioned above. A plot of $\ln (Y-X_0)$ vs. h, with $X_0 = 0.000071$, is shown in Figure 34. The linearity is clear. This indicates that one of the C's in Equation (73) is zero. The q accompanying the non-zero C thus retains effects of mass-transfer and of dispersion.

Using data from several runs, as was done in Chapter VI, values of D and K were determined. The values determined in this way are in good agreement with those found in the literature. (See Table III).

The results of this analysis indicate that a model which incorporates both mass-transfer and dispersion in column crystallization is not incompatible with data taken on a eutectic system as was previously postulated.

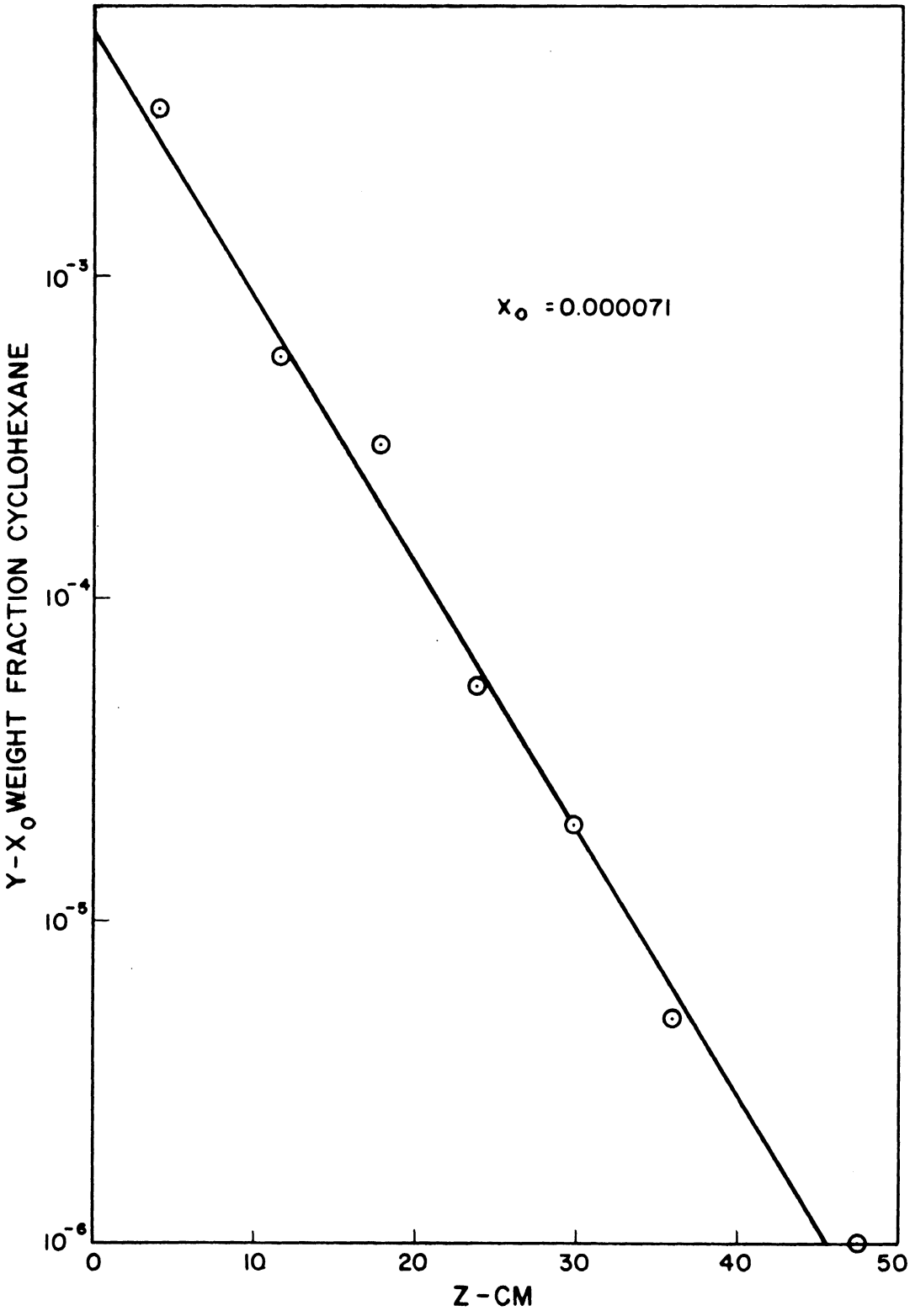

Figure 34. Re-analysis of Previously Reported Data.[1]

CHAPTER VII

SUMMARY

The data and interpretations presented in this dissertation demonstrate that the mechanisms of mass-transfer between phases and dispersion within the liquid phase effect and limit separations by column crystallization. Data from three diverse binary systems were used in this demonstration. These systems were:

1) m-bromonitrobenzene - m-chloronitrobenzene which forms a solid solution with a nearly linear phase relation;
2) azobenzene - stilbene which forms a solid solution with a highly non-linear phase relation; and
3) benzene - cyclohexane which forms a eutectic.

Four mathematical models, each based on different assumptions as to the physical nature of column crystallization, were formulated. These models were sequentially evaluated for agreement with pertinent data. Major contradictions between model and data existed for three of the models. The fourth model did not disagree with the data in any of the tested aspects.

The model which is consistent with the data describes the nature of column crystallization as being dependent on the type of system under consideration. Column crystallization of a eutectic system is basically a washing operation. A nearly pure crystal forms in the freezing section and is surrounded by an impure adhering liquid. As the crystal moves through the purification section, this impure liquid is purified by mass-transfer to the free reflux liquid. Dispersion occurs in this reflux.

Column crystallization of a system which forms a solid solution is essentially a process of melting and recrystallization. As the crystal formed in the freezing section moves through the purification section, it becomes unstable. Heat-transfer from the warmer liquid melts the unstable crystal. This heat-transfer takes place rapidly, but the exchange of material between the old crystal and the reflux liquid is limited by mass-transfer considerations. As in the eutectic system, considerable dispersion occurs in the reflux liquid.

In either type of system, however, both dispersion and mass-transfer occur. In keeping with this result, values for effective diffusivity and mass-transfer coefficient, which were determined for the first and third chemical system mentioned above, were in good agreement with literature values taken from other types of studies. The effects of agitation on diffusivity were also in good agreement with predictions of literature correlations.

CHAPTER VIII

SUBJECTS FOR FUTURE INVESTIGATION

Data obtained during the present study, as well as previous data[1], show that in the regime of operation thus far achieved, dispersion within the liquid phase is the dominant effect in column crystallization. The result of dispersion is of course to limit the separation otherwise being produced by the phase separation within the freezing section and by the mass-transfer which occurs within the purification section. Studies should be undertaken to find ways of reducing the effect of dispersion in relation to that of mass-transfer.

One obvious way of achieving the desirable reduction at total reflux would be to produce a higher flux of crystals. This is seen by examination of Equation (16) which defines H, the effectiveness of the column as a separating device. A small H is desirable. This could be attained by increasing L to the point at which H is a minimum with respect to flux. Thus a study to determine the factors which limit the flux of liquid and solid through the column should be established.

A second means of reducing the effect of dispersion is to reduce the diffusivity. This could be done by reducing the three variables which cause agitation; rate of rotation, rate of oscillation, and stroke of oscillation. Previously reported data indicate that there is an optimum set of these three variables. That is, reduction below certain values for each parameter is detrimental to separation. A method of reducing the optimum value of D should be sought. Such

a method might include changing the configuration or the orientation of the crystallizer.

BIBLIOGRAPHY

1. Albertins, R., Ph.D. Dissertation, The University of Michigan, 1967.

2. Albertins, R., W. C. Gates and J. E. Powers, in Fractional Solidification (M. Zief and W. R. Wilcox, eds.) Marcel Dekker, Inc., New York (1967).

3. Anikin, A. G., Dokl. Akad. Nauk SSSR, 151, (5), 1139 (1963).

4. Anikin, A. G., Russ. J. Phys. Chem., 37 (3), 377 (1963).

5. Arnold, P. M., U.S. Patent 2, 540, 977 (1951).

6. Carslaw, H. S., and J. C. Jaeger, Conduction of Heat in Solids, 2nd Ed., Oxford University Press, London, 1959.

7. Cohen, K. J., Chem. Phys., 8, 588 (1940).

8. Findlay, R. A. and D. L. McKay, Chem. Eng. Progr. Symp. Ser., 25, 163 (1959).

9. Findlay, R. A., U. S. Patent 2,683,178 (1954).

10. Findlay, R. A., U. S. Patent 2,676,167 (1954).

11. Findlay, R. A., U. S. Patent 2,855,100 (1958).

12. Findlay, R. A., U. S. Patent 2,898,271 (1959).

13. Findlay, R. A., and J. A. Weedman, in Advances in Petroleum Chemistry and Refining, Vol. 1, (Kobe, K. A., and John J. Mcketta, Jr., eds.), Interscience Publishers, Inc., New York (1958) p. 119.

14. Frevel, L. K., U. S. Patent 2,659,761 (1953).

15. Gates, L. J., unpublished data.

16. Green, R. M., U. S. Patent 2,765,921 (1956).

17. Hachmuth, K. H., U. S. Patent 2,894,997 (1959).

18. Hartland, S., and J. C. Mecklenburgh, Chem. Eng. Science, 21, 1209 (1966).

19. Hasselblatt, M. M., Zeit. für Physik. Chem., 83, 1 (1913).

20. Hayford, D. A., Ph.D. Dissertation, Virginia Polytechnic Institute, 1961.

21. Jones, S. C., Ph.D. Dissertation, The University of Michigan, 1962.

22. Kuster, F. W., Zeit. für Physik. Chem., 8, 577 (1891).

23. Lange, N. A., ed., Handbook of Chemistry, 10th Ed., McGraw-Hill Book Co., New York, 1961.

24. Leva, M., Fluidization, McGraw-Hill Book Co., New York, 1959.

25. Lewis, J. B., Chem. Eng. Science, 3, 248 (1954).

26. Li, N. N., and E. N. Ziegler, Ind. Eng. Chem., 59 (3), 30 (1967).

27. McKay, D. L., G. H. Dale, and J. A. Weedman, Ind. Eng. Chem., 52, 197 (1960).

28. McKay, D. L., in Fractional Solidification, (M. Zief and W. R. Wilcox, eds.) Marcel Dekker, Inc., New York (1967) p. 427.

29. McKay, D. L., and H. W. Goard, Chem. Eng. Progr., 61 (11), 99 (1965).

30. McKay, D. L., U. S. Patent 2,823,242 (1958).

31. Moon, J. S., Ph.D. Dissertation, University of California, 1964.

32. Powers, J. E., in Symposion über Zonenschmelzen und Kolonnen' Kristallisieren (H. Schildknecht, ed.) Kernforschungszentrum, Karlsruhe, 1963, p. 57.

33. Quigg, D. J., U. S. Patent 2,890,239 (1959).

34. Reid, R. C., and T. K. Sherwood, The Properties of Gases and Liquids, 2nd Ed., McGraw-Hill Book Co., New York, 1966.

35. Schildknecht, H., presented at Symp. on Crystallization, 56th Nat'l. Meeting, A.I.Ch.E., San Francisco, 1965.

36. Schildknecht, H., Anal. Chem., 181, 254 (1961).

37. Smoot, L. D., and A. L. Babb, Ind. Eng. Chem. Fund., 1, 93 (1962).

38. Tarr, T. A., U. S. Patent 2,874,199 (1959).

39. Thomas, R. W., U. S. Patent 2,854,494 (1958).

40. Thorsen G., and S. G. Terjesen, Chem. Eng. Science, 17, 137 (1962).

41. Timmermans, J., Physico-Chemical Constants of Pure Organic Compounds, Elsevier Publishing Co., Amsterdam, 1950.

42. Washburn, E. W., ed., International Critical Tables, 1st Ed., Vol. IV, McGraw-Hill Book Co., New York, 1928.

43. Weedman, J. A., and R. A. Findlay, Petrol. Refiner, 37, 195 (1958).

44. Weedman, J. A., U. S. Patent 2,747,001 (1956).

45. Yagi, S., H. Inove, and H. Sakamoto, Kagaku Kogaku, 27 (6), 415 (1963).

APPENDIX A1

DETAILED DESCRIPTIONS

a. Equipment

The equipment used in this study was very similar to that previously described by Albertins[1]. Its main parts were the column itself, a drive mechanism, a refrigerant bath, electrical control and measuring devices and an electronic temperature controller. The column used in the present study is illustrated in Figure 2.

The column was formed from a 32 mm Pyrex glass tube 54.5 cm long. This tube enclosed a 0.497 inch stainless-steel shaft and a stainless-steel spiral. The spiral fit tightly around the central shaft, and loosely along the glass column.

The bottom of the glass column consisted of the freezing section (F.S.) with a short "dead space" below it. The F.S. was defined on the inside by the glass column and on the outside by a glass jacket of 48 mm Pyrex tubing. Two glass jackets were used in this study. One was 5.0 cm long, the other 7.0 cm. The top and bottom of the F.S. were formed by nlyon rings which held the glass jacket in place. Each ring contained two taps through which refrigerant could be passed. One of these taps was positioned radially, the other tangentially. The contacts between the various pieces of the F.S. were sealed with neoprene O-rings.

The small "dead space" below the F.S. was uninsulated, and exposed to ambient. It was surrounded by approximately 11 ft. of tightly wound resistance wire. Defining this dead space at the bottom, and forming the bottom of the column, was a nylon plug. This plug fit

tightly around the stainless-steel shaft and loosely into the glass column. The seals around this plug were formed by Viton O-rings. There was a small drain through the bottom plug. This drain was capped with 1/16 inch stainless-steel tubing which was closed at one end and which could be pulled from the nylon plug.

The purification section of the column crystallizer was of various lengths as determined by the position of the melter relative to that of the stationary freezing section. 3.5 cm above the F.S. and at 5 cm intervals thereafter there were sample taps in the wall of the glass column. Each consisted of an opening through the column wall. This opening was narrow (about 1/16 in diameter) at the spiral end and about 1/4 inch at the outside. Into each tap a rubber septum was placed to form a seal.

An 18 gage hypodermic needle, with a 3/4 inch square-ended tube, passed through each septum toward the spiral. The end of the needle was within 1/8 inch of the spiral when there was no force on the needle. Each needle was wrapped with about 3 feet of resistance wire, and was capped with a rubber septum like the ones closing the taps. The resistance wire on the seven taps was connected in series to form a total resistance of 15 ohms.

The purification and melting sections were nearly surrounded with close-fitting polyurethane insulation at least 2 cm thick. A gap of less than 2 cm, for the entire length of the column, permitted visual observation of the operation of the column. This polyurethane insulation was surrounded by an air space from 1 to 5 cm in thickness which was in turn defined on the outside by polyurethane foam 5 cm

thick. The top and bottom of this air space was enclosed by polyurethane foam 3 cm thick. A cross-section of the column and the layers of insulation is illustrated in Figure 35.

The melter in the melting section was a Chromalox 75W cartridge heater, Model No. C301 INY. This heater had a resistance of 194 ohms, was 1/2 inch in diameter and 6 cm long. It was welded to the stainless steel shaft which passed from the bottom of the column through the nylon plug, the freezing section and the purification section.

The position of the melter within the column, and therefore the length of the purification section, was varied. The bottom of the melter was more than 23 cm and less than 35 cm from the top of the freezing section.

The glass column forming the crystallizer extended above the melter. The top of this column was wrapped with 9 ohms of resistance wire to form an auxilliary heater. If the melter could not melt all the crystals because insufficient energy was supplied, the auxilliary heater could be used to re-establish an energy balance quickly.

The stainless-steel spiral, which extended from the freezing section through the glass column and out its top end, had a modified, lenticular cross-section. This cross-section is sketched below. The spiral, which had 25 turns in 23.3 cm, was supplied by Specialty Design Co., Ann Arbor, Michigan.

The spiral was connected to a drive mechanism which permitted continuous variation of rate of rotation, and frequency and stroke of oscillation. This drive was supplied by The Upjohn Co., Kalamazoo, Michigan.

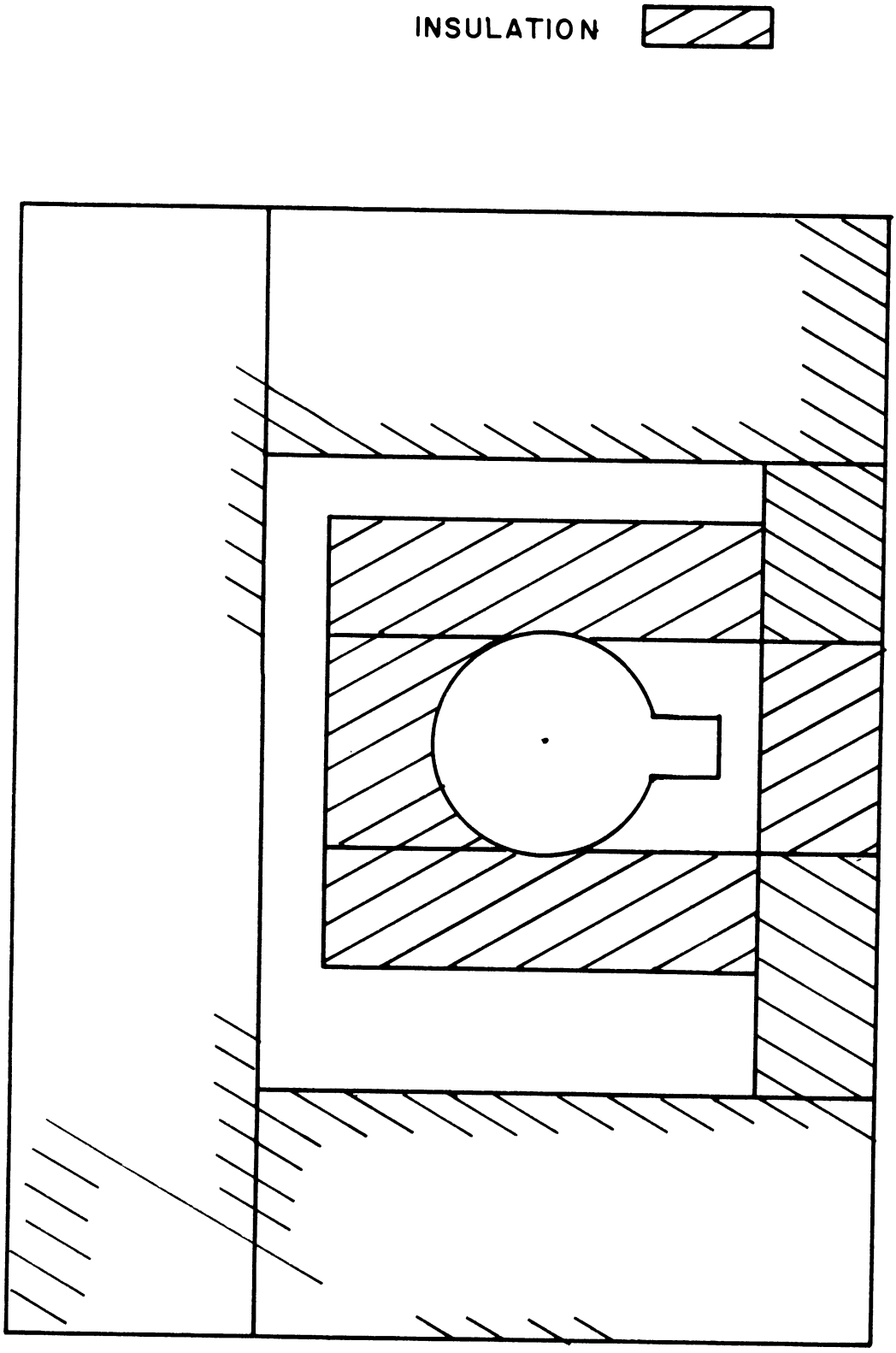

Figure 35. Cross-sectional View of Column with Insulation in Place.

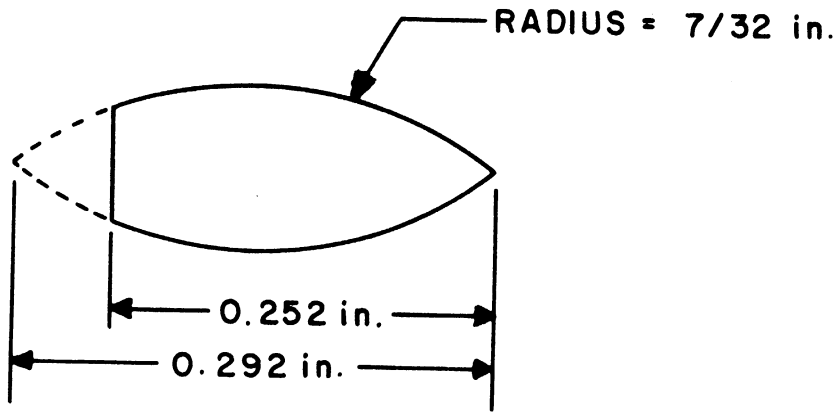

Figure 36. Cross-section of Wire from which Spiral was Wound.

Water baths, in which the temperature of the fluid could be regulated, served as sources of refrigerant. These baths had a continuous flow of tap water through them.

Electrical power to the melter was adjusted by means of a Variac V20H variable transformer. This transformer was connected to the wall circuits through two rheostats connected in series. Large changes in the main transformers setting were thus required to effect small changes in the voltage applied to the melter. This voltage was measured by two meters which had been calibrated against a Siemens-Halske voltmeter previously calibrated in the Electrical Measurements lab of the University of Michigan by Dr. Mosher.

Electrical power to the auxilliary heater at the top of the column, to the sample taps, and to the heater around the dead space below the freezing section was supplied by a 250 W Lionel transformer, model ZW, which was connected directly to the wall circuits.

A 4-channel, electronic, phase-shift, proportional controller was used to control the temperature in the water baths, and thus to the annulus of the freezing section. This device maintained the temperature of the water to about $\pm$ 0.05 C°. This value is estimated from the fact that the reading of mercury thermometers, graduated in units of 1 C°, and reading 5.5 C°/cm, did not show any observable variation in temperature. The controller controlled on the resistance of a 500 ohm, disk thermister (Fenwal model JB25J1) which was immersed in the bath.

b. Operating Procedures

The procedures followed in operating and sampling the column are described in this section.

The column, having been cleaned with benzene and dried, was assembled and put in place. The sample taps, with new septums at each end of each hypodermic needle, were set into the column. The outer layer of polyurethane foam, including the top and bottom pieces, was put in place. The inner jacket of foam insulation was not wrapped around the column. Air, heated to 65°C or more, was circulated in the space between the column and the outer enclosure for two hours or more.

While the column was being heated by the air, the material to be charged to the column was heated in a steam bath. Also during this period the water baths, used as the source of refrigerant, were heated. The temperature to which the baths were raised was sufficiently high that, when introduced, the change would not freeze in the freezing section.

Just before the charge was added to the column the refrigerant pump was turned on. Also power was supplied to the melter and to the auxilliary heater at the top of the column. In addition, the hot air was turned off and the front of the outer insulation was removed. The spiral drive was turned on and the mixture of BNB and CNB was introduced

The amount of charge varied with the position of the melter within the column. However, for all runs, the liquid level on charging was between 2 and 3 cm, above the top of the melter. This prevented the level of the slurry, which formed as the liquid was cooled, from dropping below the top of the melter.

With the column operating, the inner jacket of insulation was put in place and the front of the outer jacket was kept off. The temperature of the water (the refrigerant) was allowed to drop slowly to

the desired temperature. Crystals formed in the freezing section and filled the bottom of the column. As the level of the slurry-liquid interface rose, the front of the outer jacket of insulation was added.

The power supplied to the melter was increased gradually as the interface between the slurry and the clear liquid rose. When this interface had reached the melter, or about the middle of it, maximum power for that given run was being supplied. At this same time, the entire front part of the outer insulation was put in place. This piece was then disturbed only occasionally to observe the level of the crystals.

As the concentration gradient established itself within the column, the crystal rate changed. Consequently the power input to the melter decreased with time. A proper balance between the heat loads in the freezing and melting sections was maintained by observing the level of the crystals. After about 4 hours no changes in power input were required. After 2 to 3 hours of running with no changes in power the liquid in the column was sampled.

While a run was in progress the syringes and needles to be used in sampling were washed in boiling water containing a phosphate soap, rinsed in distilled water and then in acetone, and finally dried. During this same time 3 cc, glass sample vials were weighed to $\pm$ 0.0001 gm, and capped.

About 15 minutes prior to sampling the dried syringes were assembled and placed in a steam bath. Ten minutes later the front part of the outer jacket of insulation was removed and power was applied to the sample taps. This energy melted any solid which had formed within the syringe needle which comprised the tap.

After the tap heaters had been on for five minutes the drive for the spiral was turned off and the samples were taken. The top tap was always sampled first and the bottom one last. This prevented the act of sampling from disturbing the liquid at the taps yet to be sampled. As each sample was taken, it was injected into the previously weighed sample vials. The entire sampling procedure usually took 3-1/2 minutes.

When the last sample had been taken, either the column was drained if no further runs were to be made, or the drive was started again and a new run made.

The vials containing the samples were weighed and the weight of each sample was determined. Samples usually weighed about 0.1 gram. Each sample was then diluted with methyl chloroform (MC) (Eaton Chemical, Uninhibited trichloroethane) capped and placed in a freezer maintained at -23°C.

The dilution with MC was performed as follows. MC at room temperature was measured with a 0.5 ml syringe which was graduated in units of 0.01 ml. A volume of MC in ml equal to twice the weight of the sample in grams was added to each sample.

c. Analytical Procedures

Samples of liquid extracted from the column were analyzed by gas chromatography. A model 1522-1B Aerograph chromatograph (Ser. No. 762-0068) was used. Repeat analyses, made either sequentially or up to four months apart, indicated that the technique was highly reproducible. The entire analytical procedure is described in detail in this section.

Chromatographic columns of 1/8 inch, thin-wall, stainless-steel were used. These were 5-1/2 feet long and were filled with 2.1 ± 0.2 grams of packing. The packing material was 30/60 Chromosorb A, AW (Johns Manville, lot 02746), seived to 40/45 onto which 10 weight percent of active liquid phase had been deposited. The liquid phase was Carbowax 20M (Wilkens 82-1115). It was deposited by evaporating at room temperature the methanol (Baker, Reagent 9070 lot 32776) from a 10% solution in which the Chromosorb was slurried.

Prepurified nitrogen (Matheson, FG-4908) was used as the carrier gas. This gas gave greater responses and shorter residence times than did helium. The carrier flow was 50 ± 5 cc/min at an inlet pressure of 20 psig.

Flame ionization detectors were used. These were cleaned regularly as the materials being analyzed produced considerable residue and corrosion. Matheson prepurified hydrogen (FG-4896) was burned in the detectors. Air, supplied from the room through a prepackaged molecular sieve by small fish-tank pumps was also used.

The temperatures of the various parts of the chromatograph were as follows. The oven containing the columns was at 197°C. The injector was at 230°C and the detector block at 225°C.

Output from the detectors, after amplification, was recorded on a Brown (Model 15312V-X-30Y10, Ser. No. 324587) recorder. Simultaneously, an Infotroncis Model CRS-10H (Ser. No. 1728) integrator measured and printed out the peak areas. A sample analysis is shown on Figure 37. The integrated areas, together with the corresponding electrometer attenuations, are also presented on the figure. The quotient of the BNB

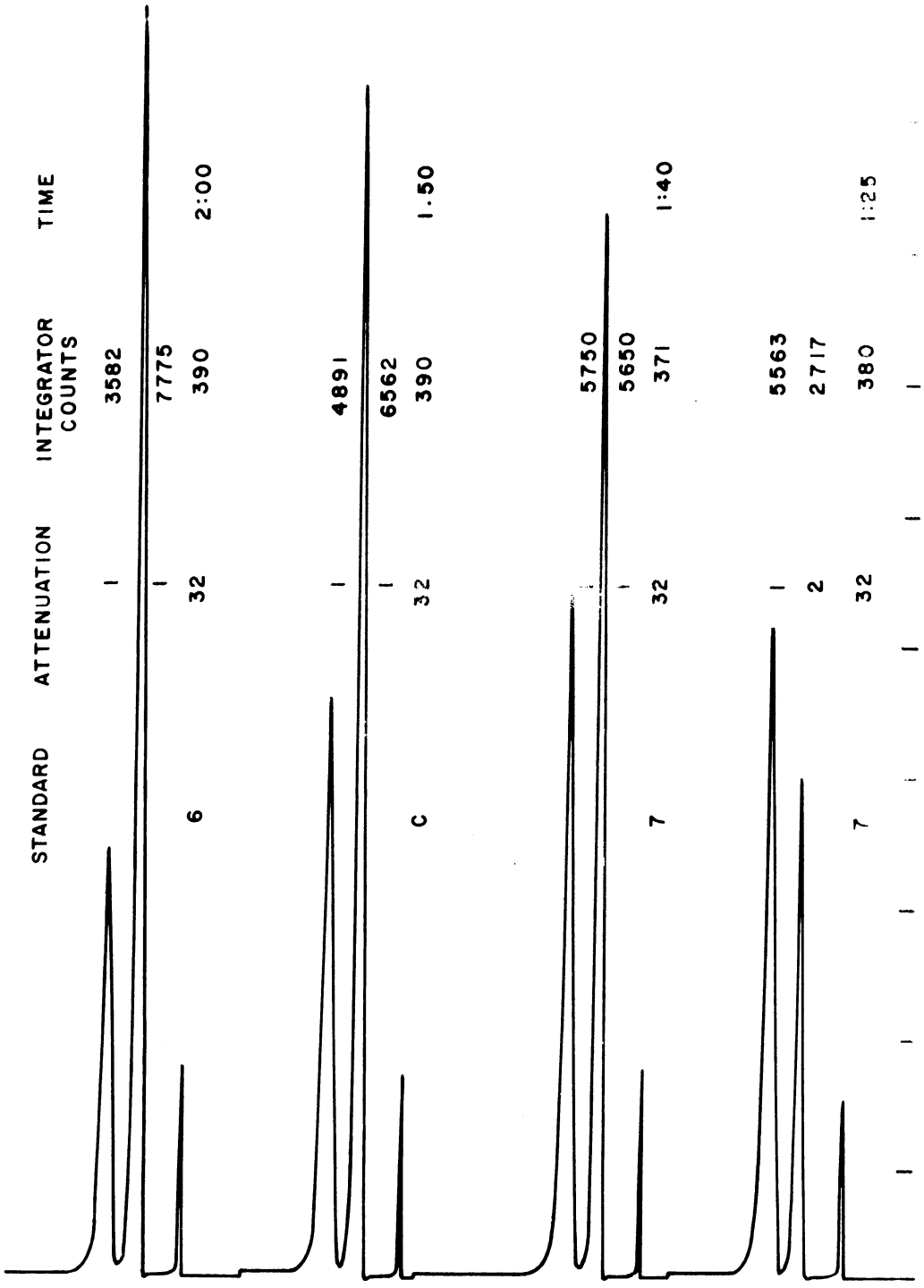

Figure . Sample Chromatogram.

peak area divided by the sum of the peak areas was determined to define a calculated mole per cent BNB.

In analyzing samples, 0.8 μl of material, prepared as described in Appendix A1-b were injected. Samples were analyzed in the following order: 6, 1, 3, 7, 4, 2, 5. After a set of samples had been run, two or three standard samples, which had been prepared by weighing in quantities of BNB, CNB and solvent (methyl chloroform-MC), were analyzed. From the analyses of these known samples, a calibration of actual composition versus experimentally determined composition was prepared. The linearity of these calibrations is demonstrated in Figure 38 and in Table X. Such calibration curves were finally used, with the chromatographic analyses of the unknown samples, to determine actual composition. This latter composition used in all treatments of the data.

TABLE X

COMPARISON OF ANALYSES
OF STANDARD SAMPLES

Sample	Analysis of Standard Sample	
	mole fraction BNB	
	by weighing	by GC
5	0.072	0.065
6	0.313	0.315
C	0.430	0.427
7	0.502	0.505
B	0.600	0.595, 0.608
D	0.742	0.743
A	0.880	0.879

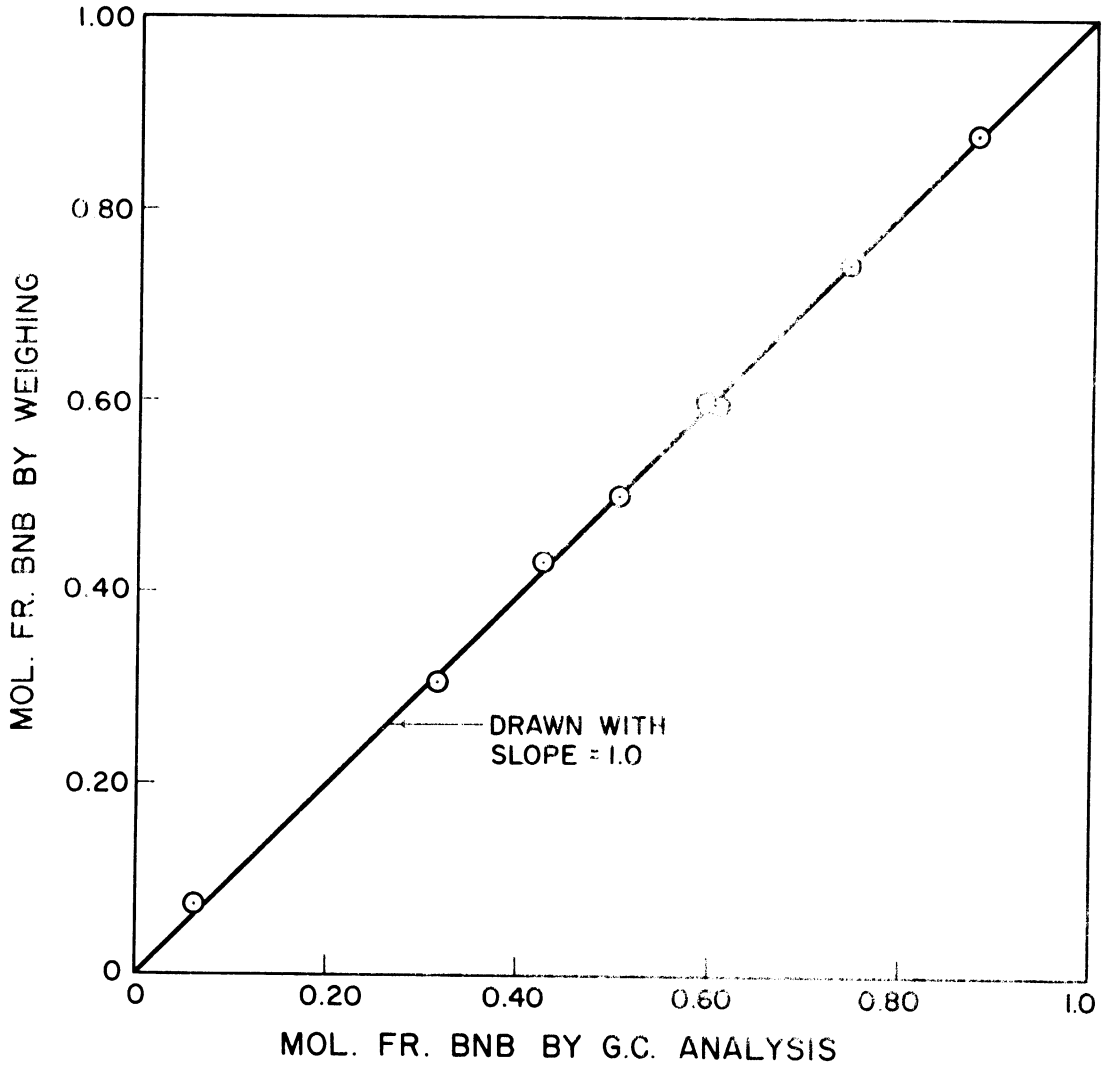

Figure 38. Linearity of Calibration of Gas Chromatograph.

APPENDIX A2

TESTS OF OPERATIONS

a. Attainment of Steady-State

All the data reported in this dissertation were taken at steady-state. The procedure by which the time required to reach steady-state was determined is described in this section.

The column was charged, operated and sampled as described in Appendix A1. The conditions of operation were chosen so that a severe test for steady-state would be made. These conditions included a low rate of agitation, a high crystal rate, and a slow approach to the ultimate crystal rate.

When the first set of samples had been taken, after 6 hours of operation, the drive to the spiral was restarted and a second run was made at the same conditions as the first. This second run lasted 2 to 3 hours from the time that equilibrium was reestablished. A second set of samples was taken about 4 hours after the first set.

The samples from the two runs were analyzed as described in Appendix A1-c. To determine whether the two runs were the same a plot of composition - run 1 vs. composition - run 2 was made. Each point on the plot thus represented two samples taken from a single tap. If there were no difference between the runs, then the slope of the line drawn through the seven points would be one. Figure 39 is such a plot. The slope of the line, as determined by a least squares analysis, is 1.012. Clearly there was no significant difference between the profiles at 6 and at 10 hours for the test illustrated. A second test for steady-state, made with a lower crystal rate, also showed no significant

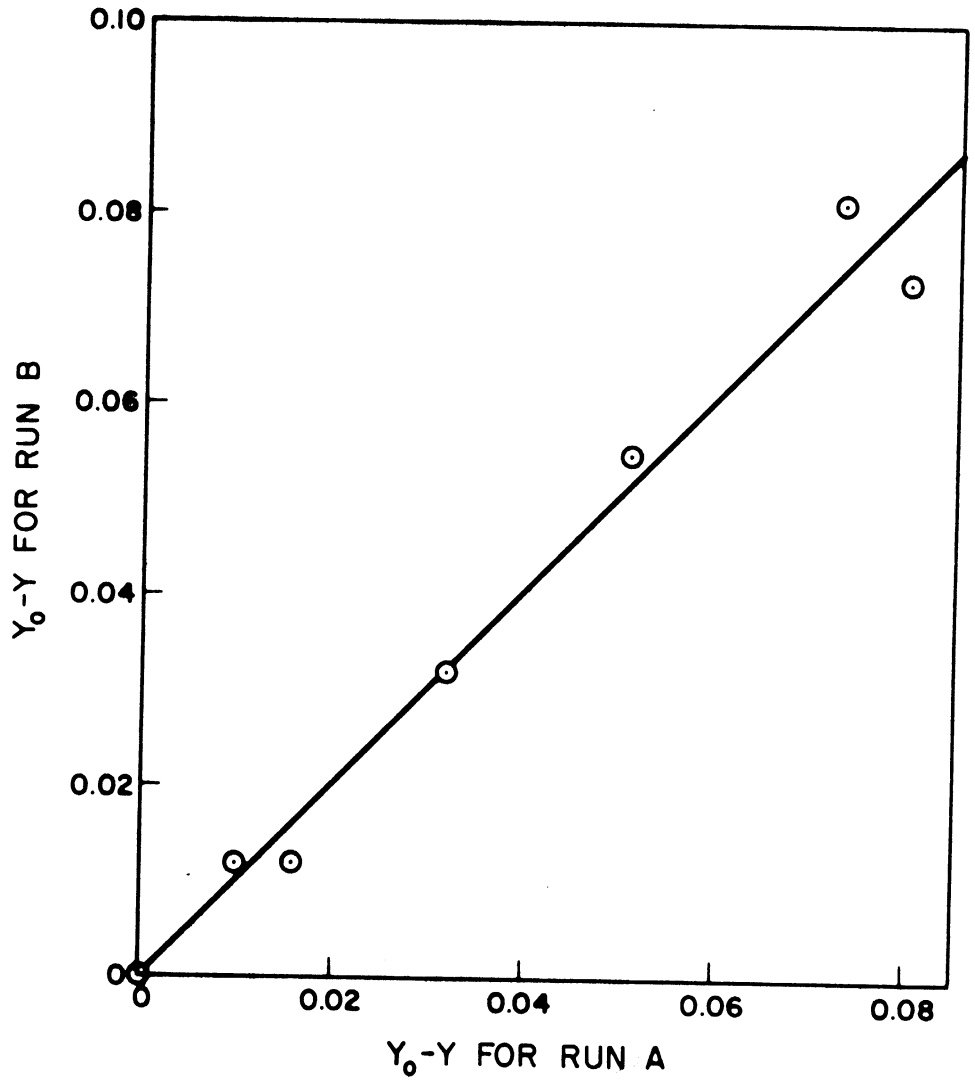

Figure 39. Illustration of Attainment of Steady-State.

difference between the two runs (slope = 1.024). As a result of these two tests, all data were taken at least 6 hours after charging.

b. Constancy of Crystal Rate

The model which describes column crystallization assumes that the flows of crystals and reflux liquid are independent of position in the column. Three pieces of evidence which support this assumption are discussed in this section. However, no direct tests of constancy were made.

The best evidence is that the model agrees with the data. Equation (22) presents the model as derived.

$$Y = Y_o - (Y - X^*)_o \, h / [E/L + L/F] \qquad (22)$$

For the most part, the term E/L was much greater than the term L/F. Thus, the concentration gradient in the liquid phase is very nearly proportional to the crystal rate (See Equation (75)).

$$Y \approx Y_o - (Y - X^*)_o \, hL/E \qquad (75)$$

If L had varied appreciably, the concentration gradient would not have been linear.

The crystal rate was measured at the top of the column by determining the power supplied to the melter. As the material in the column was more than 200° above room temperature, one would expect this measured value would be the maximum value. Thus, the "flooding" phenomenon (Appendix A3-a) which occurred at high crystal rates would have been most severe at the top of the column. In fact, there was no apparent trend in the flooding behavior.

When flooding occurred, it started essentially uniformly throughout the column. It seems reasonable, therefore, that there was no change in the crystal rate within the column.

The last evidence confirming the constancy of crystal rate occurred during the start-up period. Consequently, it is a transient effect and should not be weighed heavily. However, it is consistent with the two previous results.

Two runs were made in which the liquid charged to the column was cooled to the freezing point throughout the column. The insulation was put in place, the melter turned off, and the crystal bed allowed to form. The time required for the bed to form was determined as were the eventual crystal rate and the volume fraction solids. From this knowledge, the time required to generate the volume of crystals which were held in the column was determined.

For both runs, this latter time was about 20% more than the actual time required for the bed to form. It can be concluded that crystals were formed more rapidly than the final rate would indicate. There was either an appreciable heat leak through the insulation, or the rate of formation within the freezing section decreased with time. The latter conclusion is certainly reasonable.

When the run was started, the composition of the liquid in the freezing section was about 35% BNB. As a run progressed this value dropped to about 30%. As the temperature of the refrigerant was maintained constant throughout a run, the temperature difference between the slurry and the refrigerant decreased with time. Thus a lower crystal rate was produced at the end of a run than at the beginning.

This last discussion may not be satisfying in that it does not directly indicate that there were no heat leaks from the column. However, the described difference in times can be explained qualitatively by the mentioned phenomenon. Together with the first two results described in this section, it is felt that an adequate case for the constancy of the crystal rate is presented.

APPENDIX A3

RESULTS NOT PERTAINING TO IDENTIFICATIONS OF MECHANISMS

The previous sections of the report concern the determination of the mechanisms involved in the column crystallization of solid solutions. This section presents results which do not bear on that determination. These results concern:

1. the maximum crystal rate,
2. the effect of agitation, and
3. the effect of the spiral.

a. Maximum Crystal Rate

The maximum obtainable crystal rate was influenced by hydrodynamic factors within the column and by the construction and operation of the freezing section. The factors relating to the freezing section were the surface area and the heat-transfer coefficient between the refrigerant and the liquid being frozen.

Hydrodynamic Factors

Jackets which enclosed surface areas of 22.4 cm^2 and 16.0 cm^2 in the freezing section were used in this study.

The maximum crystal rate with the larger jacket in place was 0.040 grams solid/sec. This is equivalent to 0.027 cm^3/sec and to 0.06 cm^3/cm^2-sec. These values are low in comparison to those obtained by other workers. McKay reports0.6 cm^3/cm^2-sec for a column without a spiral, operating on cyclohexane-isooctane. Albertins[1] reported a maximum crystal rate of 0.100 gram/sec. for a spiral column of

similar dimensions to that used in the current study. This value is equivalent to 0.100 cm^3/sec and 0.16 cm^3/cm^2-sec.

Attempts to increase the crystal rate beyond the maximum produced voids throughout the column. The crystals seemed to be more tightly packed than was usual. The liquid which formed in the melting section could not percolate through the dense bed to the freezing section. This situation is similar to flooding in a gas absorption. At high gas rates, liquid is blown from the absorber. Similarly, at high crystal rates, the liquid is "blown from the purification section".

The low value obtained for the maximum crystal rate in the present study can be explained only qualitatively. It is suggested that there were smaller crystals in BNB-CNB than in the benzene-cyclohexane used by Albertins. No measurements were taken to support this contention. However, three observers at various times suggested that the BNB solids appeared small. Leva[24] reported that the maximum flow of liquid through a packed bed rises with the square of the particle diameter. Thus the ratio of the maximum flows mentioned above could be explained by a ratio of particle diameters equal to 1.7.

Surface Area

The maximum obtainable crystal rate when the small jacket was in place was 0.032 gram/sec. The limiting factor in this case was the surface area of the freezing section.

At the maximum crystal rate, crystals began to appear on the inner wall of the freezing section. If the crystal rate were not reduced, this buildup of crystals soon choked the column. In a choked column,

the spiral could not break the crystals from the wall and very quickly it no longer rotated freely. At such time, the whole column began to rotate.

When the maximum crystal rate was obtained, the temperature difference between the freezing section and the liquid was 5.1 ± 0.2C°. It is believed that at this temperature difference the temperature of the inner surface of the freezing section was low enough to permit rapid initiation and growth of crystals. The growth generated large crystals which collectively interferred with the rotation of the spiral. The alleviation of this difficulty was the use of a larger jacket, which provided an equal crystal rate from a higher inside surface tem- ure.

sfer Coefficient

arly in the experimental work, crystal rates no higher than ec could be achieved. The factor restricting the crystal time was a high, local heat-transfer coefficient.

the column was constructed, the taps for the refrigerant w radially. Thus, when the refrigerant entered the fi , it impinged directly on the inner wall. A high local hea fficient was produced. As a result, a heavy build-up of t als occurred on the wall inside the column at rather low t ferences. These crystals soon restricted the rotation of the

tion of this problem was the construction of new taps for nt. These taps were placed tangentially so that

liquid flowed around the column rather than directly against the inner wall.

b. Effect of Agitation

The effect of agitation on two variables, separation and density of slurry, is discussed in the following paragraphs.

Separation

It has been mentioned previously (Chapter V-A) that the separation increased as the agitation decreased. This is to be expected if dispersion in the liquid phase is the largest factor limiting separation.

The results discussed before were, however, all taken from runs in which the slurry in the column appeared to be uniform. That is, there was no settling of the crystals between turns of the spiral. Such runs were therefore made with an agitation higher than some minimum allowable value.

When a run was made with less than this minimum agitation, the separation decreased significantly. For such runs, the crystals settled measurably. There was in effect then two non-mixing bulk phases. One was the slurry moving upward toward the melting section. The other was the free liquid moving down. These two phases did not mix together so there was little opportunity for mass-transfer between phases.

Table XI presents data which describe the effect of agitation on separation. In Run 20 segregation of the crystals occurred. It is evident that a lower separation occurred in this run.

TABLE XI

EFFECT OF SLURRY SEGREGATION ON SEPARATION

Run	Agitation		Separation per cm of column
	OPM	RPM	weight fraction per cm
21	43	45	.0031
20	31	29	.0014

Density of Slurry

It was observed several times that the density of the slurry (the volume fraction solids) decreased as agitation increased. This observation is based on the fact that the interface between the crystal slurry and the liquid above it rose or fell rapidly as the agitation was increased or decreased, respectively. No data concerning the extent of the rise and fall were taken, but the effect was real and reproducible.

c. Effect of Spiral

Previous investigators have referred to the spiral as an agitator and as a conveyor. The results of the present study indicate that the latter description is not correct.

When a run was started, large crystals sometimes formed. These were generally conveyed to the melting section quite rapidly. However, once an appreciable bed of crystals had been established, no large crystals were formed and a fairly sharp interface between slurry and clear liquid was produced. The position of this interface could be

maintained any place in the column by balancing power input in the melting section and the heat load in the freezing section. The interface dropped when the melter power was too high, and it rose when the power was too low. If the two heat loads were dropped to zero, the interface remained stationary. It did not rise as one would expect if the spiral were acting as a conveyor.

APPENDIX A4

AREAS OF FUTURE WORK PERTAINING TO COLUMN OPERATION

The results described in the previous appendix raise several questions which might form the basis for future studies. The questions are discussed briefly in this section.

The results presented in the previous section indicate that a crystal rate, greater than that corresponding to $H_{minimum}$ which is defined as L_{min}, could not be produced. However, Albertins did attain a crystal rate equal to L_{min}. It was also suggested in this report that the maximum crystal rate, L_{max}, is fixed by the diameter of the particles. It would seem advantageous to determine the parameters which limit the crystal size. Then perhaps rates equal to L_{min} could be achieved regularly.

Low separations accompanied the segregation which occurred at very low agitation. The adverse effect of segregation might be eliminated if a column crystallizer were oriented, not vertically, but diagonally. Diagonal orientation would cause the crystals to settle along the column wall rather than on the spiral. The settled slurry would thus form a porous seal through which the reflux liquid would have to pass to reach the freezing section. Therefore, although there would still be segregation between the slurry and the free liquid, the by-passing present in a vertical column would be eliminated. The result would be similar to the effect achieved by an Archimedes' screw which will deliver water when set diagonally, but not when set vertically.

Diagonal operation might have another benefit. If, as described above, interphase contact were maintained by diagonal positioning, then the agitation currently used to effect such contact could be drastically reduced. This reduction would limit the diffusivity within the liquid. Because dispersion is currently the predominant effect limiting separations, a reduction of diffusivity would increase the separations almost proportionally.

Reducing agitation would increase separations in another way. It was mentioned earlier that the crystal bed expanded as agitation increased. Thus the separation was affected adversely by increased dispersion (η_L increased) and by decreased mass-transfer (a decreased).

APPENDIX A5

CALCULATIONS

a. Analysis of Data from Azobenzene-Stilbene

The model including mass-transfer and liquid dispersion (Equation (22)), which was developed in this report by assuming a linear equilibrium relationship, was applied stepwise to data for a system in which this relationship was not linear. The calculated profile and the experimental one agreed very well.

Data presented by Powers[32] represent the overall composition in a column crystallizer in which azobenzene was separated from stilbene. These data are the weighted average of the compositions in the liquid and in the solid phases. As Equation (22) applies to the liquid phase, Powers' data cannot be analyzed directly. To determine a liquid profile from Powers' overall profile the following assumptions were made.

1) The volume fraction liquid was 2/3. This is about the value obtained in the present study and by Albertins.
2) The liquid and solid were in equilibrium. This gives the maximum reasonable difference between the compositions in the liquid and solid phases. Powers' application of an equation describing a liquid profile to data which represent overall compositions implies that liquid and solid have the same composition.

These two assumptions define a unique relation between overall composition and liquid composition. This relation was used to prepare Table XII in which Powers' data are compared with equivalent liquid compositions.

TABLE XII

COMPARISON OF DATA REPORTED BY POWERS[32] AND PROFILE CALCULATED FROM EQUATION 22

Position	Powers' Data of Overall Composition	Equivalent Liquid Composition	Calculated Liquid Profile
cm	Weight Fractions		
48	0.99	0.99	
45		0.99	0.990
42	0.97	0.98	
40		0.97	0.968
39	0.94	0.97	
36	0.91	0.94	
35		0.93	0.908
33	0.82	0.88	
30	0.67	0.77	0.747
27	0.48	0.60	
25		0.49	0.451
24	0.35	0.41	
20		0.08	0.070
18	0.02	0.02	
15	0.01	0.01	0.000
12	0.00		

In order to apply Equation (22), values of L, ($D\eta A\rho$) and ($KaA\rho$) must be known. Unfortunately, Powers does not give any clue to these values in his paper. The following procedure was used to make estimates.

The present study indicated that in many cases the term $D\eta A\rho/L$ was 5 to 10 times greater than $L/KaA\rho$. Powers indicated in his paper that the sum of these two terms was about 4. These approximations were combined to give Equation (76).

$$H = 3.5 + m/2 \tag{76}$$

Thus Equation (22) has the form given in Equation (77).

$$Y = Y_o - (Y - X^*)_o \, h / [3.5 + m/2] \tag{77}$$

A value of Y_o equal to 0.990 at $h = 45$ cm was assumed. $(Y-X^*)_o$ and m were determined from the phase equilibrium. These values were assumed to be constant for a column length of 5 cm. Then, for a $\Delta h = 5$, a ΔY was calculated, and Y at $h = 40$ was determined. This stepwise procedure was applied repeatedly for successive intervals of the column. The results of these calculations are summarized in Table XII. As it was mentioned earlier, the profile determined by this procedure was in good agreement with the liquid profile calculated from Powers' data. In fact, the determined concentrations lay between those presented by Powers (which assume equal compositions in both phases) and those assumed here (which assume equilibrium between phases).

b. Correlation of Phase Equilibrium Data

Bromonitrobenzene-chloronitrobenzene

Data of Hasselblatt[19], taken from International Critical Tables, Vol. IV, p. 122, were used in this study. These data are in substantial agreement with those presented by Kuster[22], and with tests made during the course of the present study[15]. Table XIII presents the temperature-composition data. Figure 3, presented earlier, is a second representation of these data.

It was desired to convert these data to a more easily used form. This was done by statistically fitting curves through the data points. The statistical equations were then used to calculate temperature-composition data with a much smaller interval than given.

As demonstrated on Fig. 26, the liquidus line, from 0 to 70 mole per cent BNB, was fit very well by Equation (78).

$$T = 44.6 - 4.06 \ln (1 - Y) \qquad (78)$$

The solidus line required a second power term to give a good fit. Equation (79), again derived statistically, fit the data adequately from 0 to 70 mole per cent BNB.

$$T = 44.6 - 3.21 \ln (1-X) + 0.383 (\ln (1-x))^2 \qquad (79)$$

This equation is shown on Figure 40.

The liquidus and solidus lines at the BNB-rich end of the diagram were not statistically fit. However, as demonstrated on Figure 40, both lines are described very well by an equation of the form

$$T = A + B \ln (\text{mole fraction}) \qquad (80)$$

TABLE XIII

PHASE EQUILIBRIUM DATA OF HASSELBLATT(19)
FOR SYSTEM BNB-CNB

Composition	Temperature	
	Solidus	Liquidus
Mole Fraction BNB	°C	°C
0.00	44.6	44.6
0.05	44.7	44.8
0.10	44.9	45.0
0.20	45.3	45.5
0.30	45.7	46.0
0.40	46.3	46.7
0.50	47.0	47.4
0.60	47.8	48.3
0.70	49.0	49.5
0.80	50.7	51.1
0.90	52.3	52.5
0.95	53.1	53.2
1.00	54.0	54.0

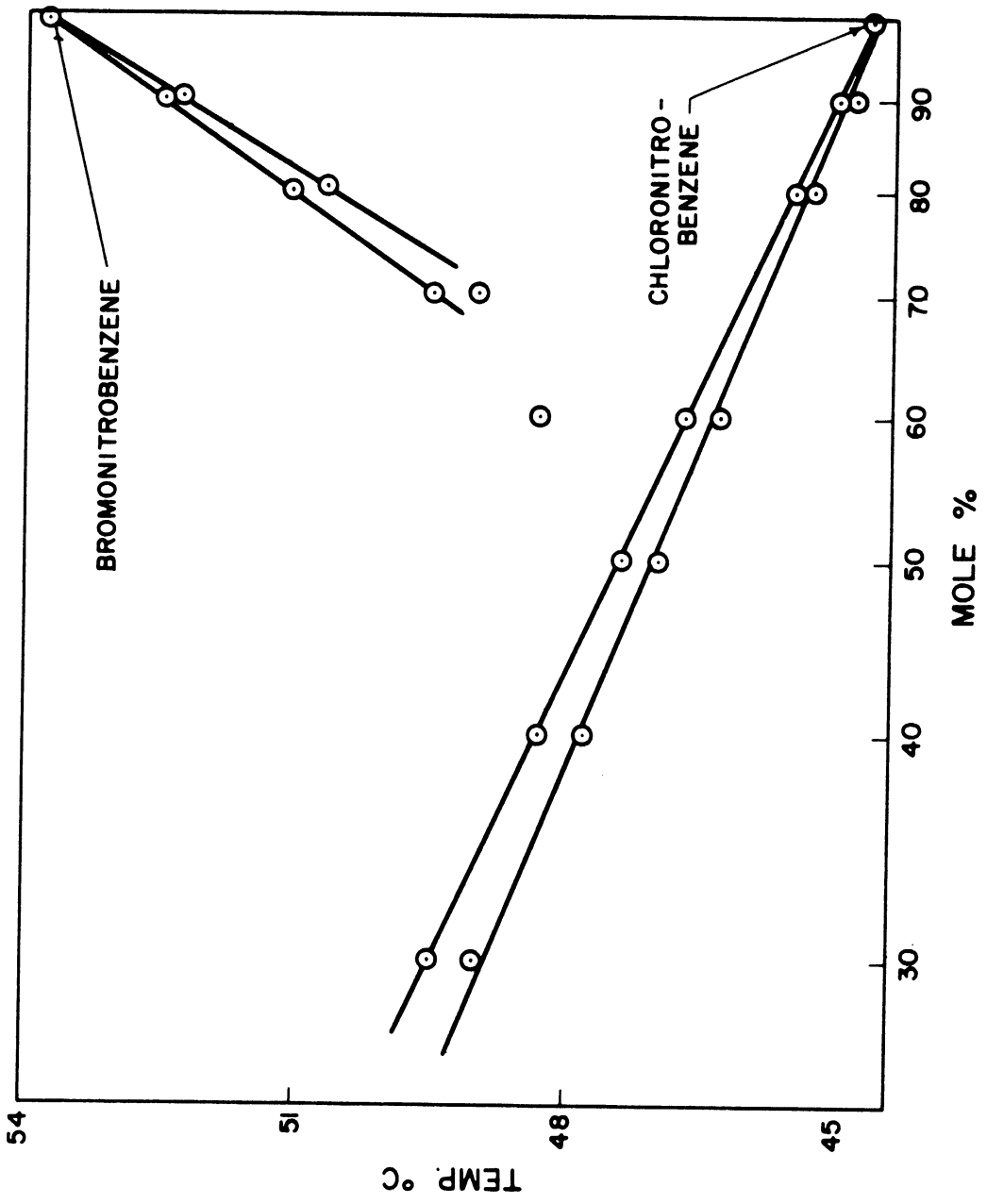

Figure 40. Analysis of Phase Equilibrium Data.

Tables of X and Y vs. T and of X^* vs. Y, were made from the equations which were derived. Figure 4 is based on such a table. The assumed linearity between X^* and Y can be tested with the figure. It is certainly clear that for a narrow range of compositions, on the order of 0.1 weight fraction, either m is in fact constant, or m can be approximated by a constant with only little error.

Azobenzene-Stilbene

Data presented by Powers[32] were used for this system. And, as in the case of BNB-CNB, the data were converted to a more useful form by fitting them with logarithmic equations. The data, and the resultant equations, are shown on Figure 41. It is clearly seen that the liquidus line at the stilbene end of the diagram and the solidus line at the other end were of the form given in Equation (80). The other ends of these lines were fit by quadratics of the form given in Equation (81).

$$T = A + B(\ln(\text{mole fraction})) + C(\ln(\text{mole fraction}))^2 \qquad (81)$$

The statistically evaluated constants for these several equations are presented in Table XIV.

As in the case of BNB-CNB, the statistical equations were used to make tables of X^* and Y vs. T, and of X^* vs. Y. The data on Figure 26, which presents X^* vs. Y, were taken from these tables. Clearly for this system X^* vs. Y is highly non-linear.

c. Correction of Diffusivities

The diffusivities calculated from Equation (18) are based on the vertical distance between sample taps. Liquid does not follow this

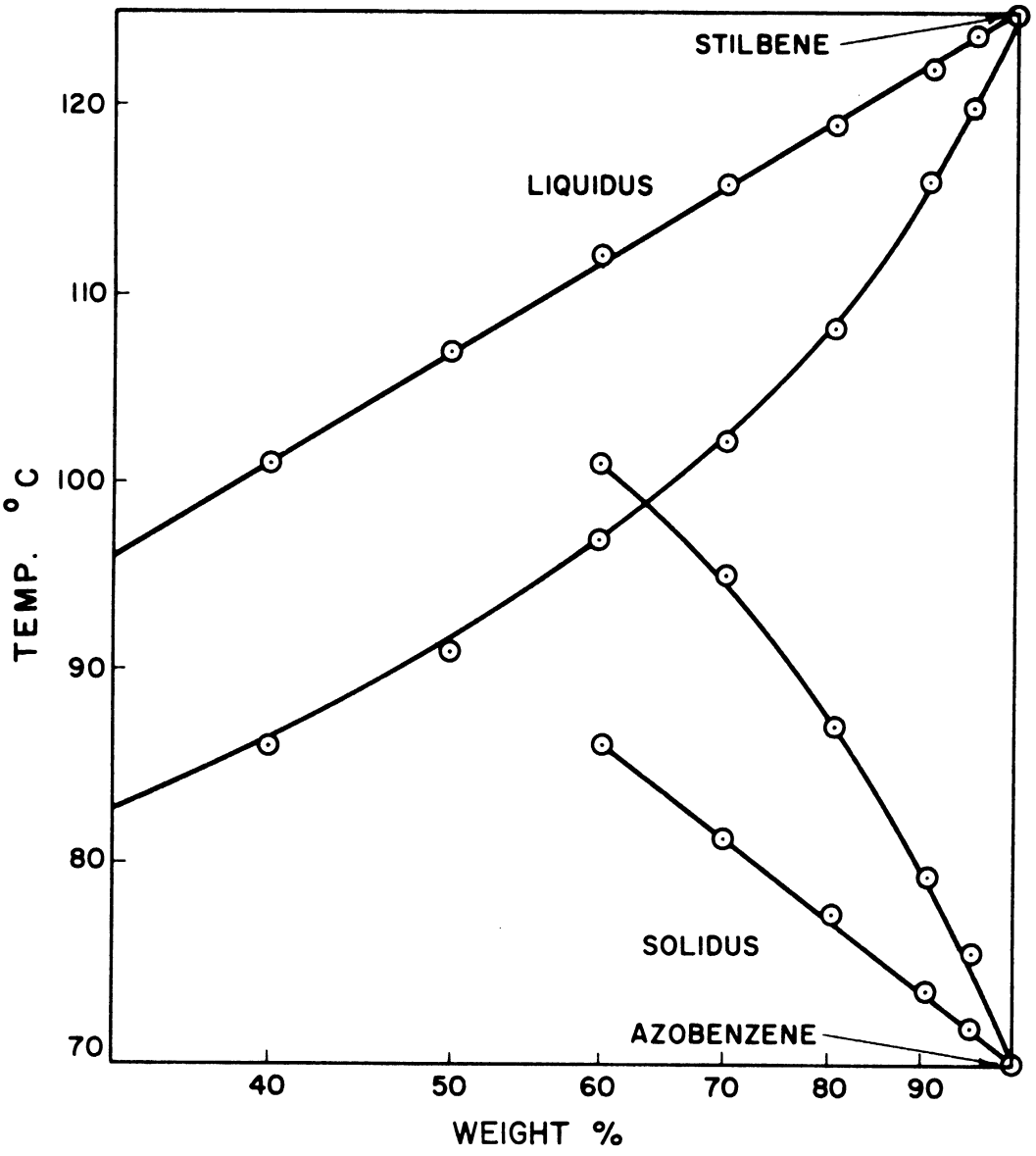

Figure 41. Analysis of Phase Equilibrium Data.

TABLE XIV

CONSTANTS USED IN CORRELATION OF PHASE EQUILIBRIUM DATA

Argument of Logarithm	A	B	C
$X_{azobenzene}$	69.5	-31.7	-
$Y_{stilbene}$	125.3	26.4	-
$X_{stilbene}$	124.7	89.6	69.8
$Y_{azobenezene}$	69.6	-94.1	-64.1

path, however, but flows spirally around the central shaft of the column. Thus, the diffusivities calculated directly must be corrected. The correction factor is derived in this section.

In order to determine the effective path length per cm of column, the dimensions of the spiral must be considered. As described in Appendix A1-a, the spiral was 2.58 cm OD by 1.26 cm ID. The pitch was 0.92 cm per turn and the solid volume of the spiral was 0.93 cm^3/cm. Thus, the void volume of the spiral was 3.23 cm^3/cm and the area through which liquid flowed at right angles was 0.5 cm^2.

The void volume is equal to the area times the effective path length. Thus the path length was 6.5 cm/cm. This number was used to correct diffusivities. The value for diffusivity determined from Equation (18) was multiplied by 6.5 cm/cm to give the corrected diffusivity.

d. Crystal Rate at Minimum H

H, a measure of the separating power of a column crystallizer, has a minimum as a function of L . The values of H and L at this minimum are determined in this section.

The functional form for H is given by Equation (18)

$$H = E/L + L/F \tag{18}$$

In this equation E and F contain terms which relate to diffusion and mas-transfer, respectively. The derivative of H with respect to L is given by Equation (82).

$$dH/dL = - E/L^2 + 1/F \tag{82}$$

When H is a minimum, dH/dL is zero. Thus the value of L corresponding to H_{min} is given by Equation (83).

$$L_{min} = (EF)^{1/2} \tag{83}$$

The value of H_{min} is shown in Equation (84) which is determined by substituting L_{min} for L in Equation (82).

$$H_{min} = (E/F)^{1/2} + (E/F)^{1/2} \tag{84}$$

Thus it is seen that at H_{min} the effects of diffusion and mass-transfer are equal. That is, $E/L_{min} = L_{min}/F$.

APPENDIX A6

SAMPLE CALCULATIONS

A set of calculations is presented in this appendix to demonstrate the methods of calculation and to put forth the values used in the several computations.

a. Determination of the Crystal Rate

The crystal rate was determined from the power supplied to the melter and the heat of fusion of the crystals. This latter heat was assumed to be linearly related to the composition of the liquid in the melter, and to the pure component heats of fusion. The heats of fusion were assumed to be independent of temperature.

The heats of fusion of BNB and CNB are 24.3 and 33.1 cal./g, respectively.[42] From these data and the assumptions listed above, the heat of fusion of a mixture is given by $33.1-8.8X_o$ cal./g.

The values for X_o which were used in determining heats of fusion were not raw data. Rather, the least squares line through all the data was used to generate a value for X_o. Thus, for example in Run 29, X_o was calculated to be 0.707 whereas the corresponding data point was 0.702. A value of 26.9 cal/g was determined as the heat of fusion for this run.

The crystal rate was calculated by dividing the heat of fusion into the power input, V^2/R. Here V is the voltage supplied to the melter, and R is its resistance (194 ohms). For Run 29, V was 28.7 volts. Thus the crystal rate was:

$$(28.7)^2/[194 \times 4.19 \text{ watt-sec/cal} \times 26.9] = 0.038\text{g/sec}$$

b. Determination of H

The slope of the concentration profile for Run 29 (see Figure 10) was 0.088 weight fraction per 6 taps or 30.4 cm. This was determined by a least squares fit of the concentration data. The concentration at the top tap was 0.688. From tables prepared from Equations (78) and (79) a value of 0.0355 was extracted as the equilibrium difference between the composition of the liquid and solid phases, That is, $(X^*-Y)_o = 0.0355$ for Run 29.

According to Equation (22), the slope of the concentration profile is given by $(X^*-Y)_o/H$. By rearrangement, H is given by $(X^*-Y)_o/\text{slope} = 0.0355 \times 30.4/0.088 = 12.2$ cm.

c. Determination of D and K

Data for Runs 29 to 31 are shown in Figure 10, plotted as HL versus L^2 . The intercept and slope of the least squares line drawn through these data are 0.373 g-cm/sec and 64 cm/sec/g, respectively. The intercept is E , equal to $DA\eta\rho$, and the slope is F , equal to $KaA\rho/m$. Thus D and K can be calculated from values of the slope, intercept and a , A , ρ , η and m .

Area

The area A is that through which the liquid and solid flow. It is defined by the glass column, by the stainless-steel shaft, and by adjacent turns in the spiral. The width of the annular space was 0.66 cm, and the distance between turns was 0.76 cm. Thus the area was 0.50 cm^2 .

Density

The density of the liquid was assumed to be a linear combination of the pure component densities. These were:

(1) BNB = 1.50 g/cm^3

(2) CNB = 1.35 g/cm^3

Therefore the liquid density was 1.46 g/cm^3 .

Volume fraction

The volume fraction, η , was calculated by a mass balance on the column. The amount of material charged was known, and could be accounted for in the final liquid and solid. Thus, the sum of the products of volume times density for the two phases in the slurry equalled the same product for the charge. That is,

$$\text{Vol. Liq} \times \rho_L + \text{Vol. sol.} \times \rho_S = \text{Vol. chg.} \times \rho_L$$

On rearrangement this equation yields Equation (82) for η_S .

$$\eta_S = \Delta V \, \rho_L/(\rho_S-\rho_L)x(V_o-\Delta V) \qquad (82)$$

For Run 29, the change in volume, ΔV , was 8 cm^3 and the volume charged, V_o , was 225 cm^3. The densities were 1.46 and 1.65 g/cm^3 . Thus, η_L , equal to $1-\eta_S$, was 0.718.

Interfacial area

The interfacial area available for mass-transfer was estimated from an approximate particle diameter. A value of 0.04 cm was used. This value was derived from the approximation previously used by Albertins (Reference 1) and the observation previously discussed that the crystals

in the present study seemed smaller. The surface area of a particle with a diameter of 0.04 cm is

$$\pi(0.04)^2 = 5.04 \times 10^{-3} \text{ cm}^2/\text{crystal}$$

and the volume is

$$\pi(0.04)^3/6 = 3.35 \times 10^{-5} \text{ cm}^3/\text{crystal}$$

The number of crystals in 1 cm^3 of slurry is

$$(1 \text{ cm}^3)\ (1-\eta_L = 0.282)/3.35 \times 10^{-5} = 8{,}430 \text{ crystals}$$

From the above data, the surface area per cm^3 of slurry is

$$8430 \times 5.04 \times 10^{-3} = 42.5 \text{ cm}^2/\text{cm}^3$$

D and K

The values for A, ρ, η and a presented above are substituted into the expressions for E and F to determine D and K. D is given by

$$D = 0.373/0.50 \times 0.72 \times 1.46$$
$$= 0.77 \text{ cm}^2/\text{sec}$$

This value is corrected for path length by multiplying by 6.5 (see Appendix A5-C). Thus D is 5.0 cm^2/sec.

F is equal to 64 cm-sec/g so that K is given by

$$K = 0.9/64 \times 43 \times 0.50 \times 1.46$$
$$= 0.44 \times 10^{-3} \text{ cm/sec}.$$

APPENDIX A7

DATA

Charge to the Column: 0.05 Weight Fraction BNB

Sample Tap Number	Integrator Counts			
	Run 6		Run 7	
	CNB	BNB	CNB	BNB
1	9213	5852	9533	5294
2	8920	5786	9380	5945
3	8627	9718	10027	6271
4	8910	6026	9483	5658
5	9315	6166		
6			10274	5880
7	8759	6097	9681	6322
Attenuation	4	1	4	1
Operating Conditions				
Voltage to Meter-Volts		17.7		15.4
Stroke-mm		4.5		4.5
Oscillation Rate-OPM		72		72
Rotation-RPM		67		67
Column length-cm		30.3		30.3

Charge to the Column: 0.95 Weight Fraction BNB

Sample Tap Number	Integrator Counts Run 13 CNB	BNB
1	7475	11029
2	7212	11266
3		
4	6823	10302
5	8803	10322
6		
7	7468	10273
Attenuation	1	8

Operating Conditions	
Voltage to Meter-Volts	28.3
Stroke-mm	4.5
Oscillation Rate-OPM	22
Rotation Rate-RPM	67
Column Length-cm	30.3

Charge to the Column: 0.50 Weight Fraction BNB

Sample Tap Number	Integrator Counts					
	Run 14		Run 15		Run 16	
	CNB	BNB	CNB	BNB	CNB	BNB
1	3530	2676	6700	5038	4751	3521
2	3421	2529	6555	4944		
3	3689	2593	6509	4742	5097	3095
4	3603	2463	6652	4450	5589	3023
5	3532	2367	7072	4485	5661	2846
6	3670	2186	7040	4268	5633	2680
7			7369	4080	5244	3029
Attenuation	1	1	1	1	1	1

Operating Conditions			
Voltage to Meter-Volts	28.9	28.9	25.1
Stroke-mm	4.5	4.5	6.0
Oscillation Rate-OPM	25	25	40
Rotation Rate-RPM	67	32	46
Column Length-cm	30.3	30.3	30.3

Charge to the Column: 0.50 Weight Fraction BNB

Sample Tap Number	Integrator Counts			
	Run 17		Run 18	
	CNB	BNB	CNB	BNB
1	5068	3116		
2			6813	4268
3	5436	3047	3370	4063
4	5244	2801	6892	4085
5	5599	2715	3443	1875
6	5609	2579	3612	3650
7	5532	2622	3544	7185
Attenuation	1	1	1	1

Operating Conditions		
Voltage to Meter-Volts	20.6	21.0
Stroke-mm	6.0	6.0
Oscillation Rate-OPM	31	31
Rotation Rate-RPM	29	29
Column Length-cm	30.3	25.1

Charge to the Column: 0.65 Weight Fraction BNB

	Integrator Counts					
Sample Tap Number	Run 20		Run 21		Run 22	
	CNB	BNB	CNB	BNB	CNB	BNB
1						
2						
3			5053	9312	5445	9327
4	4893	7586	4695	7978	5596	9205
5	5925	8877	4980	8234	5563	8815
6	6060	9098	6176	9320	6677	10265
7	6344	8969	6560	9061	6061	8936
Attenuation	1	1	1	1	1	1

Operating Conditions			
Voltage to Meter-Volts	26.5	27.2	26.4
Stroke-mm	6.0	6.0	9.0
Oscillation Rate-OPM	31	43	43
Rotation Rate-RPM	29	45	45
Column Length-cm	20.0	20.0	20.0

Charge to the Column: 0.65 Weight Fraction BNB

Sample Tap Number	Integrator Counts					
	Run 23		Run 24		Run 25	
	CNB	BNB	CNB	BNB	CNB	BNB
1	4434	7632	4529	8674	4516	7807
2	5074	8389	5013	9050	4259	7115
3	5248	8414	4662	8420	4592	7425
4	5225	7798	4111	6797	4811	7418
5	6236	8562	5312	7905	5318	7403
6	5583	6998	5510	7313	5165	7199
7	5587	6781	5907	8111	5179	6825
Attenuation	1	1	1	1	1	1

Operating Conditions			
Voltage to Meter-Volts	27.0	27.5	27.1
Stroke-mm	6.0	6.0	6.0
Oscillation Rate-OPM	45	45	43
Rotation Rate-RPM	41	41	78
Column Length-cm	30.3	30.3	30.3

Charge to the Column: 0.65 Weight Fraction BNB

Sample Tap Number	Integrator Counts Run 26 CNB	BNB
1	4737	9171
2	4887	9098
3	4972	8777
4	5414	8757
5	5360	7969
6	2960	3913
7	5573	7405
Attenuation	1	1

Operating Conditions	
Voltage to Meter-Volts	26.6
Stroke-mm	6.0
Oscillation Rate-OPM	43
Rotation Rate-RPM	48
Column Length-cm	30.3

Charge to the Column: 0.65 Weight Fraction BNB

Sample Tap Number	Integrator Counts					
	Run 29		Run 30		Run 31	
	CNB	BNB	CNB	BNB	CNB	BNB
1	4265	8048	4205	8151	4364	8266
2	3933	7781	3991	7390	3665	7163
3	4388	8141	3810	6875	4505	8369
4	4301	7949	4511	7995	4091	7337
5	4507	7941	4423	7380	4183	7317
6	4658	7537	4659	7705		
7	4593	7455	4918	7762	4465	7410
Attenuation	1	1	1	1	1	1

Operating Conditions			
Voltage to Meter-Volts	28.7	26.8	23.3
Stroke-mm	4.2	4.2	4.2
Oscillation Rate-OPM	67	67	67
Rotation Rate-RPM	60	60	60
Column Length-cm	30.3	30.3	30.3

Charge to the Column: 0.35 Weight Fraction BNB

Sample Tap Number	Integrator Counts					
	Run 33		Run 34		Run 35	
	CNB	BNB	CNB	BNB	CNB	BNB
1	6339	4981	6861	6552	6523	4768
2	6345	4966	6611	6253	6958	5130
3	6742	5174	7287	7023	6932	5090
4	6527	4855	6871	6171	7192	4892
5	6687	5059	7488	7914	7383	5014
6						
7	6620	4654	6921	6231	6788	4781
Attenuation	1	1	1	1	1	1

Operating Conditions			
Voltage to Meter-Volts	25.2	20.4	14.0
Stroke-mm	2.0	2.0	2.0
Oscillation Rate-OPM	130	130	130
Rotation Rate-RPM	60	60	60
Column Length-cm	30.3	30.3	30.3